Hygro-Mechanics of Wood Fibre Composite Materials

Stålne, Kristian

2009

Document Version:
Publisher's PDF, also known as Version of record

LUND UNIVERSITY

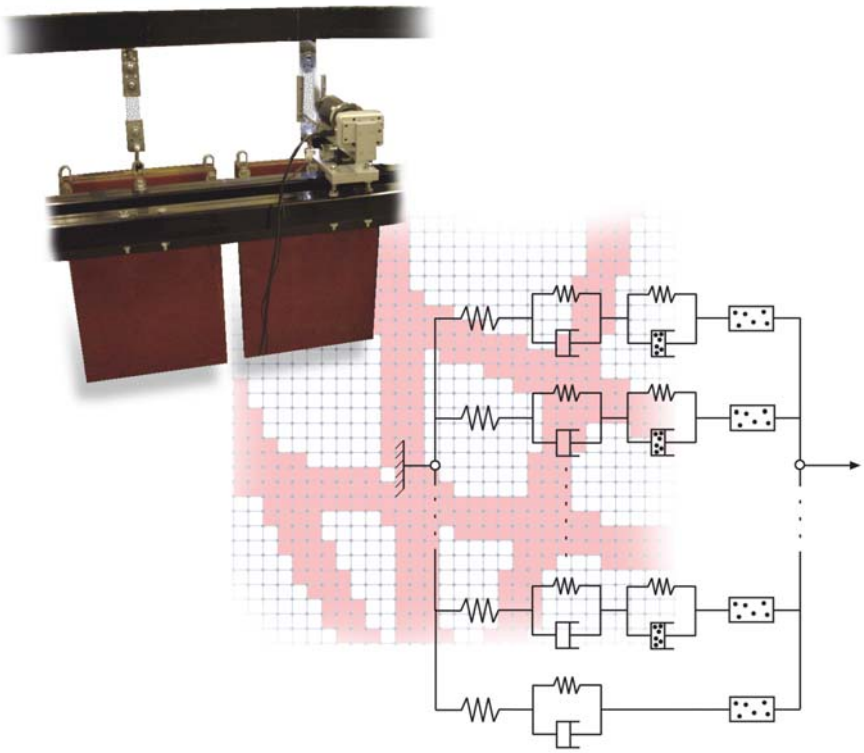

HYGRO-MECHANICS OF WOOD FIBRE COMPOSITE MATERIALS

KRISTIAN STÅLNE

Structural Mechanics

Doctoral Thesis

Department of Construction Sciences
Structural Mechanics

ISRN LUTVDG/TVSM--09/1022--SE (1-160)
ISBN 978-91-628-7753-8 ISSN 0281-6679

HYGRO-MECHANICS OF WOOD FIBRE COMPOSITE MATERIALS

Doctoral Thesis by

KRISTIAN STÅLNE

Printed by KFS i Lund AB, Lund, Sweden, March 2009.

For information, address:
Division of Structural Mechanics, LTH, Lund University, Box 118, SE-221 00 Lund, Sweden.
Homepage: http://www.byggmek.lth.se

Abstract

The work presented in this thesis deals with modelling and testing of hygro-mechanical properties of wood fibre composite materials. The material studied experimentally is high pressure laminate, HPL, which is a wood fibre network composite, made up of craft paper impregnated with phenolic or melamine resin. An analytical model for the hygro-mechanical properties has been developed. The model calculates the stiffness, hygroexpansion, creep and mechanosorption behaviour of the composite material from the given corresponding properties of the constituents.

The analytical model is based on the assumption of homogeneous strain. This assumption is validated by comparison of the stiffness and hygroexpansion predictions with the predictions of another analytical model developed as a part of the research. The model is validated also by the results of two finite element homogenisation methods, one 2-dimensional and one 3-dimensional. The comparisons show that the homogeneous strain assumption overestimates the composites stiffness by approximately 15 % and underestimates the composites hygroexpansion by approximately 15 %.

Experimental tests of two HPL materials with melamine resin as matrix material and with different fibre volume fraction were carried out. The tests comprised strength, stiffness, Poisson's ratio, free hygroexpansion, creep, mechanosorptive strains, moisture sorption isotherms and moisture equilibrium curves. Strain was recorded in the direction of the in-plane tensile load and in the transverse direction. The results show that creep, unlike the elastic stiffness, is significantly influenced by the moisture content. The creep was of very different character in transverse direction as compared to the creep in the direction of the load, and furthermore linear with respect to the stress up to at least 40 % of the failure stress. By development of an empirical hygro-mechanics model was mechanosorption identified and found to be of significant magnitude. The free hygroexpansion of the HPL composite was found to much larger than first expected.

The analytical model is compared with the test results. Material data for hygroexpansion, creep and mechanosorption of the matrix material is however lacking. This made it difficult to validate the analytical model by the test results. By assuming matrix material data it was found that the analytical model can be capable to capture the hygro-mechanical behaviour of composite materials. Tests of the matrix material are proposed.

It is believed that the proposed model can be successfully used for predicting the hygro-mechanical properties of new wood fibre composite materials. Such a model can be a useful tool in the process of optimal design of new composites and thus extending the good use and the area of application of wood fibre composites.

Populärvetenskaplig sammanfattning

Träfiberkompositer är material som består av träfibrer som blandats med en matris, t ex en härdplast. Till skillnad från massivt trä har materialet inga lokala variationer och svagheter som kvistar. En nackdel med såväl trä som träbaserade material är att de är hygroskopiska, vilket innebär att de tar upp fukt och sväller och att deras egenskaper påverkas av luftfuktigheten. Detta kan leda till oönskade deformationer och formändringar. En fördel med kompositer är att de genom lämligt val av sammansättning kan ges egenskaper, designas, för att passa en given produkt eller användning. För att kunna göra en sådan materialdesign är det nödvändigt att kunna beräkna tänkta kompositmaterials egenskaper utan att behöva göra provtillverkning. Sådana beräkningar görs med hjälp av matematiska simuleringar eller beräkningsmodeller.

Materialet som studeras i denna avhandling är ”high pressure laminate”, HPL, eller högtryckslaminat, som är en träfiberkomposit som består av kraftpapper som impregnerats av fenol- eller melaminharts och pressats under högt tryck och hög temperatur. Detta ger ett material med hög styvhet, styrka och reptålighet. Materialet används som bänk- och som golvlaminat, traditionellt i form av Perstorpsplattan. När materialet används utsätts det för fuktvariationer, dels på grund av de naturliga dygns- och årstidsväxlingarna, dels på grund av olika fuktnivå i laminatets tjockleksriktning, vilket kan leda till att laminatet kupar sig.

Arbetet i den här avhandlingen handlar om att ta fram en beräkningsmodell som kan prediktera träfiberkompositers hygro-mekaniska egenskaper. Beräkningsmodellen ska utifrån de ingående delmaterialens egenskaper och sammansättning kunna beräkna kompositens deformationsbeteende när den utsätts för en godtycklig last och fuktvariation.

I avhandlingen presenteras en analytisk beräkningsmodell som omfattar styvhet, hygroexpansion, (svällning), krypning och mekanosorption (deformation orsakad av varaktig last och varierande fuktnivå). Krypning är en deformation som orsakas av en last med lång varaktighet och mekanosorption är en ökad krypning p. g. a. en fuktvariation. För att validera att beräkningsmodellen ger riktiga resultat jämförs dessa med resultat från två numeriska modeller och med resultat från en annan analytisk modell.

Vidare har utförts en serie provningar på HPL-material med två olika sammansättningar. Materialen har provats med avseende på styrka, styvhet, fri hygroexpansion, krypning, mekanosorption samt fuktupptagning. Töjningen har mätts i både lastriktning och tvärriktning med ett beröringsfritt mätsystem som har utvecklats för de aktuella testerna. Resultat visar att mekanosorption äger rum för HPL-materialet. Uppmätt hygroexpansion var betydligt större än förväntad.

Beräkningsmodellen har jämförts med resultaten från provningarna och det visar sig att modellen kan spegla de fenomen som observeras i mätningarna med god noggrannhet.

Den föreslagna beräkningsmodellen kan med fördel användas för att prediktera hygro-mekaniska egenskaper för nya träfiberkompositer. En sådan modell kan vara ett användbart

verktyg i processen att ta fram en optimal design för nya kompositer och därmed utöka användningsområdet för träfiberkompositer.

Preface

The work presented in this thesis was carried out at the Division of Structural Mechanics, Department of Construction Sciences, Lund University, Sweden. The financial support by the Swedish Foundation for Strategical Research (SSF) programme “Wood Technology” is gratefully acknowledged. The last part of this work has been financed by the Division of Structural Mechanics, which is gratefully acknowledged, as well.

I would like to express my deepest gratitude to my supervisor, Professor Per Johan Gustafsson, for his patience and his skilful supervision during the full decade that this work has lasted. The door has always been open for questions and discussions that have guided me in the right direction of all aspects of this project.

During this time I have also received a great amount of help from the staff at the Structural Mechanics Division. During the course of work, Professors Ola Dahlblom and Göran Sandberg and Dr. Christer Nilsson have been contributing with valuable ideas, feed-back and support. Mr. Thord Lundgren has been of invaluable assistance in the experimental parts of my work, building the hardware to the DSP-system, load rigs and most parts associated to it. Mr. Bo Zadig has been of assistance with graphics and printing. All of this I am very grateful for.

I would also like to thank Perstorp AB and Pergo AB for good collaboration and providing me with high quality HPL specimens. Special thanks go to Dr. Håkan Wernersson for both professional and personal support.

Being a researcher is a hard life. Being married to one is probably even harder. This work would not have been completed without the never-ending love and support from my wife, Jenny. Thank you for always being there for me.

Lund, March 2009

Contents

1. Introduction

1.1. Composite Materials

A composite material is created when two or more materials are mixed in order to achieve different properties than those of its constituents. The regions occupied by the separate constituents are commonly considered as being homogeneous continua and assumed to be bonded together firmly at the interfaces. A main advantage of using a composite material is that it can be tailor-made for a particular application. By adding fibres aligned in one preferred direction, the material can be made stiffer and stronger in that direction. This makes it possible to achieve light but yet stiff materials. Different types of composite materials can be distinguished on the basis of their micro-structure: particle composites, fibre composites laminate composites and composites with irregular geometry, according to Figure 1.

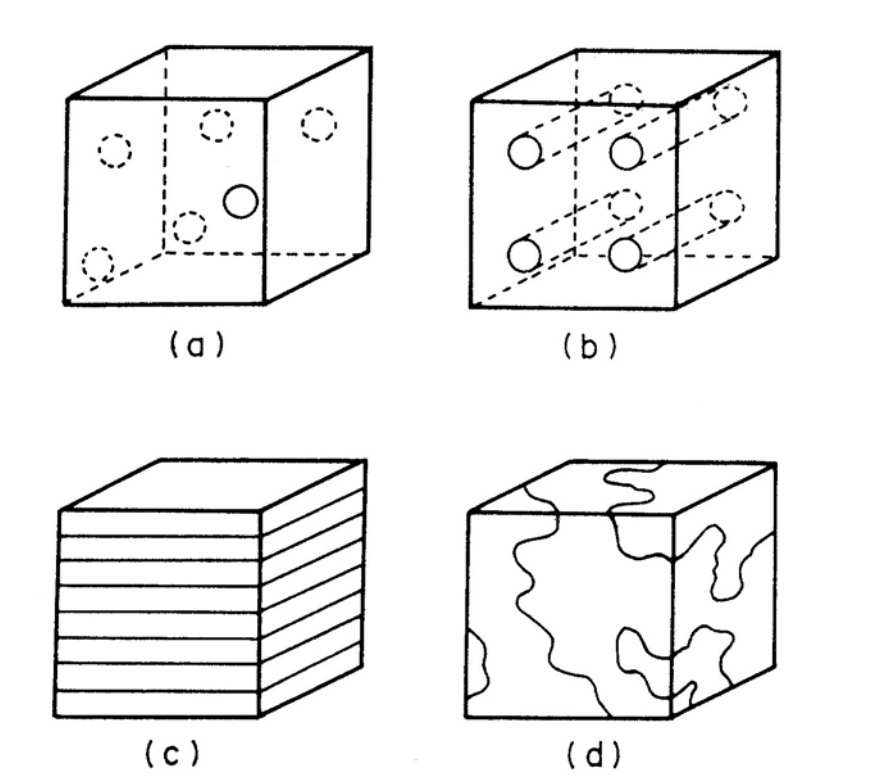

Figure 1. Principal types of composites: a) particle composite, b) fibre composite, c) laminate composite, d) composite with irregular geometry.

One of the particle composites most frequently employed is concrete. Here, cement paste is mixed with sand and small stones to produce a material that is cheaper and has improved

properties, such as being stiffer and showing less moisture-induced strains than the cement paste. Reinforcing concrete with steel bars provides it a high degree of strength, also when in tension. Concrete can also be reinforced with steel, polymeric or glass fibres, making it easier to control the stiffness. Concrete with both fibres and bars can in some cases be regarded as a composite material made up of four constituents. The composite material concrete is perhaps the most commonly and frequently used material for buildings and structures.

In a smaller scale fibre composites are used in high performance products associated with sports products, automotive and aerospace industry, and also in building components. Fibre composites are often classified according to the fibre length and the fibre orientation distribution. Fibres can either be placed in one direction, be arranged in a weave, or arranged in accordance with some continuous orientation distribution function. Fibre materials commonly used are glass, carbon, aramid and wood. The surrounding phase, or matrix, is often some polymer such as epoxy or polyester.

1.1.1. Wood Composites

Wood is in it self a natural composite material made up of strong fibres that are glued together by a matrix material. Raw material for various man-made wood based composites is produced by defibration, cutting or grinding the wood. Composite materials containing fibres or particles obtained from wood or from plants such as flax and hemp are gaining in popularity, both by environmental reasons and due to their good performance, their low cost and their low weight. Wood-based composites are commonly created either by joining wood particles by some adhesive, by mixing wood flour with a thermoplastic [1] or by impregnating paper with a thermoset resin. Advantages of wood composites as compared with solid wood are that they are more homogeneous, e.g. without knots, they can be assigned other anisotropic properties and products can be designed in almost any shape.

Often wood particles are taken from waste from sawmills [2] and used in composites as fillers with a matrix material with poor mechanical properties and poor adhesion. This type of particle composite is not very high performing due to the fact that the wood particles are not in contact with each other and that a significant part of the load has to be carried by the matrix phase.

Wood based composites and products are hygroscopic, like wood [3, 4]. Studies of the hygroscopic nature of wood based products are presented in [5] and [6]. Research on the mechanical and hygro-mechanical performance of wood and other natural fibre composites are presented in e.g. [7-10].

1.1.2. High Pressure Laminates

The most significant mechanical property of wood that one wants to take advantage of in a composite is its high stiffness in the longitudinal fibre direction. A composite with well connected fibres with high aspect ratio, i.e. length to width ratio, can carry load efficiently. One such composite material is High Pressure Laminate, HPL [11]. HPL is manufactured by taking craft paper, wetting it with phenolic or melamine formaldehyde resin [12], letting it dry and then

cure it at high pressure and temperature, typically at 2.6 MPa and 190°C. The HPL material origins from the material Bakelite, which was developed in the beginning of the 20th century by mixing wood flour with thermosetting phenolic formaldehyde resin [13].

The HPL material is used for applications such as flooring, panelling or as hygiene surfaces such as kitchen work benches. When used in flooring, the HPL is glued on a medium density fibreboard or any other type of bearing material. The surface is hard and resistant to scratches and heat, thanks to the melamine resin. However, being a wood based material, HPL will react to changes in moisture content by changing its dimensions. This is something that has to be taken into consideration when trying to expand the area of application and the market for HPL and other wood based materials. Shape instability could lead to cupping of the material, meaning that the edges of the laminate are raised, making it even more vulnerable to absorb moisture. There is also a risk for buckling if the laminate is not allowed to expand freely.

1.2. Modelling of Composite Materials

As mentioned, wood composite materials have certain advantages compared to solid wood. One being the possibility to make statistically homogeneous materials, compared to solid wood which has local weaknesses such as knots and cracks. Another advantage is the possibility to manufacture the composite with regard to its application; it can be tailor made and optimized with regard to the loads and the climate situations it will be exposed to in its application. This proves, however, to be a challenging task. The mechanical properties of the composite will depend on a large number of factors, such as:

- Type of paper being used
- The kind of wood fibres that constitute the paper
- Possible damage of the fibres
- Fibre orientation distribution in the paper
- Manufacturing process of the paper
- Fibre bonding properties
- Paper thickness and number of layers
- Type of resin being used
- Melamine/formaldehyde proportions
- Fibre/resin proportions
- Process parameters such as curing time, temperature and pressure.

All these factors, of which most are on the micro scale, will contribute to the physical and the mechanical properties of the resulting composite at the macro scale. For example, the composite will have a high stiffness and strength if the fibres are well separated at the paper processing stage and not damaged [14]. The composite can be considered as a black box with the above mentioned factors as input and the composites properties as the output. We could then make a large number of measurements and vary all indata parameters, one at a time, in order to make some sort of multivariable analysis, assuming that the influence of all parameters is independent

from each other. This approach would, however, be extremely costly and not very effective if we want to tailor our composites for new applications. If we want to effectively predict the properties of the composite, we need to gain a deeper understanding of the performance of the material.

In order to successfully design and optimize a composite material one has to be able to simulate and predict the properties of the composite before it is manufactured. This is essential if wood composites, and composites as a whole, shall be competitive in the future. For this reason there is a need for modelling of the mechanical properties of wood fibre composite materials. Mechanical properties here refer to the properties that decide the composites strain response to mechanical loading and changes in climate. The process of modelling the mechanical properties of the composite material regarded as a homogeneous material from the properties of the constituents is referred to as a homogenisation [15, 16].

1.3. Aim of Work

The many parameters that may affect the mechanical properties can be divided into fibre and paper properties, resin properties and process parameters. To map out the black box is a mouthful and it spans many disciplines; from chemistry, polymer science, process control, to solid and structural mechanics. The ideal scenario would be to model the entire chain from molecule, to polymer chain, to constituent property, to a homogenized material and all the way to the final product.

The aim of this work is to focus on one of those steps, which can be formulated with the following question:

Given a certain constitution of fibres and resin, and given the hygro-mechanical properties of those constituents, what hygro-mechanical properties of the composite material will this result in?

This seems, at start, like a more reasonable task. There are, however, some fundamental difficulties to this as well. One problem with predicting the mechanical properties of the composite is providing the indata. For example, the only data available for melamine formaldehyde is the Young's modulus of 8-9 GPa [17], with no information of the chemical process parameters. The sheer number of material parameters to describe the elastic stiffness of a wood fibre is extensive: 9 parameters are needed even if the fibre material is assumed to be a homogeneous linear elastic orthotropic material. Estimations of fibre stiffness are often made through testing on composites followed by a back calculation to find fibre stiffness [18], the accurate of which depends on the accuracy of the micro-mechanical model being employed. Estimations are also made by testing of single fibres [19] and by micro-mechanical modelling of single fibres from material data of the fibres constituents, cellulose, hemicellulose and lignin [20].

For a full description of the hygro-mechanical strain performance of a composite material by the analytical model presented in paper III is 48 parameters needed. The lack of indata is a problem leading to difficulties in validation of mechanical models. In order to validate if a model accurately describes a material one need both reliable indata as well as a large amount of outdata from measurements.

1.4. Research Approach and Structure of Thesis

The problem with validation of the model is central for the method of the presented work. The method, or strategy, can be summarized as follows: The outline of the work presented here is to model the mechanical properties of the composite material by means of an analytical model for stiffness, hygroexpansion, creep and mechanosorption from the known corresponding properties of the constituents. Two models are presented, one for stiffness and hygroexpansion and a second for the stiffness, hygroexpansion and time dependent properties. The first is a two step homogenisation of first a fibre with a coating of matrix material and then an integration of all fibre directions, using an interpolation between the two assumptions of homogeneous strain and homogeneous stress. The latter is solely based on the assumption of homogeneous strain and this assumption is validated and supported by comparison with the results from two numerical homogenisations using the same indata as the analytical model. Finally the results are compared to measurements from a HPL material in order to see if the phenomenons really are present in the model.

1.5. Limitations

In order to optimise and to employ composites to the fullest of its potential, there is a need for understanding and modelling the entire chain from the properties of the molecules up to the properties of the composite material product. The work in this thesis is limited to deal with the step from predicting the properties of the composite material from the properties of the constituents. Further limitations of this work are:

- Small strains – the strains in all models are assumed to be small, i.e. no geometrical effects are taken into account in the modelling.
- Service stresses – the stresses in all models are assumed to be significantly under the ultimate stress of the composite material and its constituents.
- Homogeneous continuous constituents – both constituents of the composite are modelled as homogeneous and continuous materials.
- Adhesion between phases – the adhesions between the fibre and the matrix phase and in the fibre connections are assumed to be perfect.
- No dynamic effects – the composite is assumed not to have any inertia at loading.
- Only HPL – applied modelling and testing are only done on HPL materials.
- No coupling stress-moisture – the moisture induced swelling is modelled to cause a free hygroexpansion in the constituents, but the stresses and strains in the material are assumed not to affect the moisture in any way.

- No temperature dependency – there is no modelling of how the temperature affects the composite properties. The temperature is throughout this work assumed to be constant at 23°C.

- Mechanosorption as material property – mechanosorption is modelled as a material property in the fibre and not as a structural phenomenon occurring e.g. in fibre bonds. No mechanosorption is assumed to occur in the matrix materials.

1.6. Original Features

This thesis contains some original features that have not been found in literature:

- A gradual interpolation between the homogeneous strain and the homogeneous stress assumptions for the cases of 2D and 3D analysis. The interpolation is presented in paper I and in appendix A.

- Creep properties of HPL are tested under short and long-term loading. The results from the testing are presented in paper V.

- Long-term material testing employing measurement of the entire in-plane strain field using optical metrology. The results from the testing are presented in paper V and the measurement technique is presented in appendix B.

- An analytical 3D-homogenisation of the long time behaviour of fibre network composite materials. The model presented in paper III comprises, first, a homogenisation of the different fibre direction of the fibre phase, and second, a homogenisation between the fibre network and the matrix material.

- Mechanosorption is modelled in a composite homogenisation in paper III.

- The mechanosorption phenomenon is observed in a test on HPL materials. The results from the test are presented in paper V.

1.7. Summary of Publications

This thesis consists of this introduction and overview, five appended papers and two appendices. Here follows a summary of the papers and the appendix and their part of the strategy.

Paper I

An analytical model for stiffness and hygroexpansion is developed. The model is divided into two steps; first a particle composite model that takes into consideration a single fibre in an environment of matrix material, and then integration over all fibre directions. The results from the model are compared to measurements of a composite material. The model is estimated to be

best suited to particle composite materials since there is no contact between fibres. All fibres are modelled with a coating of matrix material.

Paper II

The results from the analytical model are compared to the results from a numerical finite element model. The finite element model is a 3D homogenisation of a representative volume element with three different configurations of five fibres each. The material is modelled with phenolic resin as matrix material with a fibre volume fraction of 45%, which is the maximum amount of fibres that can be fitted in the RVE. The results from the FE model are compared with results from the analytical model presented in paper I. In this introduction, in section 3.2, are the stiffness results compared also with the stiffness results from the analytical model presented in paper III. The comparison validates the accuracy of the assumptions made in analytical model.

Paper III

An analytical model for stiffness, hygroexpansion, creep and mechanosorption is developed. The model assumes a serial coupling of the elastic, hygroexpansion, creep and mechanosorption strains, respectively, for the constituent materials, and then a state of homogeneous strain, i.e. parallel coupling, between the phases in the composite material. The model is presented with example simulations of a composite exposed to constant load and varying climate.

Paper IV

The validity of the homogeneous strain assumption is investigated. A numerical model is developed in order to validate the homogeneous strain assumption by comparing it to results from a finite element simulation. The homogenisation is made for stiffness and hygroexpansion strain and the conclusion is that the homogeneous strain assumption leads to an overestimation of the stiffness by approximately 15 % and to an underestimation of hygroexpansion strain by approximately 15 %.

Paper V

Results from measurements of two melamine/formaldehyde-fibre composite materials with different fibre volume fractions are presented. The paper comprises results from measurements of stiffness, hygroexpansion, long- and short-term creep, mechanosorption, moisture absorption and desorption. An empirical model is developed in order to describe the hygro-mechanical properties of the composite materials. Parameter values of the empirical model are evaluated from the above mentioned test results.

Appendix A

Appendix A presents mathematical considerations of composite homogenisation using parallel coupling, serial coupling and integration of fibre orientation. The foundations for coordinate transformations, composite stiffness, hygroexpansion and integration of different fibre orientations under the assumptions of homogeneous strain and homogeneous strain are derived. The interpolation between the assumptions of homogeneous strain and of homogeneous stress is introduced.

Appendix B

Appendix B presents the theory and the application of the optical strain measurement system employed in paper V. The measurement system is based on the principal of digital speckle photography, DSP, and uses image correlation in order to calculate the deformation field of the surface of the specimen. From derivation of the deformation field all in-plane components of the strain are evaluated.

2. Modelling of the Mechanical Properties of Wood Fibre Composites

Here the basis of the procedure for the present modelling of the hygro-mechanical properties will be presented. A number of assumptions need to be made: that no chemical interaction between the different phases occurs, that the phases are homogeneous and distinctly separated, and that there is statistical homogeneity allowing one to define a volume element which is representative of the structure as a whole. In order to calculate the stiffness, hygroexpansion, creep and mechanosorptive properties of a composite made up of two materials, one needs information on the corresponding material properties of the constituents.

Formulated as strain increments, the total strain increment of a constituent is expressed as a serial coupling of all strains increments from the stiffness, hygroexpansion, creep and mechanosorption strains, respectively, according to

$$d\varepsilon = d\varepsilon_e + d\varepsilon_h + d\varepsilon_{cr} + d\varepsilon_{ms} \tag{1}$$

where $d\varepsilon$ is the total strain increment of the constituent, $d\varepsilon_e$, $d\varepsilon_h$, $d\varepsilon_{cr}$ and $d\varepsilon_{ms}$, is the elastic, the hygroexpansion, the creep, and the mechanosorptive strain increment, respectively.

2.1. Modelling of Stiffness

Modelling of stiffness of composites has by natural causes been of greatest interest due to the importance of stiffness and probably also due to the fact that it is comparatively simple to make estimations of stiffness. The most important and general models are the Voigt approximation from 1889 and the Reuss approximation from 1929 [21], based on the assumption of homogeneous strain and of homogeneous stress, respectively. The former of those will be extensively used in this work, but also the Reuss approximation and a gradual scale of intermediate models will be studied. The stiffness matrix can, according to the Voigt and the Reuss approximations, be expressed as

$$\mathbf{D}_c = \left[\sum_i V_i \mathbf{D}_i^{\alpha} \right]^{\frac{1}{\alpha}} \tag{2}$$

where $\mathbf{D}_i$ is the stiffness matrix of the i:th phase and V_i is the corresponding volume fraction and where $\alpha = 1$ leads to the Voigt approximation and $\alpha = -1$ leads to the Reuss approximation. The stiffness matrix is defined as the relationship between the incremental stress and the strain vector according to

$$d\boldsymbol{\sigma} = \mathbf{D}_i d\boldsymbol{\varepsilon} \tag{3}$$

The case of $\alpha = 1$ is equivalent to the assumption of a state of uniform stress in all phases [22]. The Voigt approximation overestimates the composites stiffness, since it gives an extra constrain to all phases. Hill, who showed that these two approximations are in fact boundaries for all components of the stiffness matrix regardless of the geometry of the constituents in crystalline

aggregates [23], formulated a number of fundamental theoretical principles [24]. One approach that is proposed in paper I, and further explained in Appendix A, is to make an interpolation between the Reuss and the Voigt bounds by allowing arbitrary α, $-1 \leq \alpha \leq 1$, in Equation 2.

The development of mathematical and, to various degrees, empirical models increased in the early 1960s when the technical importance of composites came clear. Models for unidirectional fibre composites were created, such as the Halpin-Tsai equations [25] which are probably the most frequently employed. A number of methods for calculating transverse stiffness of composites containing fibres of differing geometries, such as the method of Hashin-Shtrikman bounds, were derived [26, 27].

Models for particle composites are usually derived by considering a single particle in an effective medium of some sort. Models of this type include the Eshelby equivalent inclusion method [28] for elliptical particles, the Mori-Tanaka theory [29], the self consistent scheme and the generalized self consistent scheme [30, 31]. All existing models for particle composites assume the particles to be isotropic. A directional average for the particle phases can also be obtained, however without any great difficulty.

In this work two different strategies are used when modelling the stiffness. The first model, presented in the paper I, uses a two-step homogenisation process. First a homogenisation of a single fibre surrounded by a coating of matrix material, and then a homogenisation over all possible direction under the assumption of homogeneous strain. This model is best suited for particle composites, or short fibre composites where there is no direct interaction between different fibres and the load between fibres have to be transferred through the matrix material.

In order to integrate the stiffness over an orientation distribution of fibre directions, the following expression is employed

$$\mathbf{D}_{fn} = \int_0^{\pi} \mathbf{D}_f \, f(\varphi) d\varphi \tag{4}$$

where $\mathbf{D}_{fn}$ is the stiffness matrix of the homogenised fibre network, $\mathbf{D}_f$ is the stiffness matrix of the single fibre and $f(\varphi)$ is the fibre orientation distribution function. Also here, the interpolation between homogeneous strain and homogeneous stress is possible. The second model, presented in paper III, assumes all phases in the composite to be in uniform state of strain. This is probably more accurate than assuming no fibre to fibre interaction. This is also a simplification from the previous strategy. It is, however, necessary in order to handle the complexity of the time dependent properties. The assumption is further motivated from the fact that fibre stiffness in the transverse direction is close the stiffness of the matrix material of HPL materials.

2.2. Modelling of Hygroexpansion

Hygroexpansion strain occurs from a change in the materials moisture content according to

$$d\boldsymbol{\varepsilon} = \boldsymbol{\beta} dw \tag{5}$$

where $\boldsymbol{\beta}$ is the vector containing the hygroexpansion coefficients and dw is a change in the materials moisture content. The change in moisture content comes usually from a change in relative humidity in the surrounding environment. In order to model the hygroscopic behaviour of the composite there is also needed information of the moisture uptake. This information is provided by the moisture sorption isotherms and the moisture equilibrium curves. The materials moisture content $w(t)$ can be expressed as

$$w(t) = g(RH(t)) \tag{6}$$

where $RH(t)$ is the relative humidity in the surrounding climate at a given moment. $g(RH(t))$ gives information about the time it takes for the material to reach moisture equilibrium and if the material is under sorption or desorption.

The problem of hygroexpansion is often compared to that of thermal expansion since from a mathematical point of view the problems are similar. There is however an important difference. In thermal expansion the temperature in the environment will cause a temperature in both phases that are equal to each other and to the surrounding temperature. In hygroexpansion the surrounding relative humidity will cause moisture contents w_1 and w_2 in phase *1* and *2* that are not necessarily the same since both phases generally have different moisture sorption isotherms and moisture equilibrium curves. Information about the phase's moisture uptake is not known in HPL and the two possibilities investigated here are

- the moisture content is equal in both phases, and
- the entire change in moisture content is taking place in the fibre phase.

These are of course not accurate assumptions and information about the sorption isotherms and moisture equilibrium curves of the two phases should be determined separately.

An equation for the effective hygroexpansion coefficients of a general 2-phase material or for the thermal expansion coefficients was derived by Levin [32]. The equation was extended by Rosen and Hashin [33] to generally anisotropic 2-phase composites and to an arbitrary phase geometry.

Hygroexpansion can also be modelled similarly to stiffness, according to assumptions of homogeneous strain or homogeneous stress. In the case of homogeneous strain the composite hygroexpansion will be

$$d\boldsymbol{\varepsilon}_h = \mathbf{D}_i^{-1} \sum_i V_i \mathbf{D}_i d\boldsymbol{\varepsilon}_{hi} \tag{7}$$

where $d\boldsymbol{\varepsilon}_h$ is the hygroexpansion strain increment of the composite and $d\boldsymbol{\varepsilon}_{hi}$ is the hygroexpansion strain increment for the i:th phase. This gives the hygroexpansion coefficients for the composite according to

$$\boldsymbol{\beta}_c = \mathbf{D}_i^{-1} \sum_i V_i \mathbf{D}_i \boldsymbol{\beta}_i \tag{8}$$

where $\boldsymbol{\beta}_i$ are the hygroexpansion coefficients for the *i*:th phase of the composite. In the case of a fibre orientations distribution and assumption of homogeneous strain the hygroexpansion strain increment of the fibre network, $d\boldsymbol{\varepsilon}_{hfn}$, will be

$$d\boldsymbol{\varepsilon}_{hfn} = \mathbf{D}_{fn}^{-1} \int_0^{\pi} \mathbf{D}_f \, d\boldsymbol{\varepsilon}_{hf} \, f(\varphi) d\varphi \tag{9}$$

where $d\boldsymbol{\varepsilon}_{hf}$ is the hygroexpansion strain increment in a single fibre, expressed in the global coordinate system. Thus, the hygroexpansion coefficients of the fibre network $\boldsymbol{\beta}_{fn}$ can be expressed as

$$\boldsymbol{\beta}_{fn} = \mathbf{D}_{fn}^{-1} \int_0^{\pi} \mathbf{D}_f \boldsymbol{\beta}_f \, f(\varphi) d\varphi \tag{10}$$

However, in the case of hygroexpansion the assumptions of homogeneous stress and homogeneous strain will not be bounds for the composites free hygroexpansion. Examples of when homogeneous strain assumption will overestimate the hygroexpansion is shown in Figure 8 in paper IV.

2.3. Time-dependent Material Modelling

2.3.1. Creep

Micro-mechanical modelling of time-dependent properties of composite materials has not rendered in as much interest as modelling of stiffness. General surveys of models of time-dependent properties of composite materials are provided by Aboudi [21]. Theoretical analysis of the linear viscoelastic behaviour of unidirectional transversal composite materials have been presented by Kaliske [34], Luciano [35], Barbero [36] and Klasztorny [37].

In wood and wood-based material creep is generally moisture dependent. An increase in moisture content tends to increase the creep of the material. Comprehensive investigations and modelling of the load- and moisture-induced straining of solid wood have been reported in doctoral dissertations of Mårtensson [38], Hanhijärvi [39] and Ormarsson [40].

The most common way of modelling creep is by means of serial and parallel coupling of spring and dash-pot elements [41, 42, 43]. The most basic element is called a Kelvin element, which consists of a parallel coupled spring and dashpot.

As an example, a material's one dimensional stiffness and creep properties are modelled with a spring to model the stiffness serial coupled with a Kelvin element to model the creep behaviour. The elastic spring stiffness of the material is *E* according to

$$d\sigma = E\, d\varepsilon_e \tag{11}$$

The creep behaviour is modelled with a creep spring with stiffness E_{cr}, which is associated with the elastic spring stiffness E according to

$$E_{cr} = \frac{1}{\mu} E \tag{12}$$

where μ is a dimensionless constant, and with a creep dashpot, which will act as a fluid where the strain time increment is proportional to the stress over the dashpot, according to

$$\dot{\varepsilon}_{cr} = C_{cr}\sigma \tag{13}$$

where C_{cr} is the creep compliance of the dashpot. The creep compliance is associated with the elastic spring stiffness E with the creep time constant τ according to

$$C_{cr} = \frac{1}{\tau} E^{-1} \tag{14}$$

The stress-strain relationship for a Kelvin element thus becomes

$$\sigma = C_{cr}{}^{-1}\dot{\varepsilon}_{cr} + E_{cr}\varepsilon_{cr} \tag{15}$$

Combining these two elements according to Figure 2 and applying a constant stress at time $t = 0$ on the material, according to $\sigma(t) = \sigma_0$, will result in a strain as a function of time. This is achieved through integration of the strain increment over time t according to

$$\varepsilon(t) = \int_0^t e^{\frac{t'-t}{\mu\tau}} \frac{\sigma(t)}{\tau E} dt' = \frac{\sigma_0}{E}\mu\left(1 - e^{-\frac{t}{\mu\tau}}\right) \tag{16}$$

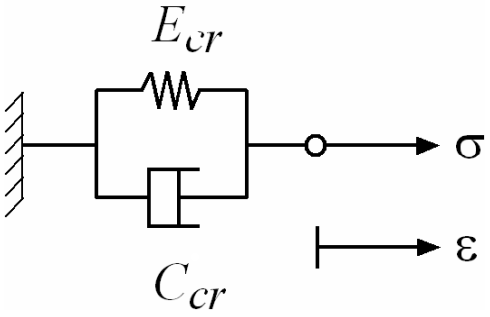

Figure 2*. Kelvin element consisting of a spring and a dash-pot.*

This use of Kelvin elements is employed in paper III for description of the properties of the phases and in paper V in modelling the composite material. In both cases the material parameters λ and τ are assumed to be functions of moisture content.

The Kelvin element can be serial coupled to more Kelvin elements with other time constants τ_i in order to model the creep behaviour over a broader time range. This is the case when modelling the creep behaviour of the HPL material in paper V. In this case the creep strain will be

$$\varepsilon(t) = \frac{\sigma_0}{E}\sum_i \mu_i \left(1 - e^{-\frac{t}{\mu_i \tau_i}}\right) \tag{17}$$

2.3.2. Mechanosorption

When a wood or wood-based material specimen is kept under constant loading and the moisture content is changed creep tends to accelerate, which is referred to as mechanosorption. The phenomenon has been investigated and modelled for solid wood [38], paper [44-46], and also been observed in concrete, wool and synthetic fibres. There is no consensual mechanism found to explain the phenomenon. This work will assume mechanosorption to be a material parameter of the wood fibre in the same way as stiffness, hygroexpansion and creep. Mårtensson [38] proposes a model on tensor form for mechanosorptive strain, here presented on matrix form:

$$\dot{\boldsymbol{\varepsilon}}_{ms} = \mathbf{m}\boldsymbol{\sigma}\,|\,\dot{w}\,| \tag{18}$$

where **m** is the mechanosorption matrix which act as a creep compliance that is proportional to the absolute of the time derivative of the materials moisture content. In the model introduced in paper III mechanosorptive creep is, as in the case of creep, parallel coupled to a stiffness spring making it possible to limit the total mechanosorptive strain according to Figure 4. The equation presented in its uniaxial formulation is

$$\sigma = \left(A_{ms}\,|\,\dot{w}\,|\right)^{-1}\dot{\varepsilon}_{ms} + E_{ms}\varepsilon_{ms} \tag{19}$$

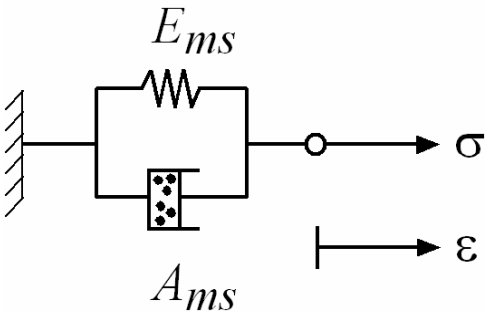

Figure 4*. Kelvin element for mechanosorption consisting of a spring and a moisture dash-pot.*

where, similar to the creep Kelvin element, A_{ms} and E_{ms} are related to the elastic spring stiffness E according to

$$A_{ms} = \frac{1}{\alpha} E^{-1} \tag{20}$$

and

$$E_{ms} = \frac{1}{\lambda} E \tag{21}$$

where the mechanosorptive time constant α and the dimensionless constant λ are introduced, which are assumed to be constant and not dependent on the moisture content. The mechanosorptive strain can be expressed as

$$\varepsilon(t) = \int_0^t e^{G(t')-G(t)} \left|\frac{dw}{dt'}\right| \frac{1}{\alpha E} \sigma(t') dt' \tag{22}$$

which for a large number of moisture cycles have the following approximate solution

$$\varepsilon(t) = \int_0^t e^{\frac{t'-t}{\alpha\lambda}|\dot{w}|} \left|\frac{dw}{dt'}\right| \frac{1}{\alpha E} \sigma(t') dt' \tag{23}$$

3. Numerical Verification of Model

Any model developed, and the assumptions it relies on, in order to predict the behaviour of a composite needs to be verified. In this case the most important of the assumptions made is the one of homogeneous strain. It is difficult to verify this assumption experimentally due to the lack of reliable data of the constituent's material properties. In this thesis are investigations of the homogeneous strain assumption made by means of two kinds of finite element homogenisation, presented in paper II and in paper IV. The verifications are made by comparing the results of the finite element homogenisations with the results of the analytical models.

3.1. Verification by means of 2D finite element model

One of the homogenisations, presented in paper IV, is made on a representative volume element, i.e. on a representative area element since the model is two dimensional plane stress, of the micro-structure of the composite containing a number of fibres. The results from the homogenisation are based on simulations on 100 different unit cells. The homogeneous strain assumption is found to overestimate the composites stiffness by approximately 15 % and underestimate the composites hygroexpansion by approximately 15 % for a fibre volume fraction typical for HPL, 60 %. This is considered not to be greater than it can be justified to use the assumptions in analytical modelling of HPL materials. There is also a possibility to introduce a correction factor of 1.15 to an analytical model to take the deviation into account.

3.2. Verification by means of 3D finite element model

A 3D finite element model of a representative volume element of a micro-structure with five fibres surrounded with matrix material was developed. Three different fibre configurations with five fibres were analysed and homogenised with respect to stiffness. Material data represent a phenolic resin matrix material and a fibre volume fraction of 45 %. The Young's modulus of the resin was set to 5.75 GPa. Comparison between the analytical model, with a random fibre orientation distribution, and the mean values of the results from the three fibre configurations and means of *x*- and *y*-directions are presented in Table 1.

Table 1. Young's modulus for HPL with phenolic resin and random fibre orientation distribution.

	FE-model	Analytical model presented in paper III	Analytical with correction factor 1.15
E (GPa)	9.2	11.4	9.9

3.3. Comparison between Analytical Models

The two analytical models, the two step model presented in paper I and and the homogeneous strain model presented in paper III, are compared. The comparison is made with phenolic resin as matrix phase, with a fibre volume fraction of 75 % and a fibre orientation distribution with 1.8 times higher fibre density orientation in the machine direction (MD) than in the cross direction (CD). The results are presented in Table 2.

Table 2. *Young's modulus in GPa, comparison between analytical models.*

	Analytical model from Paper I	Analytical model from Paper III	Analytical model from Paper III with correction factor 1.15
E_{MD} (GPa)	14.4	16.9	14.7
E_{CD} (GPa)	10.6	13.3	11.6

The results from Table 2 show a good correspondence between the analytical model presented in paper I and the model from paper III with the correction factor of 15 %.

4. Comparison between Model and Experimental Tests

4.1. Stiffness

The results from the stiffness measurements presented in paper V are compared to modelled stiffness by means of the analytical model presented in paper III. The comparison is made for two fibre volume fractions, V_f = 53 % and V_f = 58 %, denoted O53 and O58, respectively. The results are presented in Table 3.

Table 3. Young's modulus measured and modelled in the papers machine direction.

		Measured	Analytical model from Paper III	Analytical model from Paper III with correction factor 1.15
O53	E_{MD} (GPa)	11.4	14.5	12.6
O58	E_{MD} (GPa)	13.8	15.2	13.2

The modelled stiffnesses with a correction factor of 1.15 lies in the same range as the measured stiffnesses. The large measured differance between the two fibre volume fractions (2.4 GPa) is not captured by the model (0.6 GPa).

4.2. Hygroexpansion

The measured hygroexpansion coefficients of the two composite materials made in paper V are compared to modelled hygroexpansion coefficients. The results from the measurement show some unexpected results, which can be seen in Table 4.

Table 4. Composite hygroexpansion coefficients measured and modelled.

Material	Direction	Measured	Analytical model from paper III	Analytical model from Paper III with correction factor 1.15	Analytical model, all moisture in fibres, and corr.factor.	Analytical model, equal moisture, $\beta_m = 0.4$
O53	β_{MD} (-)	0.158	0.022	0.025	0.039	0.155
	β_{CD} (-)	0.225	0.034	0.039	0.061	0.205
O58	β_{MD} (-)	0.112	0.023	0.026	0.038	0.140
	β_{CD} (-)	0.223	0.036	0.041	0.061	0.188

The difference between measured and modelled values is conspicuous. The measured values of hygroexpansion are 5 to 7 times greater than the modelled. One explanation could be that all moisture is stored in the fibres. This assumption, together with the correction factor associated with the homogeneous strain assumption, leads to 4 times higher values of modelled hygroexpansion.

The analytical model assumes same moisture content in both phases, and estimates a hygroexpansion coefficient in the matrix material to $\beta_m = 0.01$. A value of β_m necessary to explain the large hygroexpansion coefficient values in measured values of the composite is $\beta_m = 0.4$. This could also explain why β_{MD} is larger for material with less fibres volume fraction, O53, than for the material O58. A more accurate evaluation of the hygroexpansion of the HPL requires further information about the moisture uptake and the hygroexpansion coefficient of the individual phases.

4.3. Creep and Mechanosorption

Data on creep and mechanosorption for a single wood fibre as well as for melamine resin is scarce. Mechanosorption phenomenon occurring in melamine has not been found reported in literature. Since sufficient data of the constituent's mechanical properties is lacking, the analytical model cannot be validated by means of comparisons with experimental data. In the following are example calculations based on assumed material data presented and compared to the results of the measurements presented in paper V.

The analytical model calculations and the measurements relate to a constant tensile stress of 33 MPa, at a constant temperature of 23 °C and at a cyclically varying RH between 30 % and 70 %, starting at 30 %.

The indata employed in the example calculations are presented in Table 5 and in Table 6. Elastic data of wood fibres are from Persson [20], initial values of creep data are from creep results of solid wood [39], Young's modulus of melamine resin is from Hagstrand [17] and initial values of melamin resin creep data are from Niemz [47].

Table 5. *Material data for orthotropic wood fibre, x corresponding to the fibres longitudinal direction. * E_x = 50 000 MPa for material O58.*

E_x	$E_y = E_z$	$\nu_{xy} = \nu_{xz}$	ν_{yz}	$G_{xy} = G_{xz}$	G_{yz}
(MPa)	(MPa)	(-)	(-)	(MPa)	(MPa)
40 000*	5 000	0.2	0.3	4 000	2 000
β_x	$\beta_y = \beta_z$	τ	μ	α	λ
$(1/10^4)$	$(1/10^4)$	(h)	(-)	(-)	(-)
1	26	300	0.5	5	0.6

Table 6. *Material data for the isotropic matrix material, melamine formaldehyde.*

E_m	ν_m	β_m	τ_m	μ_m
(MPa)	(-)	$(1/10^4)$	(h)	(-)
9	0.3	40	300	0.5

Young's modulus in the fibres longitudinal direction was for material O58 changed to E_x = 50 000 MPa in order to compensate for the large measured difference in stiffness between the materials O53 and O58. The matrix materials hygroexpansion coefficient is assumed to be $\beta_m = 40 \cdot 10^{-4}$ in correspondence with results and the discussion presented in Table 4.

First simulations from the analytical model are compared to results from the empirical model developed and calibrated in paper V. The results are shown in Figure 3 and Figure 4 for the two materials.

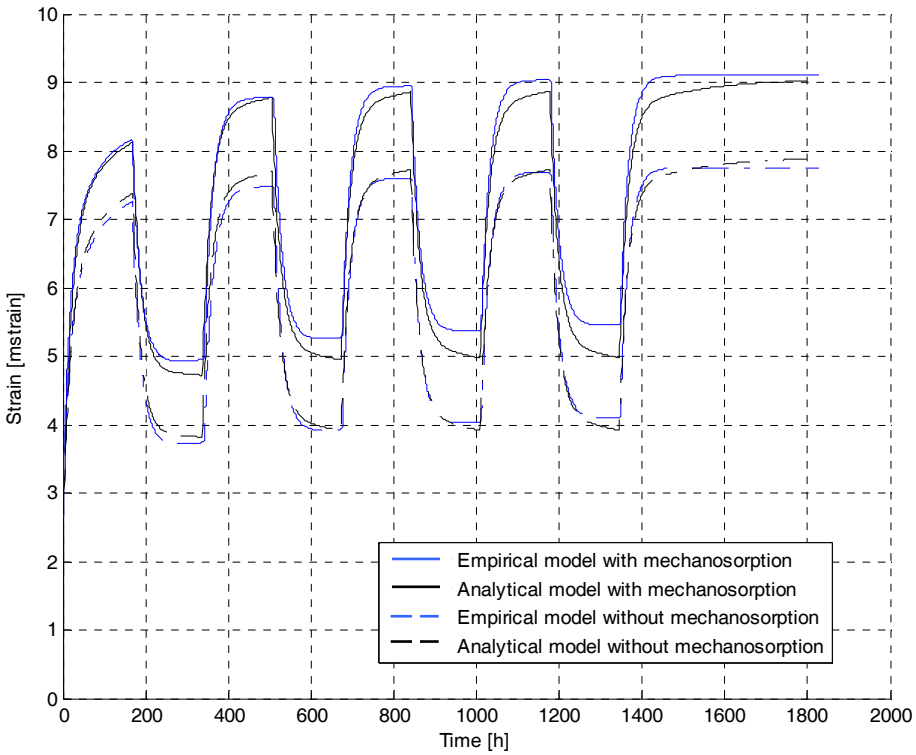

Figure 3. *Empirical and analytical model with and without mechanosorption for material O53.*

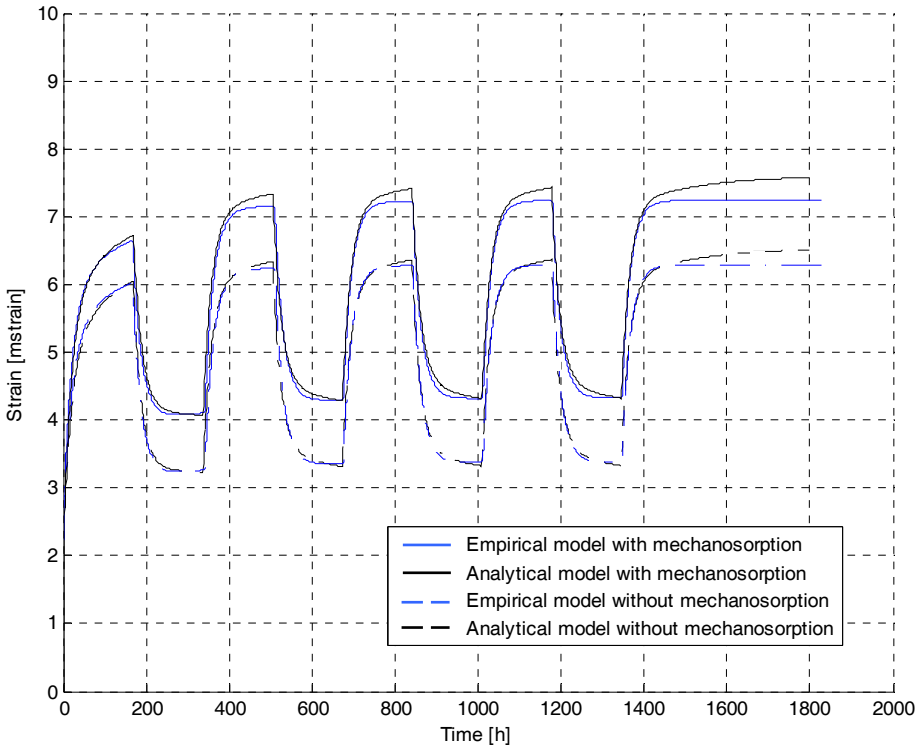

Figure 4. *Empirical and analytical model with and without mechanosorption for material O58.*

The diagrams clearly show that the analytical model is capable of reproducing the results from the measurements, with and without the presence of mechanosorption.

The analytical model is further compared with measurement results from paper V, in both loading and transverse direction, MD and CD, respectively. The comparisons, presented in Figure 5 and Figure 6, show a good agreement except for the hygroexpansion in the x-directions of the materials, which is not fully captured by the model.

It should be noted that the indata to the analytical model are not optimised by an algorithm, but adjusted by hand to get a good agreement in order to illustrate that the model is capable of capturing the measured behaviour of the composite material.

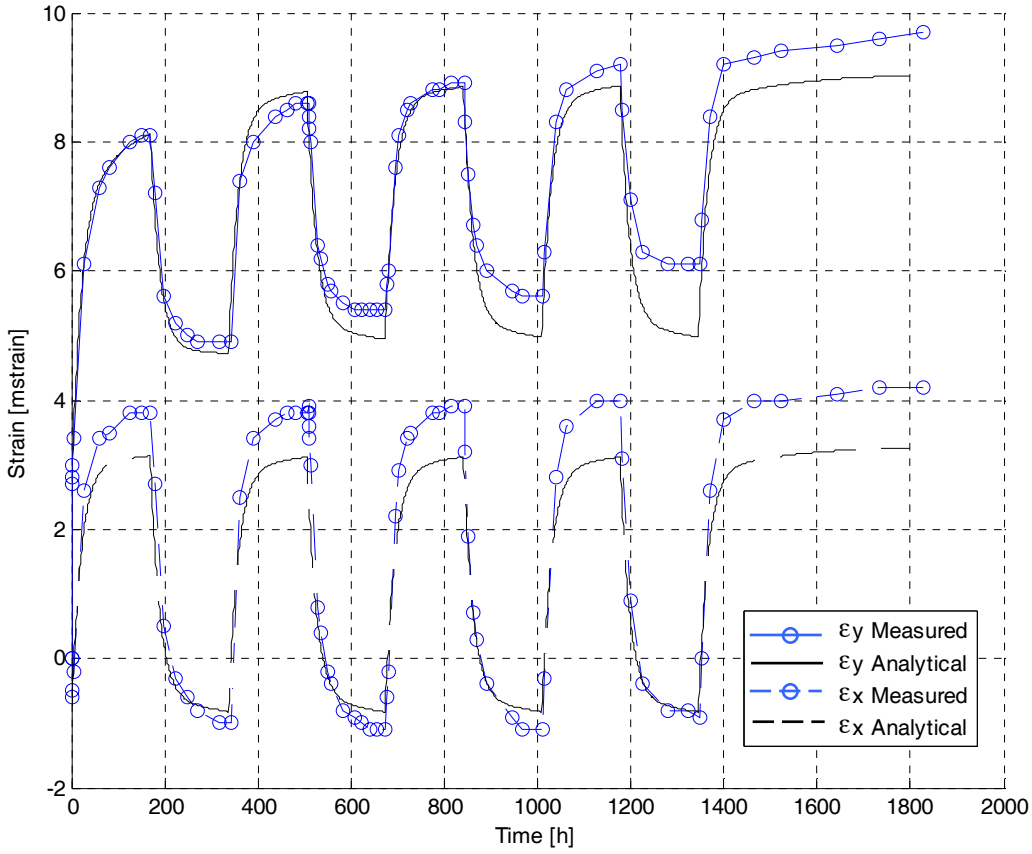

Figure 5. *Measured strain in y- and x-direction and corresponding results from analytical model for material O53.*

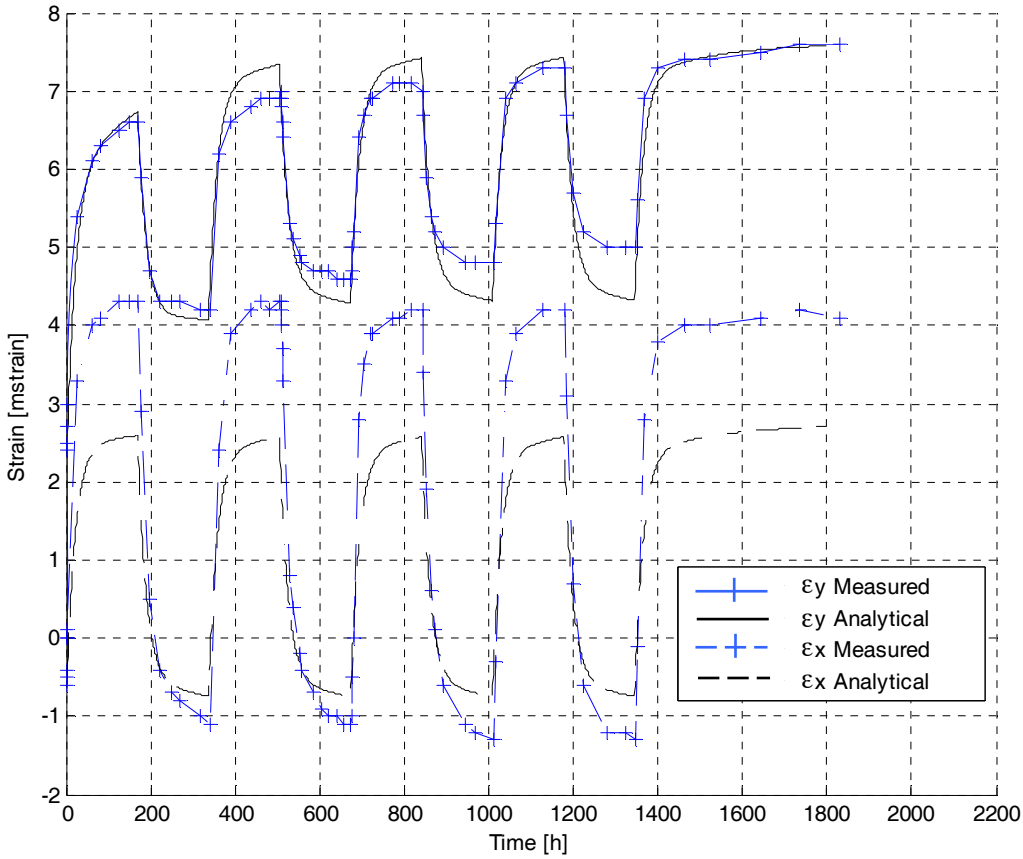

Figure 6. *Measured strain in y- and x-direction and corresponding results from analytical model for material O58.*

5. Concluding Remarks

5.1. Conclusions

The foundation of this work lies in the analytical model of the composite material presented in paper III. The model predicts the time-dependent hygro-mechanical behaviour of the composite and comprises stiffness, hygroexpansion, creep and mechanosorption. The assumption of homogeneous strain made in the analytical model is investigated and supported by the stiffness results from the analytical model in paper I, the 3D finite element model in paper II and the 2D finite element model in paper IV. In all cases the analytical model, corrected with the factor 1.15, show a good agreement with results from numerical models, the other analytical model and results from measurements.

Results from measurements presented in paper V show that mechanosorption is occurring in the composite material. Results from the hygroexpansion measurements are conspicuously high compared to predicted results from analytical models. Besides, the measurements show that an increase in fibre volume fraction leads to a decrease in hygroexpansion in the machine direction. The measurements have been repeated with the same material, but new specimens. These results need to be recreated by further new measurements to verify that the hygroexpansion coefficient of the melamine formaldehyde is extremely high, or that a new phenomenon is occurring that cannot be explained by the presented models.

The model presented in this thesis can be used as a tool for predicting the time dependent hygro-mechanical properties of HPL laminates.

5.2. Future work

The work presented is to be seen as an introductory step towards full modelling of the time dependent hygro-mechanical behaviour of wood composites in general and HPL in particular. Much work needs to be done in order to further verify the type of models presented in this thesis. Both theoretical, numerical validations, as carried out in paper IV, and validations by measurement, as carried out in paper V. The model also needs to be compared with finite element models with time dependent constitutive models in order to verify that also those parts are modelled accurately. Also needed, of course, is more reliable indata in order to use the model to make predictions about future composites mechanical behaviour. Further more, other factors needed to be investigated and modelled are process parameters of the manufacturing of composite materials.

Mechanical properties of pure melamine resin are hard to obtain due to its brittleness. A way to achieve indata about the moisture behaviour, moisture sorption isotherms and moisture equilibrium curves, and hygroexpansion is through conditioning, weighing and measuring the strain by means of the DSP system, as described in paper V. This would spread some more light over the discussion in section 2.2 and the questions regarding the hygroexpansion measurements raised in section 4.2.

Indata can also be acquired by means of the analytical modelling. In order to use the model for back-calculations of e.g. creep and mechanosorption data for the constituents that are hard to obtain, e.g. experimentally on single fibres, some sort of optimisation strategy or algorithm is needed. The algorithm should for a given set of measurement data calculate the optimal indata for the analytical model, such that the analytical model corresponds to the measured results. An example of this is shown in section 4.3. For this, of course, a large amount of measurement data is needed from tests on composite materials with variations in all mechanical, geometrical and physical properties mentioned in section 1.2.

References

1. **Oksman, K.** *Improved Properties of Thermoplastic Wood Flour Composites.* Doctoral Thesis, Luleå University of Technology, Sweden, 1997.

2. **Nilsson, L.-O., Hjort, S., Pettersson, H., Gustafsson, P. J., Molin, N.-E., Sjödahl, M., Ståhle, P., Gunnars, J., Ericsson, M., Oksman, K., Vilander, Y., Lindberg, H.** *Wood Composites Based on Recycled Plastics – Mechanical Properties.* Structural Mechanics, Lund Institute of Technology, Sweden., 1997.

3. **Dinwoodie, J. M.** *Wood – Nature's Cellular, Polymeric Fibre-composite.* The Institute of Metals, London, UK., 1989.

4. **Siau, J. F.** *Wood: Influence of Moisture on Physical Properties.* Dept of Wood Science and Forest Products, Virginia, Polytechnic Institute and State University, USA, 1995.

5. **Fellers, C., Norman, B.** *Pappersteknik.* Division of Paper Technology, Royal Institute of Technology, Sweden, 1996.

6. **Niskanen, K.** *Paper Physics.* Jyväskylä, Fapet, 1998.

7. **Marklund, E.** *Modelling the Mechanical Performance of Natural Fiber Composites.* Doctoral Thesis, Division of Polymer Engineering, Luleå University of Technology, Sweden, 2007.

8. **Brauns, J.** Hygromechanical Behaviour of Wooden Composites. 1997, Vol. 31(3).

9. **Ebrahimzadeh Pirshahid, R.** *Dynamic Mechanical Studies of Wood, Paper and som Polymers Subjected to Humidity Changes.* Doctoral Thesis, Department of Polymeric Materials, Chalmers University of Technology, Sweden, 1997.

10. **Salmén, N.L., Back, E.L.** Moisture-dependent softening of paper, evaluated by its elastic modulus. *Tappi.* 1980, Vol. 63 (6).

11. **Adl Zarrabi, B.** *Hygro-Elastic Deformation of High Pressure Laminates.* Doctoral Thesis, Division of Building Material, Chalmers University of Techology, Sweden, 1998.

12. **Voigt, B.** *New Melamine-Formaldehyde Composites.* Licentiate Dissertation, Department of Polymeric Materials, Chalmers University of Technology, Sweden, 2001.

13. Bakelite - Wikipedia. *Wikipedia.* [Online] http://en.wikipedia.org/wiki/Bakelite.

14. **Nordin, L.-O.** *Wood fiber composites : from processing and structure to mechanical performance.* Doctoral Thesis, Department of Applied Physics and Mechanical Engineering, Luleå University of Technology, Sweden, 2004.

15. **Persson, L.-E., Persson, L., Svanstedt, N., Wyller, J.** *The Homogenization Method – An Introduction.* Studentlitteratur, Lund, Sweden, 1993.

16. **Lukkassen, D., Persson, L.-E. and Wall, P.** *Some Engineering and Mathematical Aspects on the Homogenization Method for Computing Effective Moduli and Microstresses in Elastic Composite Materials.* Research Report 2, Dept of Mathematics, Luleå University of Technology, Sweden, 1994.

17. **Hagstrand, P.-O.** *Mechanical Analysis of Melamine-Formaldehyde Composites.* Doctoral Thesis, Department of Polymeric Materials, Chalmers University of Technology, Sweden, 1999.

18. **Neagu, R.C., Gamstedt, E. K., Berthold, F.** Stiffness contribution of various wood Fibers to composite materials. *Journal of Composite Materials.* 2006, Vol. 40(8).

19. **Page, D. H., El-Hosseiny, F., Winkler, K. and Lancaster, A. P. S.** *Elastic Modulus of Single Wood Pulp Fibres. Part V. Elastic Modulus.* 1977, Tappi, Vol. 60 (4), pp. 114-117.

20. **Persson, K.** *Micromechanical Modelling of Wood and Fibre Properties.* Doctoral Thesis, Division of Structural Mechanics, Lund Institute of Technology, Sweden, 2000.

21. **Aboudi, J.** *Mechanics of Composite Materials.* Elsevier, Amsterdam, The Netherlands, 1991.

22. **Stålne, K., Gustafsson, P. J.** Three-Dimensional Model for Analysis of Stiffness and Hygroexpansion properties of Fibre Composite Materials. *Journal of Engineering Mechanics, ASCE.* 2002, Vol. 128 (6).

23. **Hill, R.** Elastic Behaviour of a Crystalline Aggregate. *Proceedings of the physical Society.* 1952, Vol. Section A.

24. **Hill, R.** Elastic Properties of Reinforced Solids: Some Theoretical Principals. *Journal of the Mechanics and Physics of Solids.* 1963, Vol. 11.

25. **Halpin, J. C., Kardos, J. L.** The Halpin-Tsai Equations: A Review. *Polymer Engineering and Science.* 1976, Vol. 16.

26. **Hashin, Z., Shtrikman, S.** A Variational Approach to the Theory of the Elastic Behaviour of Multiphased Materials. *Journal of the Mechanics and Physics of Solids.* 1963, Vol. 11.

27. **Hashin, Z.** On Elastic Behaviour of Fibre Reinforced Materials of Arbitrary Transverse Phase Geometry. *Journal of the Mechanics and Physics of Solids.* 1965, Vol. 13.

28. **Eshelby, J. D.** The Determination of the Field of an Elliptical Inclusion and Related Problems. *Proccedings of the Royal Society.* 1958, Vol. A (241).

29. **Mori, T., Tanaka, K.** Average Stress in Matrix and Average Elastic Energy of Materials with Misfittning Inclusions. *Acta Metallurgica.* 1973, Vol. 21, pp. 571-574.

30. **Hashin, Z.** Analysis of Properties of Fibre Composites with Anisotropic Constituents. *Journal of Applied Mechanics.* 1983, Vol. 9, pp. 481-505.

31. **Hill, R.** A Self Consistent Mechanics of Composite Materials. *Journal of the Mechanics and Physics of Solids.* 1965, Vol. 13.

32. **Levin, V. M.** On the Coefficients of Thermal Expansion of Heterogeneous Materials. *Mechanics of Solids.* 2, 1967, pp. 58-61.

33. **Rosen, B. W., Hashin, Z.** Effective Thermal Expansion Coefficients and Specific Heats of Composite Materials. *International Journal of Engineering Science.* 1970, Vol. 8, pp. 157-173.

34. **Kaliske, M.** A Formulation of Elasticity and Viscoelasticity for Fibre Reinforced Materials at Small and Finite Strains. *Computational Methods in Applied Mechanical Engineering.* 2000, Vol. 185, pp. 225-243.

35. **Luciano, R., Barbero, E. J.** Analytical Expressions for the Relaxation Moduli of Linear Viscoelastic Composites with Periodic Microstructure. *Transactions of the ASCE.* 1995, pp. 786-793.

36. **Barbero, E. J., Luciano, R.** Micromechanical Formulas for the Relaxation Tensor of Linear Viscoelastic Composites with Transversely Isotropic Fibres. *International Journal of Solids and Structures.* 1995, Vol. 32(13), pp. 1859-1872.

37. **Klasztorny, M., Wilczynski, A. P.** Constitutive Equations of Viscoelasticity and Estimation of Viscoelastic Parameters of Unidirectional Fibrous Polymeric Composites. *Journal of Composite Materials.* 2000, Vol. 34 (9), pp. 1624-1639.

38. **Mårtensson, A.** *Mechanical Behaviour of Wood Exposed to Humidity Variations.* Doctoral Thesis, Department of Structural Engineering, Lund Institute of Technology, Sweden, 1992.

39. **Hahnijärvi, A.** *Modelling of Creep Deformation Mechanisms in Wood.* Doctoral Thesis, Technical Research Centre of Finland, Espoo, 1995.

40. **Ormarsson, S.** *Numerical Analysis of Moisture-Related Distortions in Sawn Timber.* Doctoral Thesis, Division of Structural Mechanics, Chalmers University of Technology, Sweden, 1999.

41. **Dahlblom, O.** *Constitutive Modelling and Finite Element Analysis of Concrete Structures with Regard to Environmental Influence.* Report TVSM-1004, Division of Structural Mechanics, Lund Institute of Technology, Sweden, 1987.

42. **Flügge, W.** *Viscoelasticity.* Springer, Berlin, Germany, 1975.

43. **Nielsen, L. E.** *Mechanical Properties of Polymers and Composites. Vol 1.* Marcel Dekker, inc New York USA, 1974.

44. **Fellers, C., Panek, J.** Effect on relative humidity cycling on mechanosorptive creep. *Moisture and creep effects on paper, board and containers: 5:t int. sym., Marysville, Victoria, Australia.* 2001.

45. **Alftan, J.** *Micro-Mechanically Based Modeling of Mechano-sorptive Creep in Paper.* Doctoral Thesis, Department of Solid Mechanics, Royal Institute of Technology, Sweden, 2004.

46. **Strömbro, J.** *Micro-Mechanical Mechanisms for Deformation in Polymers-Material Structures.* Doctoral Thesis, Department of Solid Mechanics, Royal Institute of Technology, Sweden, 2008.

47. **Niemz, P.** *Physik des Holzes und der Holzwerkstoffe.* Leinfelden-Echterdingen: DRW, 1993.

Appended Papers

Paper I

A 3D Model for Analysis of Stiffness and Hygroexpansion Properties of Fibre Composite Materials.

Kristian Stålne and Per Johan Gustafsson

Paper II

A 3D Finite Element Fibre Network Model for Composite Material Stiffness and Hygroexpansion Analysis

Kristian Stålne and Per Johan Gustafsson

Paper III

3D Homogenisation of Hygroscopic Anisotropic Fibre Network Composites

Kristian Stålne

Paper IV

Numerical Investigation of the Homogeneous Strain Assumption for Wood Fibre Composite Materials

Kristian Stålne and Per Johan Gustafsson

Paper V

Measurement of Hygro-Mechanical Properties of a High-Pressure Laminate Composite Material

Kristian Stålne and Per Johan Gustafsson

Appendix A

Analysis of Fibre Composite Models for Stiffness and Hygroexpansion

Kristian Stålne

Appendix B

Measurement of Strain using Digital Speckle Photography

Kristian Stålne

Paper I

I

A 3D Model for Analysis of Stiffness and Hygroexpansion Properties of Fibre Composite Materials

Kristian Stålne and Per Johan Gustafsson

Published in Journal of Engineering Mechanics, ASCE

Volume 128, Number 6, 2002, pp 654-662

A 3D Model for Analysis of Stiffness and Hygroexpansion Properties of Fibre Composite Materials

Kristian Stålne*, Per-Johan Gustafsson†

Keywords: wood, fibre, particle, composite, analytical, modelling, stiffness, hygroexpansion, homogenisation

Abstract

A three dimensional model for stiffness and hygroexpansion of fibre and particle composite materials is presented. The model is divided into two steps, first a homogenisation of a single fibre with a coating representing the matrix material, then a network mechanics modelling of the assembly of coated fibres that constitutes the composite material. The network modelling is made by a fibre orientation integration including a linear and an exponential interpolation between the extreme case of homogenous strain and the extreme case of homogenous stress. A comparison between the modelled prediction and measurement data are made for stiffness, Poissons ratio and hygroexpansion. The matrix material is assumed to have isotropic properties and the fibre or particle material may have arbitrary orthotropic properties.

*Grad. Student, Div. of Structural Mechanics, Lund University, P.O. Box 118, S-221 00 Lund, Sweden. E-mail: kristian.stalne@byggmek.lth.se

†Prof., Div. of Structural Mechanics, Lund University, P.O. Box 118, S-221 00 Lund, Sweden. E-mail: bmpjg@byggmek.lth.se

1 INTRODUCTION

The use of advanced wood fibre composite materials is increasing in building and automotive industry applications. In the building industry, the market for high pressure laminates, HPL, made up of layers of impregnated paper, has seen a strong development during the last decade. HPL is a water-resistant material, and its surface can be made very durable and be given almost any appearance of wood. A key issue for present and future usage of products made of wood fibre composites such as HPL is shape stability. Very often, moisture-induced deformations and shape instability are the limiting factors. In this study a new composite model for the analysis of hygroexpansion properties and stiffness is discussed. The aim is to develop a model by which the 3D stiffness and hygroexpansion can be predicted, making it possible to make a good and rational design of wood fibre and particle composite materials.

For analysis of the in-plane orthotropic stiffness of fibre materials such as paper, several network mechanics models have been proposed, both analytical and numerical [4], [10]. For stiffness analysis of composites made up of unidirectional fibres and a continuous matrix material, the model of Halpin and Tsai [8] is the most frequently used. Boundaries for stiffness have also been developed, e.g. the Reuss and the Voigt approximations [1] which are valid for a general composite and the Hashin-Shtrikman bounds [9] for the effective elastic moduli of unidirectional fibre composites. Theoretical analysis of the influence of fibre length and orientation distribution on stiffness have been made by Fu *et al.* [7], Sayers [14] and Dunn *et al.* [6], who have a large list of further references. It appears that modelling of hygroexpansion or the confinement stress at restricted expansion has been awarded much less interest.

The model discussed here focuses on analytical composite modelling of 3D stiffness and hygroexpansion properties, taking into account geometrical shape, anisotropic properties and arbitrary orientation distribution of the particles. The model is developed from rigorous elasticity calculations, and relates to long fibre materials such as HPL, to short fibre materials made up of short fragments of wood fibres and a polymer matrix material, and to composites made up of pieces of wood such as a particle board. It may also be applied to network materials such as paper without any matrix material. Dunn *et al.* state that no model exists that satisfies all the theoretical benchmarks that should be used to validate any model. The model discussed here possesses such qualities as symmetric resulting stiffness matrix, correct results in the high and low concentration limits, and coincidence with the exact solutions that exist for the extreme cases of laminate geometries and continuous-fibre systems with equal shear ridgities.

The constituents are assumed to be orthotropic and linear elastic and without any chemical interaction or absorption of matrix material into the fibre walls. Time and rate effects such as creep and mechanosorption are not considered. The orientation distribution of the fibres is defined by $\psi(\varphi, \theta)$, where $0 \leq \varphi \leq \pi$ denotes the in-plane angle with the global $x-$axis and $0 \leq \theta \leq \pi$ denotes the out-of-plane angle.

2 OUTLINE OF MODEL

The model is a two-step composite model with calculation of homogenized material properties at two levels of the material structure. First, a model for the properties of a single fibre or particle with a coating representing the matrix material is developed. Then a network mechanics model is developed for the composite material made up of the fibres with a coating. The homogenized material representing a single fibre or particle with a coating is, in the following, called the *cf*-material, *cf* indicating coated fibre.

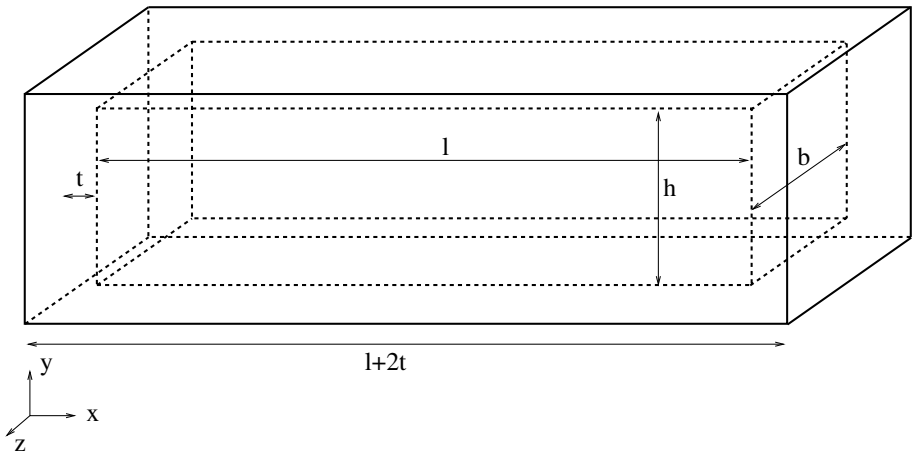

Figure 1: *Fibre, $l \times b \times h$, coated with a matrix material layer with thickness t.*

The fibre is assumed to have the shape of a right angle block and the coating is assumed to be of equal thickness, t, at all surfaces of the fibre, Figure 1. Knowing the shape and volume of the fibre, $V_f = lbh$, and of the matrix material, $V_m = (l + 2t)(b + 2t)(h + 2t) - lbh$, the thickness t can be calculated from the fibre to matrix volume ratio,

$$\frac{V_f}{V_m} = \frac{lbh}{(l + 2t)(b + 2t)(h + 2t) - lbh} \quad . \tag{1}$$

The total volume is $V_{tot} = V_f + V_m + V_p$, where V_p is the volume of possible pores. The fibre volume fraction is

$$v_f = \frac{V_f}{V_{tot}} \quad . \tag{2}$$

The properties of the *cf*-material are in general orthotropic due to the more or less oblong shape of the fibre and due to orthotropic properties of the fibre. The homogenised properties of the composite material are obtained by integration over the fibre orientation directions. This integration is made with respect to a function containing the properties of the *cf*-material. This function has a free parameter, $\alpha, -1 \leq \alpha \leq 1$, such that $\alpha = 1$ corresponds to the extreme of parallel coupling with complete interaction and equal strain for the variously oriented *cf*-material, and $\alpha = -1$ corresponds to the extreme of series coupling with equal stress. Two types of functions of α are studied: a linear function and an exponential function.

3 HOMOGENISATION OF COATED FIBRE

The general principle used for calculating the properties of the homogenous *cf*-material is that the response to load and to moisture change should be the same in terms of deformation of the *cf*-material and the coated fibre composite structure. In the present analysis the response of the composite structure is determined by minimization of potential energy. This minimization is carried out to a finite number of parameters, degrees of freedom, which, together with an assumption regarding the shape of the deformed structure, defines the strains. The present choice of shape functions fulfills the conditions of compatibility. Hence the calculated stiffness of the structure will, in general, somewhat overestimate the true stiffness. The deformed shape valid for loading by normal force in the $x-, y-$ or $z-$direction and for the change of moisture content is, for the 3D case, defined by 3 times 2 normal strain parameters, see Figure 2b. The shape for shear loadings is defined by 3 times 3 independent shear strain parameters, see Figure 2c.

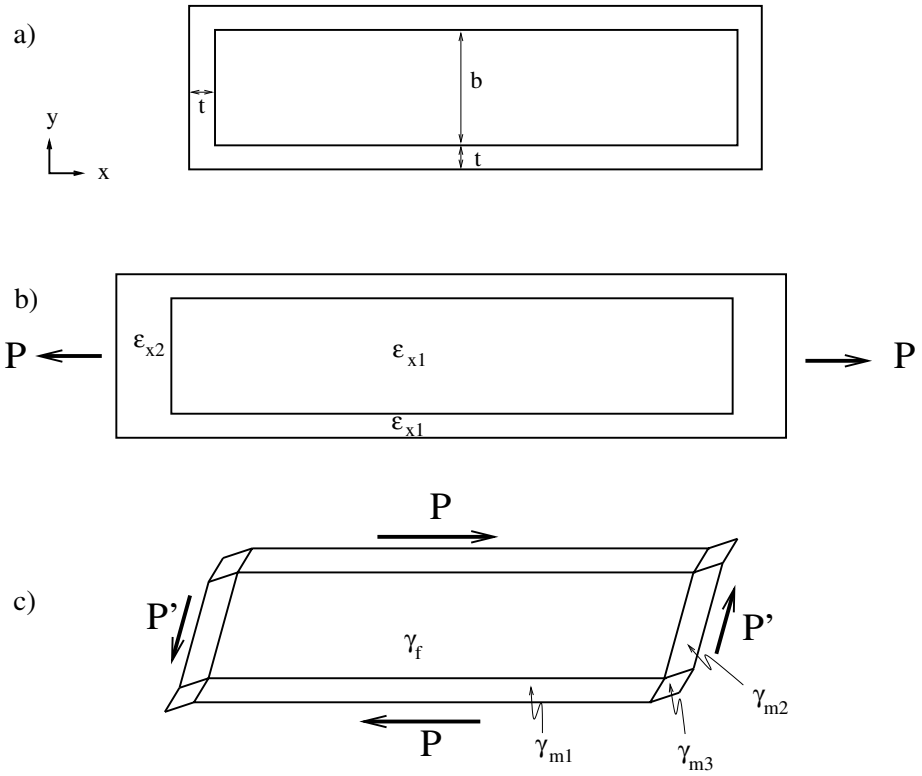

Figure 2: *Shape of coated fibre, a) unloaded, b) loaded in tension, c) loaded in shear.*

The potential energy for a structure or body and the loads acting on the body is

$$\Pi = U - W = \frac{1}{2}\int_V \varepsilon^T \boldsymbol{\sigma} dV - \int_S \mathbf{u}^T \mathbf{f} dS \tag{3}$$

where U is the strain energy and W is the potential energy of the loads. Minimization of Π with respect to the free parameters

$$\frac{\partial \Pi}{\partial \varepsilon'} = 0, \tag{4}$$

provides the equations from which the free strain parameters can be calculated.

3.1 E-moduli and Poissons ratios of *cf*-material

The stiffness properties of the homogenized *cf*-material are defined by a 6×6 compliance matrix, $\overline{\mathbf{C}}_{cf}$, relating a stress vector and a strain vector $\overline{\boldsymbol{\varepsilon}} = \overline{\mathbf{C}}_{cf}\ \overline{\boldsymbol{\sigma}}$ in the local coordinate system of the *cf*

$$\begin{bmatrix} \varepsilon_x \\ \varepsilon_y \\ \varepsilon_z \\ \sqrt{2}\varepsilon_{xy} \\ \sqrt{2}\varepsilon_{xz} \\ \sqrt{2}\varepsilon_{yz} \end{bmatrix} = \begin{bmatrix} \frac{1}{E_x} & -\frac{\nu_{yx}}{E_y} & -\frac{\nu_{zx}}{E_z} & 0 & 0 & 0 \\ -\frac{\nu_{xy}}{E_x} & \frac{1}{E_y} & -\frac{\nu_{zy}}{E_z} & 0 & 0 & 0 \\ -\frac{\nu_{xz}}{E_x} & -\frac{\nu_{yz}}{E_y} & \frac{1}{E_z} & 0 & 0 & 0 \\ 0 & 0 & 0 & \frac{1}{2G_{xy}} & 0 & 0 \\ 0 & 0 & 0 & 0 & \frac{1}{2G_{xz}} & 0 \\ 0 & 0 & 0 & 0 & 0 & \frac{1}{2G_{yz}} \end{bmatrix} \begin{bmatrix} \sigma_x \\ \sigma_y \\ \sigma_z \\ \sqrt{2}\sigma_{xy} \\ \sqrt{2}\sigma_{xz} \\ \sqrt{2}\sigma_{yz} \end{bmatrix}. \tag{5}$$

The shear components in $\overline{\boldsymbol{\varepsilon}}$ and $\overline{\boldsymbol{\sigma}}$ are defined with a factor $\sqrt{2}$ which facilitates subsequal analysis of the composite material. The six independent elastic stiffness parameters in the upper left of $\overline{\mathbf{C}}_{cf}$ are obtained by analysing the performance of the *cf* structure when exposed to normal force, Figure 2b. The three shear stiffness parameters are obtained separately by analysing the performance at shear loading, Figure 2c.

The deformation during loading according to Figure 2b is defined by six parameters:

ε_{x1} - normal strain in the $x-$direction in the interval $0 \leq x \leq l$,
ε_{x2} - normal strain in the $x-$direction in the interval $l \leq x \leq l + 2t$,
ε_{y1} - normal strain in the $y-$direction in the interval $0 \leq y \leq b$,
ε_{y2} - normal strain in the $y-$direction in the interval $b \leq y \leq b + 2t$,
ε_{z1} - normal strain in the $z-$direction in the interval $0 \leq z \leq h$,
ε_{z2} - normal strain in the $z-$direction in the interval $h \leq z \leq h + 2t$.

This yields $2^3 = 8$ subvolumes, see Figure 3, with different sets of $\varepsilon_x, \varepsilon_y$ and ε_z , e.g $\overline{\boldsymbol{\varepsilon}}_f = [\, \varepsilon_{x1} \;\; \varepsilon_{y1} \;\; \varepsilon_{z1} \;\; 0 \;\; 0 \;\; 0]$ for the first subvolume, denoted f.

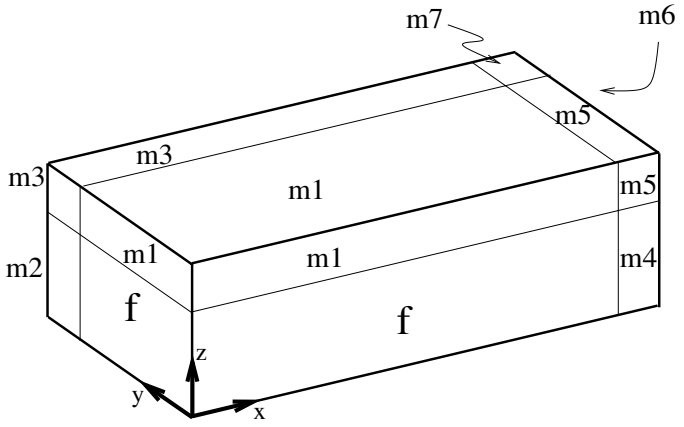

Figure 3: *Subvolumes with different strain.*

From equation (3)

$$\Pi = \frac{1}{2} V_f \overline{\boldsymbol{\varepsilon}}_f^T \overline{\mathbf{D}}_f \overline{\boldsymbol{\varepsilon}}_f + \sum_{i=1}^{7} \frac{1}{2} V_{mi} \overline{\boldsymbol{\varepsilon}}_{mi}^T \overline{\mathbf{D}}_m \overline{\boldsymbol{\varepsilon}}_{mi} - P(l\varepsilon_{x1} + 2t\varepsilon_{x2}) \tag{6}$$

where the stiffness matrices, $\overline{\mathbf{D}}_f$ and $\overline{\mathbf{D}}_m$ are equal to $\overline{\mathbf{C}}_f^{-1}$ and $\overline{\mathbf{C}}_m^{-1}$ defining the stiffness properties of the fibre and the matrix material respectively, in analogy with equation (5). $V_f = lbh$, $V_{m1} = 2tlb$, $V_{m2} = 2tlh, \ldots$ etc are the volumes of the respective region. Partial derivatives, equation (4), with respect to the six free parameters, $\boldsymbol{\varepsilon}' = [\varepsilon_{x1}, \varepsilon_{x2}, \varepsilon_{y1}, \varepsilon_{y2}, \varepsilon_{z1}, \varepsilon_{z2}]^T$, gives, for loading in the x-direction, a system of equations

$$\begin{cases} V_f \mathbf{e}_x^T \overline{\mathbf{D}}_f \overline{\boldsymbol{\varepsilon}}_f + V_{m1} \mathbf{e}_x^T \overline{\mathbf{D}}_m \overline{\boldsymbol{\varepsilon}}_{m1} + V_{m2} \mathbf{e}_x^T \overline{\mathbf{D}}_m \overline{\boldsymbol{\varepsilon}}_{m2} + V_{m3} \mathbf{e}_x^T \overline{\mathbf{D}}_m \overline{\boldsymbol{\varepsilon}}_{m3} = Pl \\ V_f \mathbf{e}_y^T \overline{\mathbf{D}}_f \overline{\boldsymbol{\varepsilon}}_f + V_{m1} \mathbf{e}_y^T \overline{\mathbf{D}}_m \overline{\boldsymbol{\varepsilon}}_{m1} + V_{m4} \mathbf{e}_y^T \overline{\mathbf{D}}_m \overline{\boldsymbol{\varepsilon}}_{m4} + V_{m5} \mathbf{e}_y^T \overline{\mathbf{D}}_m \overline{\boldsymbol{\varepsilon}}_{m5} = 0 \\ V_f \mathbf{e}_z^T \overline{\mathbf{D}}_f \overline{\boldsymbol{\varepsilon}}_f + V_{m2} \mathbf{e}_z^T \overline{\mathbf{D}}_m \overline{\boldsymbol{\varepsilon}}_{m2} + V_{m4} \mathbf{e}_z^T \overline{\mathbf{D}}_m \overline{\boldsymbol{\varepsilon}}_{m4} + V_{m6} \mathbf{e}_z^T \overline{\mathbf{D}}_m \overline{\boldsymbol{\varepsilon}}_{m6} = 0 \\ V_{m4} \mathbf{e}_x^T \overline{\mathbf{D}}_m \overline{\boldsymbol{\varepsilon}}_{m4} + V_{m5} \mathbf{e}_x^T \overline{\mathbf{D}}_m \overline{\boldsymbol{\varepsilon}}_{m5} + V_{m6} \mathbf{e}_x^T \overline{\mathbf{D}}_m \overline{\boldsymbol{\varepsilon}}_{m6} + V_{m7} \mathbf{e}_x^T \overline{\mathbf{D}}_m \overline{\boldsymbol{\varepsilon}}_{m7} = 2tP \\ V_{m2} \mathbf{e}_y^T \overline{\mathbf{D}}_m \overline{\boldsymbol{\varepsilon}}_{m2} + V_{m3} \mathbf{e}_y^T \overline{\mathbf{D}}_m \overline{\boldsymbol{\varepsilon}}_{m3} + V_{m6} \mathbf{e}_y^T \overline{\mathbf{D}}_m \overline{\boldsymbol{\varepsilon}}_{m6} + V_{m7} \mathbf{e}_y^T \overline{\mathbf{D}}_m \overline{\boldsymbol{\varepsilon}}_{m7} = 0 \\ V_{m1} \mathbf{e}_z^T \overline{\mathbf{D}}_m \overline{\boldsymbol{\varepsilon}}_{m1} + V_{m3} \mathbf{e}_z^T \overline{\mathbf{D}}_m \overline{\boldsymbol{\varepsilon}}_{m3} + V_{m5} \mathbf{e}_z^T \overline{\mathbf{D}}_m \overline{\boldsymbol{\varepsilon}}_{m5} + V_{m7} \mathbf{e}_z^T \overline{\mathbf{D}}_m \overline{\boldsymbol{\varepsilon}}_{m7} = 0 \end{cases} \tag{7}$$

where $\mathbf{e}_x^T = [1\ 0\ 0\ 0\ 0\ 0], \mathbf{e}_y^T = [0\ 1\ 0\ 0\ 0\ 0]$ and $\mathbf{e}_z^T = [0\ 0\ 1\ 0\ 0\ 0]$ are unit vectors. In matrix form this linear system of equations can be written as $\mathbf{K}_n \boldsymbol{\varepsilon}' = \mathbf{f}_x$ where $\mathbf{f}_x = P\,[l\ \ 0\ \ 0\ \ 2t\ \ 0\ \ 0]^T$ and $\mathbf{K}_n$ contains components from $\overline{\mathbf{D}}_f$, $\overline{\mathbf{D}}_m$ and volumes of the respective regions. When the strains have been solved, Young's modulus E_x and Poisson's ratios ν_{xy} and ν_{xz} of the *cf*-material are calculated from

$$E_x = \sigma_{x,mean} / \varepsilon_{x,mean} = \frac{P}{(b+2t)(h+2t)} \Big/ \frac{l\,\varepsilon_{x1} + 2t\,\varepsilon_{x2}}{l+2t} \tag{8}$$

$$\nu_{xy} = -\frac{\varepsilon_{y,mean}}{\varepsilon_{x,mean}}, \quad \nu_{xz} = -\frac{\varepsilon_{z,mean}}{\varepsilon_{x,mean}}\ . \tag{9}$$

Properties in the other two directions are calculated analogously by redefining the force vector to $\mathbf{f}_y$ and $\mathbf{f}_z$ respectively.

3.2 Shear moduli of *cf*

The shear stiffness parameters of the *cf*-material are obtained in a similar way. Since the $x-y$-shear strain is constant in the z-direction, the assumed deformation pattern at loading in the $x-y$ plane is defined by three independent parameters, γ_f, γ_{m1} and γ_{m2}, see Figure 2c. The fourth shear strain parameter, γ_{m3}, is determined by the condition of compatibility, giving

$$\gamma_{m3} = \gamma_{m1} + \gamma_{m2} - \gamma_f\ . \tag{10}$$

From equation(3) the potential, Π, is

$$\begin{aligned}\Pi &= \frac{1}{2}V_f G_{fm}\gamma_f^2+\frac{1}{2}V_{m1}G_m\gamma_{m1}^2+\frac{1}{2}V_{m2}G_m\gamma_{m2}^2+\frac{1}{2}V_{m3}G_m(\gamma_{m1}+\gamma_{m2}-\gamma_f)^2- \\ & P[(b-\frac{b+2t}{l+2t}2t)\gamma_f+2t\gamma_{m2}+\frac{b+2t}{l+2t}2t\gamma_{m1}] \end{aligned} \tag{11}$$

where G_{fm} is the mean shear modulus of the fibre in region f and the matrix in region $m1$. In these two regions the shear strain is the same at loading in the $x-y$ plane.

$$G_{fm} = \frac{hG_f+2tG_m}{h+2t} \tag{12}$$

where G_f and G_m are the $x-y$-plane shear moduli of the fibre and matrix, respectively. Minimization of the energy

$$\frac{\partial \Pi}{\partial \boldsymbol{\gamma}'} = 0 \tag{13}$$

where $\boldsymbol{\gamma}' = [\gamma_f \;\; \gamma_{m1} \;\; \gamma_{m2}]$ yields the shear strain parameters by solving the equation

$$\begin{bmatrix} blG_{fm}+4t^2G_m & -4t^2G_m & -4t^2G_m \\ -4t^2G_m & (2bt+4t^2)G_m & 4t^2G_m \\ -4t^2G_m & 4t^2G_m & (2lt+4t^2)G_m \end{bmatrix} \begin{bmatrix} \gamma_f \\ \gamma_{m1} \\ \gamma_{m2} \end{bmatrix} = P \begin{bmatrix} b-2t\frac{b+2t}{l+2t} \\ 2t \\ 2t\frac{b+2t}{l+2t} \end{bmatrix}. \tag{14}$$

Now the shear strain of the homogenised *cf*-material can be obtained from the displacements of the corners of the *cf*-structure, Figure 2c, expressed in γ_f, γ_{m1} and γ_{m2}. The shear stress in the *cf*-material when loaded by P and P' is $P/((l+2t)(h+2t)) = P'/((b+2t)(h+2t))$, giving

$$G_{xy} = \frac{\tau_{(cf)xy}}{\gamma_{(cf)xy}} = \frac{P}{(l+2t)(h+2t)} \Bigg/ \left(\frac{2t\gamma_{m1}+b\gamma_f}{2t+b} + \frac{2t(\gamma_{2m}-\gamma_f)}{2t+l} \right) \tag{15}$$

where G_{xy} is the shear modulus of the *cf*-material. G_{xz} and G_{yz} are calculated analogously by applying the load in the $x-z$ and $y-z$ planes respectively.

3.3 Hygroexpansion of *cf*-material

The free expansion of the fibre material is assumed to be

$$\overline{\varepsilon}_f^o = \left[\varepsilon_{(f)x}^o \;\; \varepsilon_{(f)y}^o \;\; \varepsilon_{(f)z}^o \;\; 0 \;\; 0 \;\; 0 \right]^T \tag{16}$$

and the free hygroexpansion of the matrix material is assumed to be

$$\overline{\boldsymbol{\varepsilon}}_m^o = \left[\varepsilon_{(m)x}^o \;\; \varepsilon_{(m)y}^o \;\; \varepsilon_{(m)z}^o \;\; 0 \;\; 0 \;\; 0\right]^T \quad . \tag{17}$$

The free hygroexpansion of the constituents is thus assumed to be isotropic or orthotropic with material axes according to the axes of the fibre geometry. At free hygroexpansion of a coated fibre, any difference between $\overline{\boldsymbol{\varepsilon}}_f^o$ and $\overline{\boldsymbol{\varepsilon}}_m^o$ will in general produce stresses and normal strains in the 8 regions of the *cf*-structure. From equation (3) the potential of the structure is then

$$\Pi = \frac{1}{2} V_f (\overline{\boldsymbol{\varepsilon}}_f - \overline{\boldsymbol{\varepsilon}}_f^o)^T \overline{\mathbf{D}}_f (\overline{\boldsymbol{\varepsilon}}_f - \overline{\boldsymbol{\varepsilon}}_f^o) + \sum_{i=1}^{7} \frac{1}{2} V_{mi} (\overline{\boldsymbol{\varepsilon}}_{mi} - \overline{\boldsymbol{\varepsilon}}_m^o)^T \overline{\mathbf{D}}_m (\overline{\boldsymbol{\varepsilon}}_{mi} - \overline{\boldsymbol{\varepsilon}}_m^o) \tag{18}$$

which by minimization according to equation (4) with respect to the free parameters, $\boldsymbol{\varepsilon}' = [\varepsilon_{x1} \;\; \varepsilon_{x2} \;\; \varepsilon_{y1} \;\; \varepsilon_{y2} \;\; \varepsilon_{z1} \;\; \varepsilon_{z2}]^T$, gives a system of equations

$$\mathbf{K}_n \boldsymbol{\varepsilon}' = \mathbf{f}_{hyg} \tag{19}$$

where $\mathbf{f}_{hyg}$ contains the free hygroexpansion components from $\overline{\boldsymbol{\varepsilon}}_f^o$ and $\overline{\boldsymbol{\varepsilon}}_m^o$, and $\mathbf{K}_n$ is defined in the above, see equation (7). From this the strain parameters, $\boldsymbol{\varepsilon}'$, are solved. The free hygroexpansion of the *cf*-material in the x-, y- and the z-directions can then be calculated by summation of the strains in the different regions of the *cf*-strucutre:

$$\varepsilon_{x(cf)} = \frac{l\varepsilon_{x1} + 2t\varepsilon_{x2}}{l + 2t}, \quad \varepsilon_{y(cf)} = \frac{b\varepsilon_{y1} + 2t\varepsilon_{y2}}{b + 2t}, \quad \varepsilon_{z(cf)} = \frac{h\varepsilon_{z1} + 2t\varepsilon_{z2}}{h + 2t} \quad . \tag{20}$$

which gives the free hygroexpansion, $\overline{\boldsymbol{\varepsilon}}_{cf}^o$, of the *cf*-material. There will be no shear strain at hygroexpansion due to the assumption of orthotropic properties of the constituents.

4 HOMOGENISATION OF COATED FIBRE NETWORK

4.1 Composite material stiffness properties

The composite material is built up of coated fibres with arbitrary orientation distribution. The global coordinate system and material properties in that system are here given without overline, i.e. x, y, z, while the local coordinate system of the fibre is indicated here by an overline, $\overline{x}, \overline{y}, \overline{z}$, see Figure 4 where the $\overline{x}$-direction is the orientation of the fibre.

From the properties calculated in the previous section, a constitutive relation of the coated fibre is defined in (5), or in a shorter matrix notation

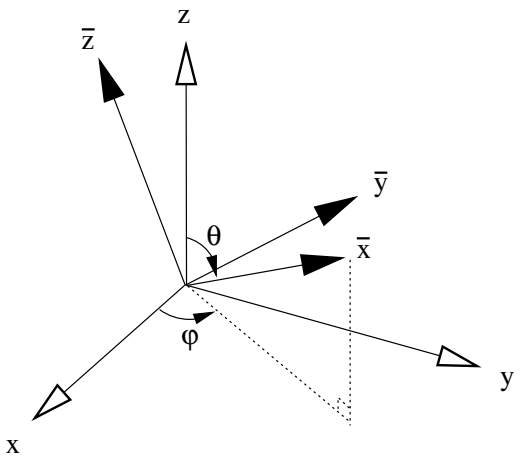

Figure 4: *Three dimensional coordinate transformation. The fibre is oriented in the x-direction.*

$$\overline{\boldsymbol{\varepsilon}} = \overline{\mathbf{D}}_{cf}^{-1}\overline{\boldsymbol{\sigma}} \tag{21}$$

The shear components in $\overline{\boldsymbol{\varepsilon}}$ and $\overline{\boldsymbol{\sigma}}$ are defined with a factor $\sqrt{2}$ in order to make the coordinate transformations from the local to the global coordinate system for stresses and strains identical [15], i.e.

$$\overline{\boldsymbol{\varepsilon}} = \mathbf{T}\boldsymbol{\varepsilon}, \quad \overline{\boldsymbol{\sigma}} = \mathbf{T}\boldsymbol{\sigma} \tag{22}$$

where the transformation matrix, $\mathbf{T}$, consists of sines and cosines of the rotation angles φ and θ. This is necessary to make the interpolation in (28) coordinate frame independent.

The transformation of the stiffness matrix becomes

$$\mathbf{D}_{cf} = \mathbf{T}^{-1}\overline{\mathbf{D}}_{cf}\mathbf{T} \tag{23}$$

The orientation distribution of the fibres is described with the scalar function $\psi(\varphi, \theta)$ so that the share of fibres in a small interval, $d\varphi d\theta$, is $\psi(\varphi, \theta)\sin\theta d\varphi d\theta$. ψ is in the subsequent applications assumed to have the form

$$\psi(\varphi, \theta) = f(\varphi)g(\theta) = (k_1 + k_2\cos^2\varphi)(k_3 + k_4\sin^2\theta) \tag{24}$$

where $k_1..k_4$ are distribution shape parameters. A 2-dimensional orientation distribution is achieved with $g(\theta) = \delta(\pi/2)$, the Dirac delta function.

For the homogenous strain assumption (the Voigt approximation or parallel coupling) the composite material stiffness matrix, $\mathbf{D}_{c(p)}$, is calculated by integration of the stiffness in all directions

$$\begin{aligned}\mathbf{D}_{c(p)} &= \int_0^\pi \int_0^\pi \mathbf{D}_{cf}\psi(\varphi,\theta)\sin\theta\, d\varphi d\theta \\ &= \int_0^\pi \int_0^\pi \mathbf{T}^{-1}\overline{\mathbf{D}}_{cf}\mathbf{T}\psi(\varphi,\theta)\sin\theta\, d\varphi d\theta \end{aligned} \tag{25}$$

For the homogenous stress assumption (the Reuss approximation or serial coupling) the stiffness matrix is calculated as the inverse of the integrated compliance according to

$$\mathbf{D}_{c(s)} = \left[\int_0^\pi \int_0^\pi \mathbf{T}^{-1}\overline{\mathbf{D}}_{cf}^{-1}\mathbf{T}\psi(\varphi,\theta)\sin\theta\, d\varphi d\theta\right]^{-1} \tag{26}$$

According to Hill's theorem these two cases are the extreme cases of the composite stiffness. A linear interpolation between the two cases gives

$$\mathbf{D}_c = \frac{1+\alpha}{2}\mathbf{D}_{c(p)} + \frac{1-\alpha}{2}\mathbf{D}_{c(s)} \tag{27}$$

where α can be considered as a fitting parameter between the Voigt approximation ($\alpha = 1$) and the Reuss approximation ($\alpha = -1$).

Another way of interpolating the Voigt and the Reuss approximations is by raising the stiffness matrices by the scalar α:

$$\mathbf{D}_{c(s)} = \left[\int_0^\pi \int_0^\pi \mathbf{T}^{-1}\overline{\mathbf{D}}_{cf}^{\alpha}\mathbf{T}\psi(\varphi,\theta)\sin\theta\, d\varphi d\theta\right]^{1/\alpha} \tag{28}$$

where, as with the linear interpolation, $\alpha = 1$ corresponds to the Voigt and $\alpha = -1$ to the Reuss. Since $\mathbf{D}_{cf}$ is positive definite in all coordinate systems, α can assume any value in between in analogy to the linear interpolation. It can by use of matrix theory be shown, see Stålne [15], that material property analysis according to equation (28) fulfills the condition of coordinate frame independence.

4.2 Composite hygroexpansion

The hygroexpansion of the coated fibre network homogenisation is first calculated by the homogenous strain assumption

$$\overline{\boldsymbol{\varepsilon}}_{c(p)} = \int_0^\pi \int_0^\pi \mathbf{D}_{c(p)}^{-1}\mathbf{T}^{-1}\overline{\mathbf{D}}_{cf}\overline{\boldsymbol{\varepsilon}}_{cf}^{o}\psi(\varphi,\theta)\sin\theta\, d\varphi d\theta \tag{29}$$

which gives the lower boundary of the free composite hygroexpansion strain. The upper boundary is given by the homogenous stress assumption

$$\overline{\varepsilon}_{c(s)} = \int_0^{\pi} \int_0^{\pi} \mathbf{T}^{-1} \overline{\varepsilon}_{cf}^{o} \psi(\varphi, \theta) \sin\theta \, d\varphi d\theta \quad . \tag{30}$$

The linear interpolation can be applied here by defining the composite hygroexpansion

$$\overline{\varepsilon}_c = \frac{1+\alpha}{2} \overline{\varepsilon}_{c(p)} + \frac{1-\alpha}{2} \overline{\varepsilon}_{c(s)} \tag{31}$$

where, as before, $\alpha = 1$ corresponds to the case of homogenous strain and $\alpha = -1$ to homogenous stress. The only plausible interpolation is this linear interpolation since the power interpolation does not give the same hygroexpansion as the constituents when all constituents hygroexpansion are set equal.

5 COMPARISON TO EXPERIMENTAL RESULTS

Results from the model are compared to results from measurements made on composites with different fibre-matrix fractions. First, the results from a study of the stiffness of a polypropylene and wood flour composite [12] are investigated. Stiffness and hygroexpansion properties are then studied in relation to an experimental study of high pressure laminates made of paper impregnated with phenolic or melamine formaldehyde resin [2].

5.1 Polypropylene-wood flour composite

Polypropylene is a synthetic polymer used in injection molded products, and it can be modified with sawdust in order to increase its stiffness. The matrix material, the polypropylene, is considered isotropic and the sawdust as particles of solid wood, pine. The fibre orientation distribution was recorded experimentally (Nilsson, L.-O.,et.al."Wood composites based on recycled plastics - mechanical properties." unpublished internal report. of Structural Mechanics, Lund University, Sweden) and the orthotropic distribution found was used in the calculation. The shape of the wood particles was determined by optical inspection to $[\, l \;\; b \;\; h \,] = [\, 3 \;\; 1 \;\; 1 \,]$ and the interpolation parameter α was set equal to 0, being a reasonable first value in between the limits -1 and 1. This value can, if needed, be adjusted by fitting to experimental data. The mechanical properties of the wood flour listed in Table 1 are from [5] and the properties of the matrix material are determined from the tests with $v_f = 0$.

The experimental and theoretical results on composite material stiffness at various fibre volume fraction are shown in Figure 5 and in Table 2. The two

Table 1: *Mechanical properties of wood flour and polypropylene.*

Wood Particle									Matrix	
E_x [MPa]	E_y [MPa]	E_z [MPa]	ν_{xy} [-]	ν_{xz} [-]	ν_{yz} [-]	G_{xy} [MPa]	G_{xz} [MPa]	G_{yz} [MPa]	E [MPa]	ν [-]
16000	1 100	570	0.42	0.51	0.68	1170	676	66	1 370	0.41

experimental values represent two composites containing polypropylenes with different melt flow index. This seems not to affect the stiffness, and is therefore not considered in the model.

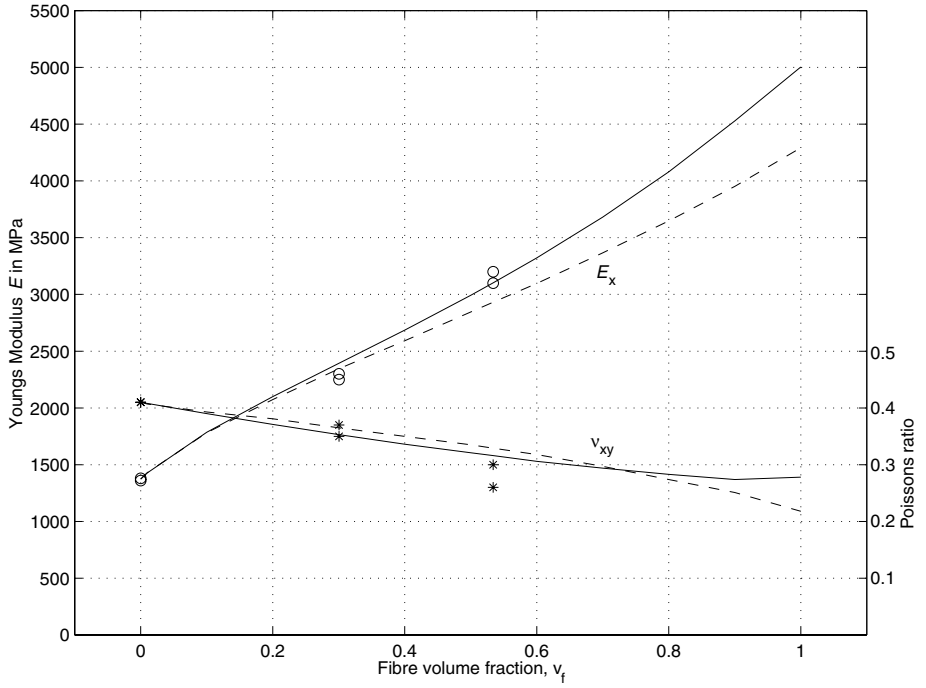

Figure 5: *Experimental values of material stiffness E_x, marked with circles, and Poissons ratio ν_{xy}, marked with stars, compared with analytical modelling with linear interpolation, marked with solid lines, and with power interpolation, marked with dashed lines.*

The theoretical predictions are in good agreement with the experimental results, both with respect to Youngs modulus and with respect to Poissons ratio.

Table 2: *Results of measurements and modelling of polypropylene-wood flour composite.*

	Measurement				Model	
	1		2			
v_f	E_X	ν	E_X	ν	E_X	ν
[-]	[MPa]	[-]	[MPa]	[-]	[MPa]	[-]
0	1380	0.41	1360	0.41	1370	0.41
0.3	2250	0.37	2300	0.35	2390	0.35
0.53	3200	0.30	3100	0.26	3100	0.31

5.2 High Pressure Laminate

A high pressure laminate (HPL) with orthotropic fibre orientation was tested for stiffness and hygroexpansion. HPL is built up of a core containing layers of phenolic resin-impregnated paper. The HPL testing was performed for tensile loading in three directions [2], and resulted in mean values of the four independent in-plane stiffness properties of an orthotropic material: 2 Youngs moduli, shear moduli and Poisons ratio, Table 4. The hygroexpansion in the two in-plane directions was measured for different intervals of the moisture content.

When modelling the HPL it is regarded as a composite with an in-plane directional orientation of continuous fibres, reflecting that the fibres are very long, $\sim$1 mm, in comparison to their width, $\sim 50\mu$m. The fibre volume fraction is measured during manufacturing to 75 per cent, and the fibre orientation distribution is considered to be 2:1 i.e. with the distribution function $f(\varphi)$ in equation (24) where the number of fibres in the x-direction is twice the number in the y-direction: $\psi(\varphi,\theta) = \frac{2}{3}\frac{1+\cos^2\varphi}{\pi} \cdot \delta(\theta{=}\pi/2)$. Exact stiffness properties for cellulose fibres are hard to estimate, e.g. an undamaged wood fibre is considered to have a longitudinal Youngs modulus of 50-60 GPa [13], which will decrease when subjected to mechanical and chemical treatment. A fibre is here assumed to have a longitudinal Youngs modulus of 40 GPa and a transversal Youngs modulus of 5 GPa, Table 3. The Youngs modulus of phenolic resin is taken from [3]. The hygroexpansion coefficient β is defined as the increase in strain per increase in moisture content in percent. Estimations of the cellulose fibre and phenolic resin hygroexpansion coefficients are from [13].

The experimental and theoretical results are summarized in Tables 4 and 5. The composite model, here used with the linear interpolation with $\alpha = 0$, appears to produce stiffness parameter values in good agreement with the experimental results. MD indicates the machine direction of the paper of the HPL, and CD

Table 3: *Mechanical properties of wood fibres and phenolic resin.*

Fibre						Matrix		
E_x [MPa]	E_y [MPa]	ν_{xy} [-]	G_{xy} [MPa]	β_x [1/%]	β_y [1/%]	E [MPa]	ν [-]	β [1/%]
40 000	5 000	0.2	4 000	0.01	0.26	5 750	0.3	0.01

the cross machine direction.

Table 4: *Experimental and theoretical stiffness properties of HPL.*

Experimental				Theoretical			
E_{MD} [GPa]	E_{CD} [GPa]	G [GPa]	ν [-]	E_{MD} [GPa]	E_{CD} [GPa]	G [GPa]	ν [-]
15.5	10.5	4.5	0.38	14.4	10.6	3.5	0.26

Table 5: *Experimental and theoretical hygroexpansion coefficients.*

Experimental		Theoretical	
β_{MD} [1/%]	β_{CD} [1/%]	β_{MD} [1/%]	β_{CD} [1/%]
0.063	0.109	0.062	0.090

The hygroexpansion was measured in the interval of 35 - 65 per cent relative humidity, which corresponds to 3.5 - 5 per cent moisture content, where the expansion can be regarded as linear with increasing moisture content. In other intervals, especially at high moisture contents, the expansion is non-linear. The fairly small deviation between theoretical prediction and experimental results with respect to hygroexpansion can very well be explained by uncertainties in the material data of the composite material constituents.

6 SUMMARY AND CONCLUDING REMARKS

A three dimensional model for all stiffness and hygroexpansion components of a fibre or particle composite material has been presented. The model is divided in two steps, first a homogenisation of a simple fibre-matrix block structure and then a homogenisation of the composite material structure by an integration for

all fibre directions. The homogenisation of the coated fibre is obtained by applying normal and shear forces one by one in various directions and computing the strains by a minimization of the potential energy. Normal stiffnesses, Poissons ratios and shear stiffnesses are then determined from definition. Thereby the whole stiffness matrix can be expressed in terms of the properties of the constituents and the shape of fibre or particle.

The composite material stiffness is first obtained for the two extremes of homogenous strain and homogenous stress. This is done by integration of the stiffness or compliance matrix of the coated fibre material for all fibre directions. Analysis of the hygroexpansion properties of a coated fibre and the composite material was carried out consistent with the stiffness analysis.

Interpolation between the two extreme cases of homogenous strain and homogenous stress can be done by a simple linear weighting of the stiffness matrices or by an exponential weighting. Both interpolations have the quality of coordinate invariance. When comparing the different procedures, the exponetial approach is more appealing from a mathematial point of view, since it is unambiguous. However, the linear interpolation is simpler, more numerically stable and demands fewer calculations. When calculating the hygroexpansion the linear interpolation is the only way possible. The two interpolations appear to give fairly similar results.

The resulting stiffness matrix for the composite material is symmetric, valid in the entire range between 0 per cent and 100 per cent fibre content, and coincident with the exact solutions that exist for the extreme cases of laminate geometries and continuous-fibre systems with equal shear rigidities. At this stage, only time-independent properties of the constituents are considered in the model. Consideration of varying fibre lengths according a fibre length distribution would be easy to implement. The present model comprise some rather extensive equations. Such qualities can however be dealt with in a convenient manner by use of *MAPLE* [11] or any other similair computer code.

Comparisons between the model and measurements gave a good agreement in stiffnesses and Poissons ratio. When comparing with the measured hygroexpansion coefficients, the calculated hygroexpansion coefficients are slightly lower. The comparison to experimental results were here made only for two types of material and it can not be generally concluded that the theoretical model underestimates hygroexpansion. The model presented is flexible in such manner that it can be used in a number of different applications and contribute to a better understanding of composite material behaviour.

7 ACKNOWLEDGEMENT

This work was financed by the Swedish Wood Technology Research Colleague.

APPENDIX I.

References

[1] Aboudi, J. (1991). "Mechanics of Composite Materials", Elsevier, Amsterdam, The Netherlands, 14-18.

[2] Andersson, B. (1999). "Composite materials' hygro-mechanical properties", Masters thesis, Report TVSM-3018, Div. of Structural Mechanics, Lund University, Sweden.

[3] Barth, Th. (1984). "Der Einfluss der Feuchteaufnahme auf die mechanischen Eigenschaften von Phenolplasten." *Z. Werkstofftech*, Verlag Chemie, Weinheim, Germany, 15, 299-308.

[4] Cox, H. L. (1951). "The elasticity and strength of paper and other fibrous materials." *Brittish J. Appl. Phys.*, London, 3, 72-79.

[5] Dinwoodie, J. M. (1989). *Wood: nature's cellular, polymeric fibre-composite*, The Institute of Metals, London, 57.

[6] Dunn, M. L., Ledbetter, H., Heyliger, P. R. and Choi, C. S. (1996). "Elastic constants of textured short-fiber composites." *J. Mech. Phys. Solids*, Elsevier, Amsterdam, The Netherlands, 44, 1509-1541.

[7] Fu, S.-Y. Lauke, B. (1998). "An analytical characterization of the anisotropy of the elastic modulus of misaligned short-fiber-reinforced polymers." *Composites Sci. Techn.*, Elsevier, Amsterdam, The Netherlands, 58, 1961-1972.

[8] Halpin, J. C., Kardos, J. L. (1976). "The Halpin-Tsai equations: A review." *Polym. Eng. Sci.*, Swets, 16, 344-352.

[9] Hashin, Z., Shtrikman, S. (1963). "A variational approach to the theory of the elastic behaviour of multiphased materials." *J. Mech. Phys. Solids*, Elsevier, Amsterdam, The Netherlands, 11, 127-140.

[10] Heyden, S. (2000). *Network modelling for the evaluation of mechanical properties of cellulose fibre fluff.*, Doctoral thesis, Report TVSM-1011, Div. of Structural Mechanics, Lund University, Sweden.

[11] *MAPLE* (2000), "A symbolic computation system or computer algebra system", Version 6.0, Waterloo Maple, Inc.

[12] Nilsson, L.-O., Hjort, S., Petterson, H., Gustafsson, P. J., Molin, N.-E., Sjödahl, M., Ståhle, P., Gunnars, J., Ericson, M., Oksman, K., Vilander, Y. and Lindberg, H. (1997). "Wood composites based on recycled plastics - mechanical properties." Div. of Structural Mechanics, Lund University, Sweden.

[13] Persson, K. (1997). *Modelling of wood properties by a micromechanical approach.*, Licentiate thesis, Report TVSM-3018, Div. of Structural Mechanics, Lund University, Sweden.

[14] Sayers, C.M. (1992). "Elastic anisotropy of short-fibre reinforced composites." *Int. J. Solid Structures*, 29, 2933-2944.

[15] Stålne, K. (1999). *Analysis of fibre composite materials for stiffness and hygroexpansion*, Report TVSM-7127, Div. of Structural Mechanics, Lund University, Sweden.

APPENDIX II.

Notation

b	width of fibre
$\mathbf{C}$	compliance matrix
c	transformation angle $\cos\theta$
$\mathbf{D}$	stiffness matrix
E	Youngs moduli
$\mathbf{e}$	unit vector
$\mathbf{f}$	force vectors
$\mathbf{f}_{hyg}$	vector containing the free hygroexpansion components
f	in-x-y-plane fibre orientation distribution function
G	shear modulus
G_{fm}	mean value of shear modulus in area f
g	out-of-x-y-plane fibre orientation distribution function
h	height of fibre
$\mathbf{K}_n$	matrix containing components from $\mathbf{D}_f$ and $\mathbf{D}_m$
$\mathbf{K}_s$	matrix containing combinations of G_f and G_m
k	coefficients of the fibre orientation distribution function
l	length of fibre
m	transformation angle $\cos\varphi$
n	transformation angle $\sin\varphi$
P	tensile and shearing load on cf
s	transformation angle $\sin\theta$

$\mathbf{T}$	coordinate transformation matrix
t	thickness of matrix material coating
U	strain energy of *cf*
$\mathbf{u}$	displacement vector
V_i	volume of phase i in *cf*
v_i	volume fraction of phase i
W	potential energy of loads acting on *cf*
α	interpolation parameter
β	hygroexpansion coefficient
γ_i	shear strain in region i
δ	Dirac delta function
$\boldsymbol{\varepsilon}^o$	free hygroexpansion vector
$\boldsymbol{\varepsilon}$	strain vector
ε_{mean}	mean strain in *cf*
$\boldsymbol{\varepsilon}'$	free strain parameter vector
θ	fibre angle to the x-y-plane
ν	Poissons ratio
Π	potential energy of *cf*
$\boldsymbol{\sigma}$	stress vector
σ_{mean}	mean stress in *cf*
τ	mean shear stress in *cf*
φ	fibre in-plane angle with the x-axis
ψ	3D fibre orientation distribution function

Superscripts

-	property in local coordinate system
o	free hygroexpansion
’	free strain parameter

Subscripts

c	composite property
$c(p)$	composite property calculated in the case of homogeous strain
$c(s)$	composite property calculated in the case of homogeous stress
cf	coated fibre property
f	fibre property
m	matrix material property
mi	matrix region i
MD	paper machine direction
CD	cross paper machine direction

Paper II

II

A 3D Finite Element Fibre Network Model for Composite Material Stiffness and Hygroexpansion Analysis.

Kristian Stålne and Per Johan Gustafsson

A 3D Finite Element Fibre Network Model for Composite Material Stiffness and Hygroexpansion Analysis

Kristian Stålne and Per Johan Gustafsson

Abstract

A 3D finite element fibre network model was developed to be used as a tool for predicting the stiffness and the hygroexpansion properties of fibre composite materials, such as high pressure laminates. The wood fibres are modelled as orthotropic or transversely isotropic solid elements surrounded by an isotropic matrix material. The fibres and the matrix are arranged in a unit cell subjected to loading or changes in moisture content. The constitutive parameters of the homogenised composite material are obtained by simulating the response of the composite structure to load and moisture. The model is evaluated by comparing the results it provides with various experimental results and with results of a recent analytical model and of various parameter studies. The model also provides in addition to properties of the homogenised material considerable information concerning stresses and strains within the material structure.

1 Introduction

High pressure laminate, HPL, is a wood fibre composite whose usage has increased much during the recent decades. It is composed of craft paper impregnated by phenolic or melamine resin. A key issue concerning wood composites is that of shape stability in relation to a moisture content gradient or to a change in moisture content. This entails the need for methods enabling the hygroexpansion and stiffness properties of wood composites such as HPL to be analysed and predicted.

Several analytical models for the stiffness of composite materials have been developed in recent decades [11, 22]. Many of these are based on the homogenisation of a single fibre surrounded by matrix material [1, 9]. These models assumes there to be no interaction between the fibres. Such an assumption is questionable in connection with HPL, however, since the particle phase of this composite material is paper, which is a network of long fibres bonded to each other.

Developments in the area of numerical simulation as based on the finite element method, for example, have made it possible to model more complicated fibre composite material structures, consisting of more than one fibre [7, 4, 6, 10, 24]. Most of these studies have dealt with estimation of the stiffness properties of plane fabric composites. These materials have a weaved fibre phase in which the fibres are crossed over and under each other at right angles [20, 8, 23, 13]. Since the fabric geometry is regular, homogenisation of a single fibre crossing is sufficient to provide a satisfactory estimate of the composite material stiffness. Composites with fibre networks of a more random types of have also been studied, using numerical simulations [15, 17, 19, 21]. There has been no study at a micro mechanical level, however, of the behaviour of composite materials of irregular geometry. Little appears to have been done either regarding simulation of the hygroexpansion or thermal expansion properties of such materials.

The aim of the model discussed is to simulate the mechanical behaviour of a wood fibre composite with an irregular fibre network, such that of paper. The model is a finite element 3D model using a square unit cell in which there are a number of fibres modelled as orthotropic solid elements surrounded by an isotropic matrix material. The response of the unit cell when exposed to an increase in moisture content and to loading in the x-, y- and z-direction, respectively, is simulated. The parameters of the model are the mechanical properties of the constituents, the fibre geometry, the fibre orientation distribution and the fibre volume fractions. The geometry of the fibres is created in a preprocessor allowing the user to decide on the location of each fibre. This enables a good rep-

resentation of the micro-structure of the fibre composite material to be obtained.

The numerical results concern primarily the influence of the model parameters on the stiffness and the hygroexpansion of the homogenised material. The predicted properties are compared with the results of a recently developed analytical model [18] and with certain test results. In addition to the homogenised material properties, the model provides considerably information on the magnitude and distribution of the stresses and strains within the material structure. This can provide estimates of the risk for development of micro-cracks, damage, creep or permanent plastic deformation within the material structure when exposed to various loads or moisture actions.

2 Description of the Model

The model concerns stiffness and hygroexpansion properties. Stiffness is analysed by exposing a square unit cell containing a number of wood fibres and a filling of matrix material to a given deformation in one direction and to zero load in all other directions. The stiffness tensor of the unit composite cell can be obtained by calculating the mean values of the stress and strain vectors for the volume of the cell. The hygroexpansion parameters of the composite cell are obtained by simulating an increase in moisture content and calculating the average strain of the unit cell in each direction.

The numerical modelling involves four steps: modelling the fibre geometry, finite element modelling, solution of the system of equations and postprocessing the results. The fibre and network geometry is created by a preprocessor written in Matlab-code [14]. It defines the volumes of the fibres and of the matrix material and generates input data to the commercial preprocessor Patran, in which the finite element mesh is created, material properties are assigned and the load cases are defined. The finite element analysis is performed by an Abaqus solver, the postprocessing being done using Patran.

2.1 General assumptions

The cross section of the fibres is assumed to be rectangular in shape, corresponding approximately to the shape of the collapsed wood fibres that the paper is made of. The height and the width of the fibres are assumed to be constant and to be the same for all the fibres, which are considered to be long and slender, no fibre ending in the cell. The space within the unit cell not occupied by fibres is occupied completely by matrix material. Thus voids are not considered in the

analysis. The fibre and matrix phases are assumed to be perfectly attached.

The constitutive relations for the fibres and matrix materials are linear elastic orthotropic or transversely isotropic and linear elastic isotropic, respectively, without any rate effect. The hygroexpansion properties of the two constituents are assumed to be linear orthotropic or transversely isotropic and to be isotropic, respectively, as well. Since the composite is formed under high pressure and temperature, an inner prestress within the material structure before any external action is applied appears likely. As long as the performance of the constituents is linear elastic, however, any eigenstress on the homogenised stiffness and expansion properties is without effect.

2.2 Geometry Preprocessing and FE-modelling

The fibre geometry preprocessor enables the user to place the fibres arbitrarily in the unit cell by mouse-clicking on a diagram such as that shown in Figure 1.

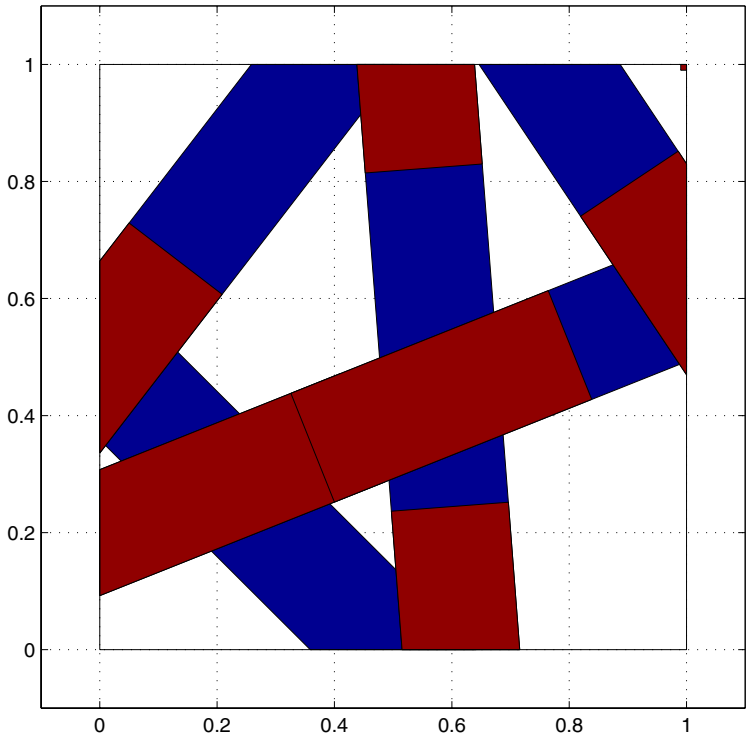

Figure 1: *Fibre geometry preprocessor.*

The first fibre crosses the square in the lowest part of the unit cell, i.e. on the

lowest "floor" of the piece of composite material. The unit cell is $1 \times 1 \times 0.1$ in size, the heigh being given from the fibre thickness, which in this case is 0.05, and the number of "floors". The next fibre generally crosses the first, climbing over it to occupy some volume on the second floor, above the first fibre, in accordance with a smooth third-degree polynomial spline, as shown in Figure 2.

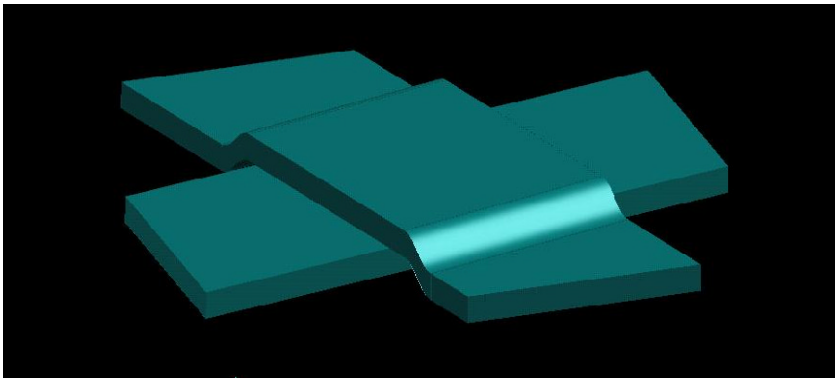

Figure 2: *Fibre crossing.*

As more fibres are added, the geometry typically becomes like that shown in Figure 3. The fibre network preprocessor also creates the geometry of the matrix material, which in boolean terms can be defined as the volume of the unit cell minus the volume of the fibre network, as shown in Figure 4.

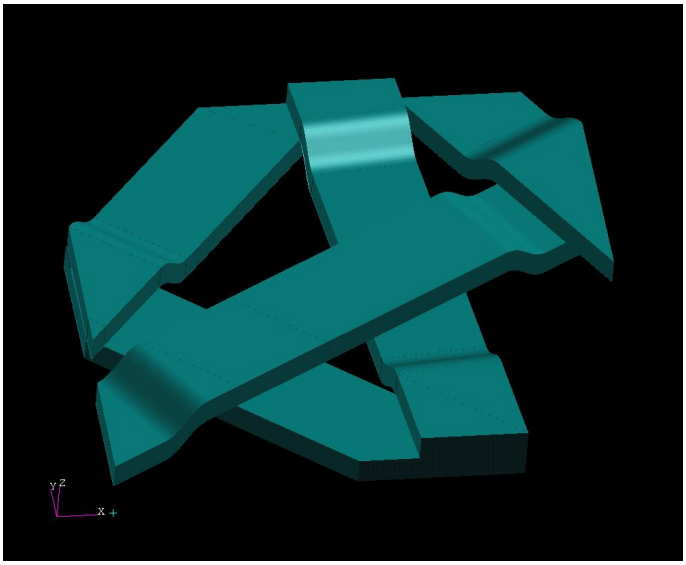

Figure 3: *Network of five fibres.*

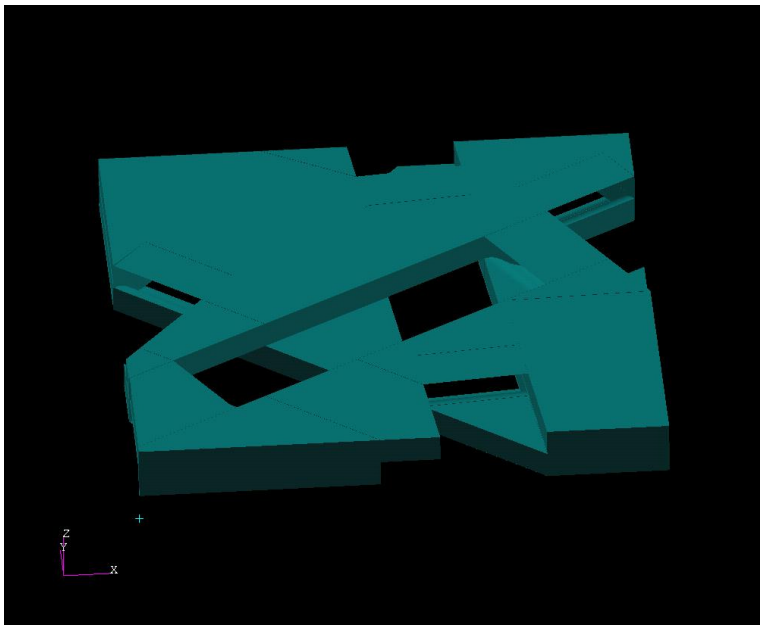

Figure 4: *Geometry of the corresponding matrix material.*

The indata to the preprocessor includes the width, thickness, orientation and location of the fibres, the number of fibres and a slope distance that determines the steepness of the fibre slope that results from the fibres climbing over each other. This determines the maximum of the fibre volume fraction. The maximum of the degree of fibre packing is achieved by use of large fibres placed in a physically realistic way so that they occupy as few "floors" as possible. In Figure 3 five fibres are placed so that they occupy only two "floors". The degree of fibre packing is limited by the slope distances and by the fact that they are assumed to be perpendicular to the longitudinal direction of the fibres. Without using very regular geometries, it is difficult, therefore, to achieve a fibre volume fraction of over 40 %.

2.3 Finite Element Calculations

The finite element mesh is generated in Patran by its producing surface elements that are extruded to the next floor to form hexagonal, iso-parametric 8-node solid elements, see Figure 5. The average element length in the x- and the y-direction is 1/20 the unit cell length. A fibre is modelled by use of about 200 elements. The five-fibre model employs an element thickness of half a "floor". This results in there being four elements in the z-direction, since the model consists of two "floors". The most difficult part of the finite element modelling is

to make the elements between two "floors" compatible, such that the mesh for both "floors" is identical. This is achieved by dividing the "floors" into smaller sections, identical for both "floors". Problems of this sort are based on the fact that Patran is not an ideal solid modeller. The finite element model typically involves about 5000 nodes, which give a system of equations with about 15000 degrees of freedom. These equations are solved in about 20 s, using a single work station.

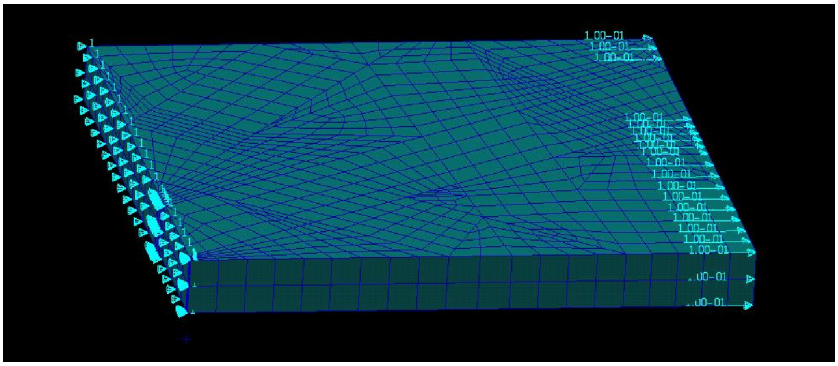

Figure 5: *Unit cell created from the geometries shown in Figure 3 and 4, with a finite element mesh.*

3 Material Properties

The matrix material considered in this study is a phenolic resin assumed to be isotropic, having a Young's modulus of 5.75 Gpa [5] and a Poisson's ratio of 0.3. The hygroexpansion coefficient, β, is defined as the increase in free strain for a given increase in moisture content, expressed in percent. The unit for β is [1/%]. A wood fibre is modelled as a transverse isotropic solid having the material properties shown in Tables 1 and 2. Note that the hygroexpansion coefficients in the transverse directions are estimated to be 26 times as great as those in the longitudinal direction [16]. The adhesion of the constituents is assumed to be perfect and without any chemical interaction or adsorption.

4 Homogenisation Procedure

Homogenisation is performed by exposing the unit cell to a prescribed deformation in the x-, y- and z-directions, respectively. During the prescribed deformation in the x-direction, the two cell boundaries with a normal vector in the

Table 1: *Elastic properties of wood fibres and of phenolic resin.*

Fibre						Matrix	
E_x [MPa]	$E_y = E_z$ [MPa]	$\nu_{xy} = \nu_{xz}$ [-]	ν_{yz} [-]	$G_{xy} = G_{xz}$ [MPa]	G_{yz} [MPa]	E [MPa]	ν [-]
40 000	5 000	0.2	0.3	4 000	1 920	5 750	0.3

Table 2: *Hygroexpansion properties of wood fibres, longitudinal and transverse, and of phenolic resin.*

Fibre		Matrix
β_L [1/%]	β_T [1/%]	β [1/%]
0.01	0.26	0.01

x-direction are forced to remain plane. The tangential forces acting on these boundaries are set equal to zero. All the other boundaries are free. The conditions when loading in the y- and z-directions are analogous. A prescribed shear deformation in the x-y-plane is achieved by giving the boundaries with a normal vector in the y-direction a displacement in the tangential, x-direction.

The average strain and the average stress are calculated according to

$$\varepsilon^*_{ij} = \frac{1}{V}\int_V \varepsilon_{ij} dV \qquad (1)$$
$$\sigma^*_{ij} = \frac{1}{V}\int_V \sigma_{ij} dV$$

where ε^*_{ij} are the estimated average strain components and σ^*_{ij} the estimated average stress components calculated over the unit cell volume, V [1]. In the finite element model the integrals are replaced by sums of the stiffnesses and strains of the element, which are constant in the case of 8-node elements. The estimated stiffness components, D^*_{ijkl}, are obtained by use of the corresponding compliance relation

$$\varepsilon^*_{ij} = C^*_{ijkl}\sigma^*_{kl} \qquad (2)$$

for an orthotropic material. From the normal strain and stress components ε^*_{xx}, ε^*_{yy} and ε^*_{zz} and σ^*_{xx} obtained for loading in the x-direction are E_x, ν_{xy} and ν_{xz} easy to calculate. The other stiffness parameters are analogously found from the stress and strain results for loading in the other directions.

The hygroexpansion coefficients are determined by exposing the unit cell to an increase in moisture content and calculating the average strain in all directions. It is assumed here that both constituents have the same increase in moisture content. The constituents increase in the moisture content may in general, depending on the properties of the constituents, be different for a given change in climate.

5 Model Verification and Comparisons

5.1 Simple Two-Fibre Model

The only possibility of reproducing a fibre volume fraction as high as 75 %, which is the volume fraction in the core layer of some HPL materials, is to model only two fibres at a single crossing. Here the width of the fibre is 75 % of the unit cell width and the fibre height is half of the unit cell height. In Table 3 the Young's moduli of this model are compared with the analytical and the measured results. The experimental values are obtained by measuring the core layer of an HPL consisting to 75 % of craft paper and to 25 % of phenolic resin [2]. The analytical model uses the material properties shown in Table 1, along with the same fibre width and height as in the numerical model.

Table 3: *Young's modulus of the composite.*

Numerical		Experimental		Analytical	
E_x [GPa]	E_y [GPa]	E_x [GPa]	E_y [GPa]	E_x [GPa]	E_y [GPa]
15.7	15.2	15.5	10.5	14.4	10.6

The simulated value for E_y here is a bit higher than the values obtained from measurements or from analytical predictions, since the numerical two-fibre model fails to reproduce the fibre orientation distribution correctly. The two-fibre model is equivalent to a cross laminate, whereas the values obtained from the measurements and from the analytical model represent orientation distributions that are continuous and involve 1.8 times more fibres in the x- than in the y-direction.

5.2 Differing Material Structure

The influence of the micro-structure geometry was studied by analysing three different unit cells, each containing five fibres and having an approximate fibre

volume fraction of 45 %. The fibre orientations are plotted in Figure 6.

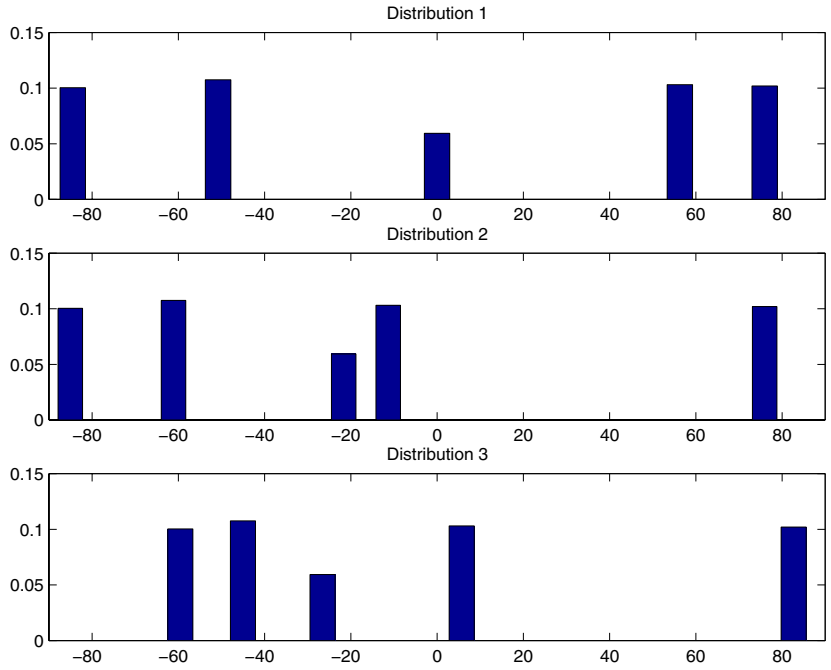

Figure 6: *Fibre angle distribution, $\varphi = 0$ indicating the x-direction. The height of the bar indicates the relative volume of the fibre.*

The Young's moduli, the shear moduli and the hygroexpansion coefficients as calculated for the three fibre distributions are shown in Table 4

Table 4: *Young's moduli and shear moduli in GPa and the hygroexpansion coefficients in 1/% for a composite.*

i	E_x	E_y	E_x	G_{xy}	G_{xz}	G_{yz}	β_x	β_y	β_z
1	9.21	6.70	5.71	1.40	2.25	2.52	0.057	0.051	0.13
2	8.80	11.51	5.71	2.12	2.33	2.42	0.050	0.041	0.12
3	10.41	8.83	5.65	2.56	2.36	2.37	0.053	0.054	-
mean	9.47	9.01	5.69	2.03	2.31	2.44	0.053	0.049	0.13

The variability of the in-plane-stiffnesses, E_x, E_y and G_{xy}, is greater than that of the out-of-plane stiffnesses, E_z, G_{xz} and G_{yz}. This is a reasonable result since it is the in-plane orientation that is varied. Micro-structure variations have less impact on the hygroexpansion coefficients than on the stiffness parameters. In addition, the variability of the hygroexpansion is of the same magnitude in all

three directions. The three structures studied can be regarded as three samples from a single composite material with a globaly uniform fibre orientation distribution. Depending on required accuracy in the calculated homogenised stiffness and hygroexpansion, the results of Table 4 give suggestions about the required number of simulations.

5.3 Differing Matrix Material Stiffnesses

A parameter study on the composite stiffness and the hygroexpansion as a function of the stiffness of the matrix material was carried out using both the analytical model and the numerical model, for a geometry of the type shown in Figure 3 and with a 40 % fibre volume fraction. For the analytical model, fibres of infinite length having an orthotropic fibre distribution were employed. The stiffness of the matrix material was varied from $E_m = 0$ to $E_m = 10$ GPa. The results are shown in Figures 7 and 8.

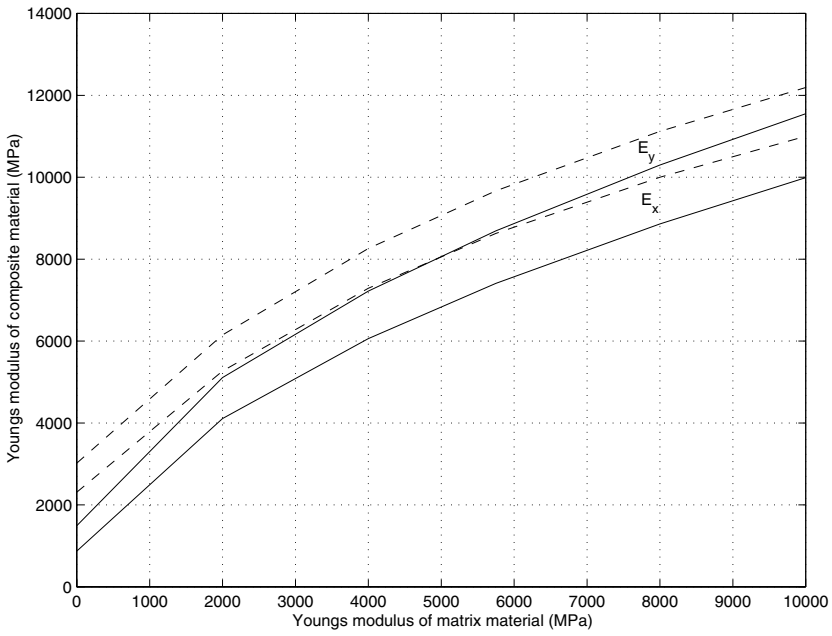

Figure 7: *Young's modulus of the composite in the $x-$ and $y-$ direction. Solid lines = numerical model, dashed lines = analytical model.*

The curves for the Young's moduli in the x- and the y-direction are similar, although the analytical results suggest the stiffness to be greater than that obtained using the numerical model, particularly in the case of low matrix stiffness. This is probably due to the steep slopes found in the numerical model, making

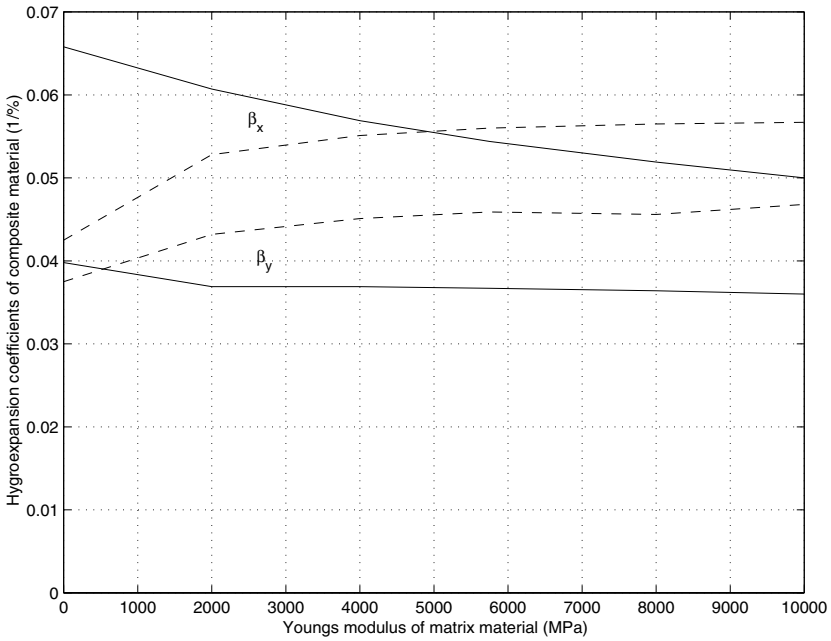

Figure 8: *Composite hygroexpansion coefficients in the $x-$ and $y-$ direction. Solid lines = numerical model, dashed lines = analytical model.*

the fibres bend under longitudinal load. The hygroexpansion coefficient values for the two models are within approximately the same range. There is a basic difference, however, in the prediction of hygroexpansion they give for low matrix material stiffness, E_m. Whereas the analytical model predicts a decrease in hygroexpansion with a decrease in E_m, the numerical model predicts an increase in hygroexpansion with a decrease in E_m. The fact that at low E_m values the hygroexpansion the numerical model predicts is greater than that which the analytical model provides appears logical, since at low E_m values the stiffness which the numerical model predicts is lower.

The stress distribution of the fibre phase of the composite under a prescribed deformation in the x-direction is illustrated in Figure 9. It can be seen that the fibre ranging from the left boundary is exposed to the highest stress, which is logical since the loading is in the x-direction. The material stresses in the matrix are illustrated in Figure 10.

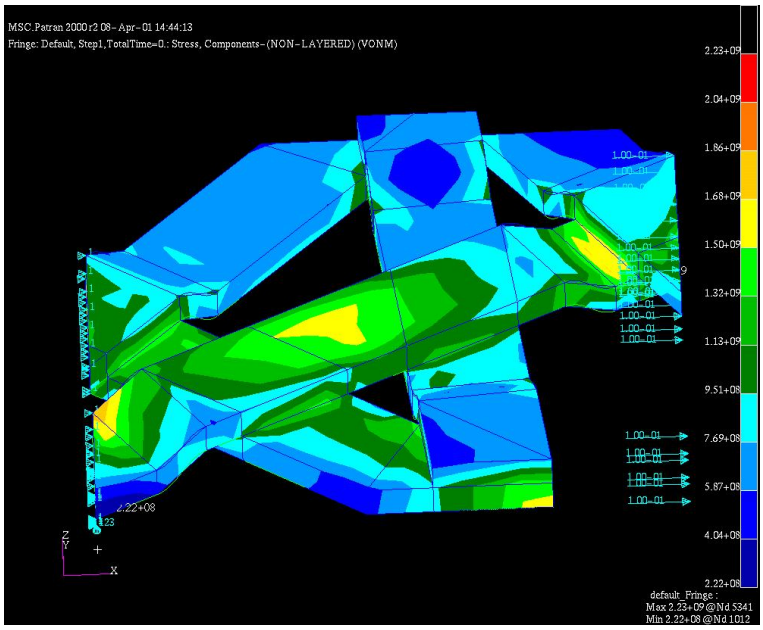

Figure 9: *A von Mises stress distribution of the fibre phase during prescribed elongation in the x-direction. Stress unit: Pa*

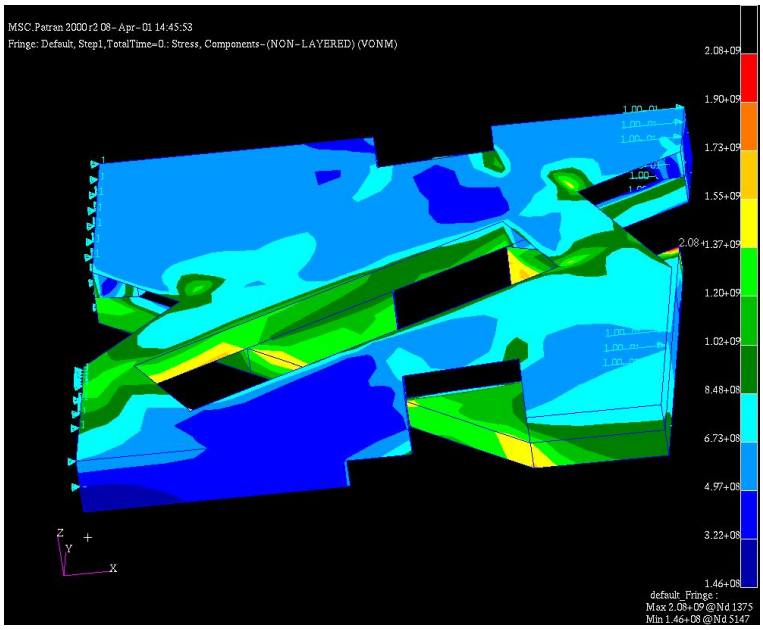

Figure 10: *A von Mises stress distribution of the matrix material phase during prescribed elongation in the x-direction. Stress unit: Pa*

6 Concluding Remarks

A 3D finite element model for the stiffness and hygroexpansion analysis of fibre composite materials was presented. The model provides a good representation of the microstructure of a composite material, such as HLP, and opens up for many possibilities, such as that of creating models of the complex microstructures of various composite materials, perhaps simply on the basis of the information contained in microscopic images. Parameter studies can also be performed of any parameter. The behaviour of new materials which do not yet exists can be analysed as well. The model can also be used to simulate network mechanics models, such as of paper, without the use of matrix material. The model provides reasonably accurate estimates of the stiffness and hygroexpansion of a composite through use of a five-fibre version of the model and of three nominally equal simulations. The five-fibre model may not be sufficient, however, for simulating fibre networks without matrix materials.

In this study only time-independent properties were investigated. The model is also intended, however, for future use in studies of time dependent properties such as creep and mechanosorption which are important for wood and wood composite materials.

7 Future Work

The model studied here was developed as a tool for the analysis of long fibre network composites such as HPL, but it can be developed further so as to achieve an even better representation of the morphology of the composite:

- The fibre packing can be increased to well above the present maximum of about 45% for a multi-fibre random geometry. This can be done by making the fibre shape more flexible, allowing the fibres to be curved in the plane, be twisted or be of varying width and thickness.

- Use of larger unit cells containing more fibres is required to obtain a better representation of a random structure with a continuous fibre orientation distribution. This will result in lesser variability between nominally equal simulations and will accordingly require fewer simulations in order for accurate mean value estimates to be made. The use of larger models will be facilitated by the ongoing development of more efficient finite element software and of faster computers.

- The fibre geometry and its internal structure can be more accurately represented by modelling it as a collapsed pipe in which the inclination of an orthotropic orientation in the fibre walls is induced by the micro-fibril angle.

References

[1] Aboudi, J. (1991). *Mechanics of Composite Materials*, Elsevier, Amsterdam, The Netherlands, 14-18.

[2] Andersson, B. (1999). *Composite Materials' Hygroexpansion Properties.* Master Thesis, Report TVSM-3018, Division of Structural Mechaics, Lund University, Sweden.

[3] Adl Zarrabi, B. (1998). *Hygro-Elastic Deformation of High Pressure Laminates*, Doctoral thesis, Div. of Building Material, Chalmers University of Technology, Göteborg, Sweden

[4] Baldwin, J. D., Altan, M. C., Rajamani, K., (1997). "Structural Analysis of an Injection Molded Short-Fiber-Reinforce Disc". *Journal of Materials Processing and Manufacturing Science*, 6, 123-145.

[5] Barth, Th. (1984). "Der Einfluss der Feuchteaufnahme auf die mechanischen Eigenschaften von Phenolplasten." *Z. Werkstofftech*, Verlag Chemie, Weinheim, Germany, 15, 299-308.

[6] Christman, T., Needleman, A., Suresh, S. (1989). "On Microstructural Evolution and Micromechanical Modelling of Deformation of a Whisker-reinforced Metal-Matrix Composite", *Materials Science and Engineering*, A107, 49-61.

[7] Dasgupta, A., Agarwal, R. K., Bhandarkar, S. M. (1996). "Three-Dimensional Modeling of Woven-Fabric Composites for Effective Thermo-Mechanical and Thermal Properties". *Composites Science and Technology*, 56, 209-223.

[8] Falzon, P. J., Herszberg, I. (1996). "Effects of Compaction on the Stiffness of Plain Weave Fabric RTM Composites". *Journal of Composite Materials*, 30, 1210-1247.

[9] Garnich, M. R., Hansen, C. (1997). "A Multicontinuum Theory for Thermal-Elastic Finite Element Analysis of Composite Materials". *Journal of Composite Materials*, 31, 71-86.

[10] Ghassemieh, E., Nassehi, V. (2001). "Stiffness Analysis of Polymeric Composites Using the Finite Element Model". Advances in Ploymer Technology, 20, 42-57.

[11] Hashin, Z. (1983) "Analysis of Composite Materials, A Survey", *Journal of Applied Mechanics*, 9, 481-505.

[12] Heyden, S. (2000). *Network modelling for the evaluation of mechanical properties of cellulose fibre fluff.*, Doctoral thesis, Report TVSM-1011, Div. of Structural Mechanics, Lund University, Sweden.

[13] Ismar, H., Schroter, F., Streicher, F. (2000). "Modeling and Numerical Simulation of the Mechanical Behaviour of Woven SiC/SiC regarding a Three-Dimensional Unit Cell". *Computational Materials Science*, 19, 320-328.

[14] Matlab - *The language of technical computation.* (1998) The Math Works Inc., Natick, Ma, USA.

[15] Nilsen, N., Niskanen, K. (1996) "A 3D simulation model for paper structure." *Progress in Paper Physics - A Seminar Proceedings.*

[16] Persson, K. (2001). *Micromechanical modelling of wood and fibre properties.* Doctoral thesis, Division of Structural Mechanics, Lund University, Sweden.

[17] Stahl, D. C., Cramer, S. M. (1998). "A Three-Dimensional Network Model for a Low Density Fibrous Composite". *Journal of Engineering Materials and Technology*, 120, 126-130.

[18] Stålne, K., Gustafsson, P. J. (2000). "A 3D Model for Analysis of Stiffness and Hygroexpansion Properties of Fibre Composite Materials", *Journal of Engineering Mechanics*, in press.

[19] Termonia, Y. (1994). "Structure-Property Relationships in Short-Fiber-Reinforced Composites". *Journal of Polymer Science, Part B: Polymer Physics*, 32, 969-979.

[20] Thom, H. (1999). "Finite Element Modeling of Plain Weave Composites" *Journal of Composite Materials*, 33, 1491-1510.

[21] Toll, S. (1998). "Packing Mechanics of Fiber Reinforcements". *Polymer Engineering and Science*, 38, 1337-1350.

[22] Tucker, C.L., Liang, E. (1999). "Stiffness Predictions for Unidirectional Short-Fiber Composites: Review and Evaluation" *Composites Science and Technology* 59, 655-671.

[23] Whitcomb, J. D., Chapman, C. D., Tang, X. (2000). "Derivation of Boundary Conditions for Micromechanics Analyses of Plain and Satin Weave Composites". *Journal of Composite Materials*, 34, 724-747.

[24] Zeman, J., Sejnoha, M., (2001). "Numerical Evaluation of Effective Elastic Properties of Graphite Fiber Tow Impregnated by Polymer Matrix". *Journal of the Mechanics and Physics of Solids*, 49, 69-90.

Paper III

III

3D Homogenisation of Hygroscopic Anisotropic Fibre Network Composites

Kristian Stålne

Submitted for publication

3D Homogenisation of Hygroscopic Anisotropic Fibre Network Composites

Kristian Stålne
Division of Structural Mechanics
Lund University
P.O. Box 118,
S-221 00 Lund, Sweden

Abstract

A 3D model of the behaviour of wood fibre composite materials exposed to loading and to changes in moisture content is presented. The model represents a homogenisation which, for a given fibre-orientation distribution predicts the time-dependent strain in a composite material from the properties of the fibre and matrix materials of which it consists. Homogenisation of the constituent materials is carried out under the assumption of homogenous strain, i.e. according to laminate theory. The constituents are modelled using a combination of spring, dashpot and expansion elements to simulate the viscoelastic, mechanosorptive and hygroexpansion parts of the strain. The resulting model is a differential equation having time-dependent coefficients. In a simplified case, the differential equation is solvable analytically, whereas for the complete model a numerical implementation is required. The model is investigated for different cases of moisture variation, loading and composite composition.

Keywords: Wood composites, analytical modelling, homogenisation, stiffness, viscoelasticity, mechanosorption, hygroexpansion, moisture.

INTRODUCTION

Wood-fibre-based composite materials have been used increasingly in the building industry, and to some extent in the automotive industry as well. One example of this is high pressure laminate, HPL, a material made up of layers of paper and impregnated with melamine and phenolic resin. Used in such applications as flooring and panelling, it is stiff, strong, durable and water resistant [2]. An important issue in the use of wood-based composite materials is their instability in shape in response to changes in climate, in terms both of their short- and long term performance. Accordingly, models are needed able to accurately predict the behaviour of wood-fibre composites when used in particularly demanding environments and for load carrying purposes.

General surveys of models of the time-dependent properties of composite materials are provided by Aboudi [1] and by Flügge [9]. Theoretical analyses of the linear viscoelastic behaviour of unidirectional transversal composite materials have been presented by Kaliske [13], Luciano [15], Barbero [4] and Klasztorny [14]. Studies have also been made of the hygrothermal behaviour of composites

[5]. Only few models of wood-fibre composites have been advanced, one made by Brauns [6]. A model of the elastic stiffness and hygroexpansion properties of wood-fibre composites has been presented earlier by the author [22]. Comprehensive investigations of the load- and moisture-induced straining of solid wood have been reported in doctoral dissertations of Mårtensson [17], Svensson [24] and Hanhijärvi [11]. These involve the measurement and modelling of strain in one dimension. More advanced constitutive modelling of solid wood taking account of three dimensional deformation has been performed by Ormarsson [19]. Micro-mechanical models of mechanosorption in paper have been developed by Alftan [3] for describing the phenomena shown in Figure 1. Any composite material modelling of the basic three dimensional behaviour of wood-fibre composites when exposed to load and to varying climatic conditions giving creep and mechanosorptive strain has not been found in available literature.

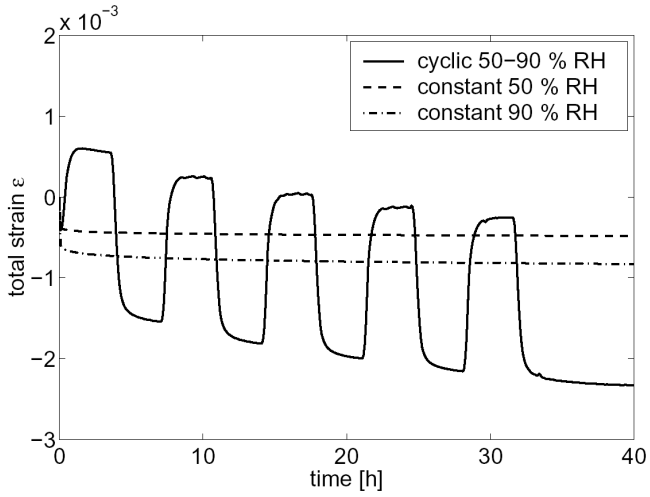

Figure 1: Example of mechanosorptive creep in paper material [8].

The aim of the model presented is to analytically predict the three-dimensional mechanical behaviour of a wood fibre network composite material under arbitrary loading and moisture conditions from the known mechanical properties of the composites constituents. Phenomenons taken into consideration by the model are elastic strain, creep, mechanosorption, hygroexpansion, a network consisting of anisotropic fibres with arbitrary orientation distribution function, proportions of the constituents and the possibility of porosity. The model is an analytical homogenisation resulting in a differential equation defining the constitutive properties of the composite material. This is achieved through rigorous calculations.

In order to make the analysis feasible a number of assumptions are required. Most important is that the homogenisation is carried out under the assumption of homogenous strain, or parallel coupling, which in composite mechanics is often referred to as laminate theory. The assumption, which gives an upper bound for the predicted stiffness of composite materials, has been shown to give a sufficiently accurate result in the case of laminated fibre network composites, such as HPL. A recent numerical study showed that the homogeneous strain assumption will overestimate the composite stiffness with approximately 15 percent for this material, using the same set of indata

[23]. The results obtained include constitutive equations for fibre network materials containing no matrix material, such as fibreboard, and for fibre composite materials.

The stress- and strain model of the constituent materials can be described by a system of springs and dashpots, the total strain being the sum of the contributions of the elastic, creep, mechanosorptive and hygroexpansion strains. It is assumed that the fibre material is orthotropic, that the matrix material neither chemically interacts with nor is absorbed by the fibre walls and that the fibre and matrix materials are completely bonded. It is likewise assumed that the matrix material is isotropic but that the composite material can be anisotropic, depending upon its fibre-orientation distribution. Porosity is taken into account by relating stress to the net cross-sectional area of the dense material. It is also assumed that the product analyzed is much larger than the micro-scale, where the homogenisation is performed, so that the composite can be regarded as a homogenous material. At the micro-scale the moisture gradient is neglected.

The homogenisation results in differential equations of varying order, depending upon the complexity assumed for the performance of the constituents. Various numerical examples presented below illustrate the performance of the composite material corresponding to particular assumptions. Numerical methods are generally required to assess the performance under a given set of conditions, although making certain material property assumptions allows analytical solutions to be found.

APPROACH OF THE MODEL

The homogenisation of the fibre network composite material is performed in three steps. First, the constitutive equations of the material in a single fibre and in the matrix material are developed in the form of two differential equations, one for each of the two constituents. Then the constitutive equation for the fibre network is calculated from the equation for the fibre material and the fibre-orientation distribution. Finally, the matrix material is taken into account in the equation for the composite material.

The choice of a constitutive model for a single fibre is based on the observed behaviour of wood and of wood-based materials and also on previously proposed models of wood materials [19, 24]. The strain increment is set equal to the sum of the elastic, creep, mechanosorptive and hygroexpansion strain increments, as shown in Figure 2. The creep part of the strain is modelled using a Kelvin element, namely a spring parallel-coupled to a dashpot. The spring prevents the fibre material from acting as a liquid as though no limits were placed on the creep strain. The mechanosorptive part is modelled by use of an element symbolically similar to the creep element, but with the strain rate in the dotted mechanosorptive dashpot made proportional to the stress and to the absolute value of the rate of change in moisture content.

The same choice of a constitutive model is employed for the matrix material, although the mechanosorptive part of the strain increment is disregarded, since no effects of that sort have been reported for thermosets or similar matrix materials like, such as for melamine-formaldehyde [10]. In addition,

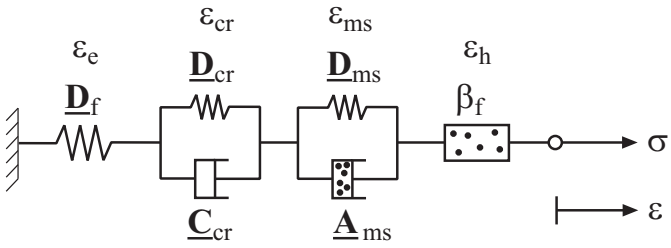

Figure 2: System of springs and dashpots describing the fibre material.

the elastic stiffness of the matrix material is assumed to be independent of the moisture content.

Certain further simplifications of the material model are necessary to make the analysis feasible. The major approximation made is to regard all time effects and moisture effects as scalar functions. This involves, firstly, all four matrices defining the creep and the mechanosorptive properties, $\mathbf{C}_{cr}, \mathbf{D}_{cr}, \mathbf{A}_{ms}$ and $\mathbf{D}_{ms}$, being assumed to be equal to the elastic stiffness matrix, $\mathbf{D}_f$, times a scalar function. Secondly, the moisture-dependent elastic stiffness matrix of the fibre material is set equal to a scalar function describing the moisture dependency times a matrix $\mathbf{D}_0$, defined as the elastic stiffness matrix at some reference level for moisture content. The same moisture dependency is assumed to be valid for the creep properties. The matrices that define the mechanosorptive material parameters are assumed to not be affected by the moisture content of the material.

The first step in development of the model from which the constitutive differential equations of the constituents are derived consists of summing strain-time derivatives of various orders involved in accordance with a scheme created for systematizing the procedure. In the second step, homogenisation from a single fibre to the fibre network is performed by integration over all the fibre directions. There are two basic alternatives for homogenizing composite materials, the one involves a homogenous strain assumption and the other a homogenous stress assumption. The homogenous strain assumption, or the parallel-coupling case, will be employed here. This means assuming that all the constituents of the composite are in the same state of strain, which although overestimating the stiffness of the composite material appears to provide a more accurate result than use of the homogenous stress assumption [21]. In the case of fibre network composite materials with long fibres bonded together the assumption is considered to give a fairly accurate homogenisation. Homogenisation is performed by integrating the fibre stresses contributing to the total stress. The fibre network equation obtained can be shown to be identical in structure with the equation describing a single fibre. This is an important result. It is based on the fact that the time effect functions chosen are scalar.

The last step in developing the model is to perform the homogenisation between the fibre network and the matrix material. This too involves making the homogenous strain assumption. The stresses and their derivatives are summed according to a scheme similar to the one described above.

The resulting constitutive equation for the composite material is a fourth-order differential equation for the strain vector, having nonlinear, matrix-valued coefficients, which in the general case are comprehensive functions of such factors as the moisture content and the material parameters.

A differential equation of lower order is obtained by making the constituents models simpler, e.g. by setting the creep spring stiffness to zero, lowering the order of the final equation by one. When modelling creep using one Kelvin element the indata, the constituents creep parameters, have to be chosen so that they give a correct description at the time scale of interest. The creep behaviour can also be described by adding further Kelvin elements in series. This increases the order of the constitutive equation by one per Kelvin element added. This way the model can be made valid at more than one time scale.

The performance of the model will be illustrated by a series of numerical examples. An analytical solution found for a simple case will be compared with the corresponding numerical solution. The numerical examples given concern predictions of the strain history of a composite under differing conditions of load and of moisture history.

THE CONSTITUTIVE EQUATION FOR A FIBRE MATERIAL

Strain Increment Components

The total strain increment of a single fibre is modelled as the sum of the increments of the elastic, creep, mechanosorptive and hygroexpansion strain contributions:

$$\dot{\underline{\boldsymbol{\varepsilon}}} = \dot{\underline{\boldsymbol{\varepsilon}}}_e + \dot{\underline{\boldsymbol{\varepsilon}}}_{cr} + \dot{\underline{\boldsymbol{\varepsilon}}}_h + \dot{\underline{\boldsymbol{\varepsilon}}}_{ms} \tag{1}$$

where $\dot{\underline{\boldsymbol{\varepsilon}}} = [\dot{\varepsilon}_x \quad \dot{\varepsilon}_y \quad \dot{\varepsilon}_z \quad \dot{\varepsilon}_{xy} \quad \dot{\varepsilon}_{xz} \quad \dot{\varepsilon}_{yz}]^T$ is the column vector containing the time derivative of all the strain components. The shear strains are defined as half the total shear angle, i.e. $\varepsilon_{xy} = (u_{x,y} + u_{y,x})/2 = \gamma_{xy}/2$, etc. Henceforth, the underlining of a matrix or a column vector and printing of the coordinate indices (x, y, z) in lower case letters will be used to indicate that the matrix or vector in question is to be evaluated in terms of the local fibre-coordinate system. Matrices and vectors appear in the global coordinate system without underlining and with the coordinate indices capitalized (X, Y, Z).

The elastic strain increment is defined in terms of the elastic stiffness matrix $\mathbf{D}_f(w)$, which is assumed to be orthotropic,

$$\dot{\underline{\boldsymbol{\varepsilon}}}_e = (\underline{\mathbf{D}}_f(w))^{-1} \dot{\underline{\boldsymbol{\sigma}}}_f \tag{2}$$

where $\dot{\underline{\boldsymbol{\sigma}}}_f = [\dot{\sigma}_x \quad \dot{\sigma}_y \quad \dot{\sigma}_z \quad \dot{\sigma}_{xy} \quad \dot{\sigma}_{xz} \quad \dot{\sigma}_{yz}]^T$ is the column vector containing the time derivatives of all the stress components in a fibre. The stiffness matrix $\underline{\mathbf{D}}_f(w)$ can vary with the moisture content w.

The creep strain increment is modelled by use of a parallel-coupled spring and a dashpot, commonly designated as a Kelvin element. The stiffness matrix of the spring is denoted as $\underline{\mathbf{D}}_{cr}(w)$ and the creep viscosity matrix as $\underline{\mathbf{C}}_{cr}(w)$, defined by $\dot{\underline{\boldsymbol{\varepsilon}}}_{cr} = \underline{\mathbf{C}}_{cr}\, \underline{\boldsymbol{\sigma}}_{cr}$. This enables the constitutive equation of the Kelvin element to be written:

$$\underline{\boldsymbol{\sigma}}_f = \underline{\mathbf{C}}_{cr}^{-1} \underline{\dot{\boldsymbol{\varepsilon}}}_{cr} + \underline{\mathbf{D}}_{cr} \underline{\boldsymbol{\varepsilon}}_{cr} \tag{3}$$

The mechanosorptive strain increment is modelled as an element consisting of an elastic spring of stiffness $\mathbf{D}_{ms}$, coupled in parallel with a moisture-rate dashpot, the resulting strain rate being proportional both to the stress and proportional to the absolute value of the rate of change in moisture content, $\mathbf{A}_{ms}|\dot{w}|$, which yields

$$\underline{\boldsymbol{\sigma}}_f = (\underline{\mathbf{A}}_{ms}|\dot{w}|)^{-1}\underline{\dot{\boldsymbol{\varepsilon}}}_{ms} + \underline{\mathbf{D}}_{ms}\underline{\boldsymbol{\varepsilon}}_{ms} \tag{4}$$

The material parameter matrices $\underline{\mathbf{A}}_{ms}$ and $\underline{\mathbf{D}}_{ms}$ are not considered to be moisture dependent.

The hygroexpansion strain increment is denoted by a moisture-dependent hygroexpansion coefficient vector $\underline{\boldsymbol{\beta}}_f(w)$, which yields a strain increment of

$$\underline{\dot{\boldsymbol{\varepsilon}}}_h = \underline{\boldsymbol{\beta}}_f(w)\ \dot{w} \tag{5}$$

Simplifications by Means of Material Parameter Coupling

In the general case, the components of the matrices $\underline{\mathbf{D}}_f$, $\underline{\mathbf{C}}_{cr}$, $\underline{\mathbf{D}}_{cr}$, $\underline{\mathbf{A}}_{ms}$, $\underline{\mathbf{D}}_{ms}$ and of the vector $\underline{\boldsymbol{\beta}}_f$, which define the properties of the material, are all independent functions of the moisture content w, which in turn is a function of time, such that $w = w(t)$. Two simplifications are introduced here. The first is to define the influence of w on the material parameters by means of two scalar dimensionless functions, $p(w)$ and $q(w)$, only. The second simplification is to assume that the material-parameter matrices $\underline{\mathbf{D}}_f$, $\underline{\mathbf{C}}_{cr}$, $\underline{\mathbf{D}}_{cr}$, $\underline{\mathbf{A}}_{ms}$ and $\underline{\mathbf{D}}_{ms}$ are coupled with each other by means of four scalar constants, τ_f, μ_f, α_f and λ_f.

According to the first simplification the elastic stiffness is

$$\mathbf{D}_f(w) = p(w)\mathbf{D}_0 \tag{6}$$

and the hygroexpansion coefficient vector is

$$\underline{\boldsymbol{\beta}}_f(w) = q(w)\underline{\boldsymbol{\beta}}_0 \tag{7}$$

where

$$\underline{\mathbf{D}}_0 = \begin{bmatrix} \frac{1}{E_x} & -\frac{\nu_{yx}}{E_y} & -\frac{\nu_{zx}}{E_z} & 0 & 0 & 0 \\ -\frac{\nu_{xy}}{E_x} & \frac{1}{E_y} & -\frac{\nu_{zy}}{E_z} & 0 & 0 & 0 \\ -\frac{\nu_{xz}}{E_x} & -\frac{\nu_{yz}}{E_y} & \frac{1}{E_z} & 0 & 0 & 0 \\ 0 & 0 & 0 & \frac{1}{2G_{xy}} & 0 & 0 \\ 0 & 0 & 0 & 0 & \frac{1}{2G_{xz}} & 0 \\ 0 & 0 & 0 & 0 & 0 & \frac{1}{2G_{yz}} \end{bmatrix}^{-1} \tag{8}$$

and

$$\underline{\boldsymbol{\beta}}_0 = [\beta_x\ \ \beta_y\ \ \beta_z\ \ 0\ \ 0\ \ 0]^T \tag{9}$$

the components of $\underline{\mathbf{D}}_0$ and $\underline{\boldsymbol{\beta}}_0$ being evaluated at the initial moisture content $w_0 = w(t_0)$. The moisture functions $p(w)$ and $q(w)$ are assumed to be independent and continuous. Equations (6)

and (7) state that a change in moisture content over time influences the stiffness and the hygroexpansion properties to the same extent in all directions.

The second simplification results in

$$\underline{\mathbf{C}}_{cr} = \frac{1}{\tau_f}\underline{\mathbf{D}}_f^{-1} \tag{10}$$

$$\underline{\mathbf{D}}_{cr} = \frac{1}{\mu_f}\underline{\mathbf{D}}_f \tag{11}$$

$$\underline{\mathbf{A}}_{ms} = \frac{1}{\alpha_f}\underline{\mathbf{D}}_0^{-1} = \frac{p(w)}{\alpha_f}\underline{\mathbf{D}}_f^{-1} \tag{12}$$

$$\underline{\mathbf{D}}_{ms} = \frac{1}{\lambda_f}\underline{\mathbf{D}}_0 = \frac{1}{\lambda_f p(w)}\underline{\mathbf{D}}_f = \frac{1}{\lambda_f \alpha_f}\underline{\mathbf{A}}_{ms}^{-1} \tag{13}$$

The constants introduced, τ_f, μ_f, α_f and λ_f, are independent of w and thus independent of t as well. The constant τ_f has the dimension time, μ_f and λ_f are dimensionless and α_f has the same dimension as $[w]$, i.e. dimensionless, e.g. kg/kg. From this it follows that the matrix products

$$\underline{\mathbf{C}}_{cr}\underline{\mathbf{D}}_{cr} = \frac{1}{\mu_f \tau_f}\mathbf{I} \tag{14}$$

$$\underline{\mathbf{A}}_{ms}\underline{\mathbf{D}}_{ms} = \frac{1}{\lambda_f \alpha_f}\mathbf{I} \tag{15}$$

are both independent of time.

These simplifications are needed not only to make the calculations feasible, but also to keep the number of material parameters at a minimum, important since each of the parameters needs to be determined by measurement or by estimation. The simplifications made represent reasonable appearing assumptions in engineering terms.

Differential Equation for the Material in a Single Fibre

The equations (2), (3), (4) and (5) are written as a single constitutive differential equation expressed in terms of the total fibre strain $\underline{\boldsymbol{\varepsilon}}$ and the total fibre stress $\underline{\boldsymbol{\sigma}}_f$. This is achieved by adding the strains and their derivatives in accordance with equation (1), which holds for all levels of the derivatives, and by derivation of both sides of equations (2), (3), (4) and (5) up to the third-order derivative. In terms of the constants introduced, for example, equation (4) can be written as

$$\dot{\underline{\boldsymbol{\varepsilon}}}_{ms} + \frac{1}{\lambda_f \alpha_f}|\dot{w}|\underline{\boldsymbol{\varepsilon}}_{ms} = \underline{\mathbf{D}}_f^{-1}\frac{1}{\alpha_f}|\dot{w}|\underline{\boldsymbol{\sigma}}_f \tag{16}$$

Derivation of both sides of the equation yields

$$\ddot{\underline{\boldsymbol{\varepsilon}}}_{ms} + \frac{1}{\lambda_f \alpha_f}|\dot{w}|\dot{\underline{\boldsymbol{\varepsilon}}}_{ms} + \frac{1}{\lambda_f \alpha_f}\dot{\overline{|\dot{w}|}}\underline{\boldsymbol{\varepsilon}}_{ms} = \underline{\mathbf{D}}_f^{-1}\frac{1}{\alpha_f}\left(|\dot{w}|\dot{\underline{\boldsymbol{\sigma}}}_f + (\dot{\overline{|\dot{w}|}} - |\dot{w}|\frac{\dot{p}}{p})\underline{\boldsymbol{\sigma}}_f\right) \tag{17}$$

and by derivation once more,

$$\underline{\boldsymbol{\varepsilon}}_{ms}^{(3)} + \tfrac{1}{\lambda_f \alpha_f} |\dot{w}| \ddot{\underline{\boldsymbol{\varepsilon}}}_{ms} + 2 \tfrac{1}{\lambda_f \alpha_f} \dot{\overline{|\dot{w}|}} \dot{\underline{\boldsymbol{\varepsilon}}}_{ms} + \tfrac{1}{\lambda_f \alpha_f} \ddot{\overline{|\dot{w}|}} \underline{\boldsymbol{\varepsilon}}_{ms} = \tag{18}$$
$$\underline{\mathbf{D}}_f^{-1} \tfrac{1}{\alpha_f} \left(|\dot{w}| \ddot{\underline{\boldsymbol{\sigma}}}_f + 2 \left(\dot{\overline{|\dot{w}|}} - |\dot{w}| \tfrac{\dot{p}}{p} \right) \dot{\underline{\boldsymbol{\sigma}}}_f + \left(\ddot{\overline{|\dot{w}|}} - 2 \dot{\overline{|\dot{w}|}} \tfrac{\dot{p}}{p} - |\dot{w}| (\tfrac{\ddot{p}}{p} - 2(\tfrac{\dot{p}}{p})^2) \right) \underline{\boldsymbol{\sigma}}_f \right)$$

since

$$\dot{\underline{\mathbf{D}}}_f = \frac{\dot{p}}{p} \underline{\mathbf{D}}_f \quad \texttt{and} \quad \dot{\overline{\underline{\mathbf{D}}_f^{-1}}} = -\frac{\dot{p}}{p} \underline{\mathbf{D}}_f^{-1} \tag{19}$$

The equations and the derivatives of these for the different strains that equations (16) to (18) represent can be combined into the system of equations shown in equation (20), where the zero- to the third-order derivatives of the strains which are to be eliminated are collected in a vector having, as sought, the third-order derivative of the total strain as its the first element. The coefficients of the strains in the equations are collected in a matrix having scalar coefficients. The elements of the vector contain all six components of each of the strains. Equations (18), (17) and (16) appear here in rows 4, 8 and 11, respectively, of the equation system. The elastic equations are found in rows 2, 6 and 10, the equations for the creep element in rows 3 and 7 and the equations for the hygroexpansion in rows 5, 9 and 12. The first row corresponds to the sum of the third derivatives of the strains $\underline{\boldsymbol{\varepsilon}}^{(3)} = \underline{\boldsymbol{\varepsilon}}_e^{(3)} + \underline{\boldsymbol{\varepsilon}}_{cr}^{(3)} + \underline{\boldsymbol{\varepsilon}}_{ms}^{(3)} + \underline{\boldsymbol{\varepsilon}}_h^{(3)}$. The sum of the second derivatives is found in row 14, equation (1) being found in row 13.

$$\begin{bmatrix}
1 & -1 & -1 & -1 & -1 & 0 & 0 & 0 & 0 & 0 & 0 & 0 & 0 & 0 \\
0 & 1 & 0 & 0 & 0 & 0 & 0 & 0 & 0 & 0 & 0 & 0 & 0 & 0 \\
0 & 0 & 1 & 0 & 0 & 0 & \frac{1}{\mu_f \tau_f} & 0 & 0 & 0 & 0 & 0 & 0 & 0 \\
0 & 0 & 0 & 1 & 0 & 0 & 0 & \frac{1}{\lambda_f \alpha_f} |\dot{w}| & 0 & 0 & 0 & 2 \frac{1}{\lambda_f \alpha_f} \dot{\overline{|\dot{w}|}} & 0 & \frac{1}{\lambda_f \alpha_f} \ddot{\overline{|\dot{w}|}} \\
0 & 0 & 0 & 0 & 1 & 0 & 0 & 0 & 0 & 0 & 0 & 0 & 0 & 0 \\
0 & 0 & 0 & 0 & 0 & 1 & 0 & 0 & 0 & 0 & 0 & 0 & 0 & 0 \\
0 & 0 & 0 & 0 & 0 & 0 & 1 & 0 & 0 & 0 & \frac{1}{\mu_f \tau_f} & 0 & 0 & 0 \\
0 & 0 & 0 & 0 & 0 & 0 & 0 & 1 & 0 & 0 & 0 & \frac{1}{\lambda_f \alpha_f} |\dot{w}| & 0 & \frac{1}{\lambda_f \alpha_f} \dot{\overline{|\dot{w}|}} \\
0 & 0 & 0 & 0 & 0 & 0 & 0 & 0 & 1 & 0 & 0 & 0 & 0 & 0 \\
0 & 0 & 0 & 0 & 0 & 0 & 0 & 0 & 0 & 1 & 0 & 0 & 0 & 0 \\
0 & 0 & 0 & 0 & 0 & 0 & 0 & 0 & 0 & 0 & 0 & 1 & 0 & \frac{1}{\lambda_f \alpha_f} |\dot{w}| \\
0 & 0 & 0 & 0 & 0 & 0 & 0 & 0 & 0 & 0 & 0 & 0 & 1 & 0 \\
0 & 0 & 0 & 0 & 0 & 0 & 0 & 0 & 0 & 1 & 1 & 1 & 1 & 0 \\
0 & 0 & 0 & 0 & 0 & 1 & 1 & 1 & 1 & 0 & 0 & 0 & 0 & 0
\end{bmatrix}
\begin{bmatrix}
\underline{\boldsymbol{\varepsilon}}^{(3)} \\
\underline{\boldsymbol{\varepsilon}}_e^{(3)} \\
\underline{\boldsymbol{\varepsilon}}_{cr}^{(3)} \\
\underline{\boldsymbol{\varepsilon}}_{ms}^{(3)} \\
\underline{\boldsymbol{\varepsilon}}_h^{(3)} \\
\ddot{\underline{\boldsymbol{\varepsilon}}}_e \\
\ddot{\underline{\boldsymbol{\varepsilon}}}_{cr} \\
\ddot{\underline{\boldsymbol{\varepsilon}}}_{ms} \\
\ddot{\underline{\boldsymbol{\varepsilon}}}_h \\
\dot{\underline{\boldsymbol{\varepsilon}}}_e \\
\dot{\underline{\boldsymbol{\varepsilon}}}_{cr} \\
\dot{\underline{\boldsymbol{\varepsilon}}}_{ms} \\
\dot{\underline{\boldsymbol{\varepsilon}}}_h \\
\underline{\boldsymbol{\varepsilon}}_{ms}
\end{bmatrix} =$$

$$\begin{bmatrix} \mathbf{0} \\ \underline{\mathbf{D}}_f^{-1}\underline{\boldsymbol{\sigma}}_f^{(3)} + 2\dot{\overline{\underline{\mathbf{D}}_f^{-1}}}\ddot{\underline{\boldsymbol{\sigma}}}_f + \ddot{\overline{\underline{\mathbf{D}}_f^{-1}}}\dot{\underline{\boldsymbol{\sigma}}}_f \\ \frac{1}{\tau_f}\left(\underline{\mathbf{D}}_f^{-1}\ddot{\underline{\boldsymbol{\sigma}}}_f + 2\dot{\overline{\underline{\mathbf{D}}_f^{-1}}}\dot{\underline{\boldsymbol{\sigma}}}_f + \ddot{\overline{\underline{\mathbf{D}}_f^{-1}}}\underline{\boldsymbol{\sigma}}_f\right) \\ \frac{p}{\alpha_f}\underline{\mathbf{D}}_f^{-1}\left(|\dot{w}|\ddot{\underline{\boldsymbol{\sigma}}}_f + 2\dot{\overline{|w|}}\dot{\underline{\boldsymbol{\sigma}}}_f + \ddot{\overline{|\dot{w}|}}\underline{\boldsymbol{\sigma}}_f\right) \\ \underline{\boldsymbol{\beta}}_f w^{(3)} + 2\dot{\underline{\boldsymbol{\beta}}}_f\ddot{w} + \ddot{\underline{\boldsymbol{\beta}}}_f\dot{w} \\ \underline{\mathbf{D}}_f^{-1}\ddot{\underline{\boldsymbol{\sigma}}}_f + \dot{\overline{\underline{\mathbf{D}}_f^{-1}}}\dot{\underline{\boldsymbol{\sigma}}}_f \\ \frac{1}{\tau_f}\left(\underline{\mathbf{D}}_f^{-1}\dot{\underline{\boldsymbol{\sigma}}}_f + \dot{\overline{\underline{\mathbf{D}}_f^{-1}}}\underline{\boldsymbol{\sigma}}_f\right) \\ \frac{p}{\alpha_f}\underline{\mathbf{D}}_f^{-1}\left(|\dot{w}|\dot{\underline{\boldsymbol{\sigma}}}_f + \dot{\overline{|w|}}\underline{\boldsymbol{\sigma}}_f\right) \\ \underline{\boldsymbol{\beta}}_f\ddot{w} + \dot{\underline{\boldsymbol{\beta}}}_f\dot{w} \\ \underline{\mathbf{D}}_f^{-1}\dot{\underline{\boldsymbol{\sigma}}}_f \\ \frac{p}{\alpha_f}\underline{\mathbf{D}}_f^{-1}|\dot{w}|\underline{\boldsymbol{\sigma}}_f \\ \underline{\boldsymbol{\beta}}_f\dot{w} \\ \dot{\underline{\boldsymbol{\varepsilon}}} \\ \ddot{\underline{\boldsymbol{\varepsilon}}} \end{bmatrix} \tag{20}$$

This system of equations can be solved, using an analytical mathematical program such as Maple [16], with respect to $\underline{\boldsymbol{\varepsilon}}^{(3)}$, resulting in the following third-order differential equation in $\underline{\boldsymbol{\varepsilon}}$ and $\underline{\boldsymbol{\sigma}}_f$

$$\underline{\mathbf{D}}_f\left(\underline{\boldsymbol{\varepsilon}}^{(3)} + H_2\ddot{\underline{\boldsymbol{\varepsilon}}} + H_1\dot{\underline{\boldsymbol{\varepsilon}}} - \underline{\boldsymbol{\beta}}_f(w^{(3)} + b_2\ddot{w} + b_1\dot{w})\right) = \underline{\boldsymbol{\sigma}}_f^{(3)} + S_2\ddot{\underline{\boldsymbol{\sigma}}}_f + S_1\dot{\underline{\boldsymbol{\sigma}}}_f + S_0\underline{\boldsymbol{\sigma}}_f \tag{21}$$

where the coefficients H_i, b_i and S_i are scalar functions of the moisture content, w, and its derivatives. The explicit expressions of the coefficients are comprehensive. The coefficients are generally not constants since w can vary over time, t.

HOMGENISATION OF THE FIBRE NETWORK

Transformation of Stresses and Strains

The stresses and strains have been expressed thus far in terms of the local fibre coordinate system, the x-axis coinciding with the longitudinal direction of the fibre. They can be transformed, however, to the global coordinate system of the composite material, as shown in Figure 3, by use of the three-dimensional transformation matrix $\mathbf{T}$ according to

$$\underline{\boldsymbol{\sigma}} = \mathbf{T}\boldsymbol{\sigma}, \quad \underline{\boldsymbol{\varepsilon}} = \mathbf{T}\boldsymbol{\varepsilon} \tag{22}$$

where the symbols that are underlined ($\underline{\boldsymbol{\sigma}}, \underline{\boldsymbol{\varepsilon}}, \underline{\mathbf{D}}_0$) and the lower-case coordinate indices denote the properties of the local coordinate system, the symbols without underlining and the indices that are capitalized denoting the global coordinates.
The three-dimensional transformation matrix, in component form, is

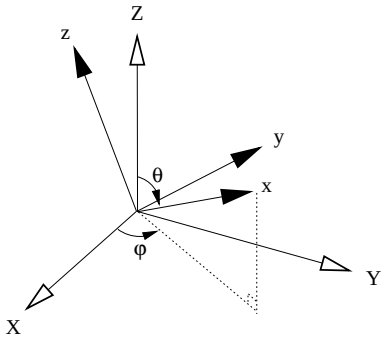

Figure 3: Coordinate transformation from local (x, y, z) to global (X, Y, Z) coordinates. The fibre is oriented in the x-direction.

$$\mathbf{T} = \begin{bmatrix} s^2m^2 & s^2n^2 & c^2 & 2s^2mn & 2csm & 2csn \\ n^2 & m^2 & 0 & -2mn & 0 & 0 \\ c^2m^2 & c^2n^2 & s^2 & 2c^2mn & -2csm & -2csn \\ -smn & smn & 0 & s(m^2-n^2) & -cn & cm \\ -csm^2 & -csn^2 & cs & -2csmn & -m(c^2-s^2) & -n(c^2-s^2) \\ cmn & -cmn & 0 & -c(m^2-n^2) & -sn & sm \end{bmatrix} \tag{23}$$

where the cosine and the sine of the rotation angles are $m = \cos\varphi$, $n = \sin\varphi$, $c = \cos\theta$ and $s = \sin\theta$ [21]. The rotation angles are defined in Figure 3. An in-plane rotation means that $\theta = \pi/2$ which gives $c = 0$ and $s = 1$. The transformation matrix is considered to be independent of time, the changes in fibre-orientation during deformation being neglected ($\dot{\mathbf{T}} = \mathbf{0}$). The transformation of a stiffness matrix is $\mathbf{D} = \mathbf{T}^{-1}\underline{\mathbf{D}}\mathbf{T}$, as given by

$$\boldsymbol{\sigma} = \mathbf{T}^{-1}\underline{\boldsymbol{\sigma}} = \mathbf{T}^{-1}\underline{\mathbf{D}}\ \underline{\boldsymbol{\varepsilon}} = \mathbf{T}^{-1}\underline{\mathbf{D}}\mathbf{T}\boldsymbol{\varepsilon} = \mathbf{D}\boldsymbol{\varepsilon} \tag{24}$$

Integration of the Fibre-Orientation Distribution

Starting from the differential equation for a single fibre, the homogenisation of a network consisting of a distribution of fibres in different directions involves the assumption of homogenous strain. Accordingly, the stress of the fibre network as a whole, $\boldsymbol{\sigma}_{fn}$, is calculated, from the stress of a single fibre, $\boldsymbol{\sigma}_f$, as the mean value

$$\boldsymbol{\sigma}_{fn} = \frac{1}{N}\sum_i^N \boldsymbol{\sigma}_f = \int_0^\pi \int_0^\pi \boldsymbol{\sigma}_f \Psi(\varphi,\theta)\sin\theta d\varphi d\theta = \int_0^\pi \int_0^\pi \mathbf{T}^{-1}\underline{\boldsymbol{\sigma}}_f \Psi(\varphi,\theta)\sin\theta d\varphi d\theta \tag{25}$$

where $\Psi(\varphi,\theta)$ is the spatial fibre-orientation distribution function containing the arguments θ and φ, which can be regarded as a probability function having the property of

$$\int_0^\pi \int_0^\pi \Psi(\varphi,\theta)\sin\theta d\varphi d\theta = 1 \tag{26}$$

In the case of a planar fibre distribution, equation (25) becomes

$$\boldsymbol{\sigma}_{fn} = \int_0^\pi \mathbf{T}^{-1}\underline{\boldsymbol{\sigma}}_f f(\varphi) d\varphi \tag{27}$$

where $f(\varphi)$ is the planar fibre-orientation distribution function having the property

$$\int_0^\pi f(\varphi)d\varphi = 1 \tag{28}$$

and where Ψ and f, in analogy to $\mathbf{T}$, are considered to be independent of time, i.e. $\dot{\Psi} = \dot{f} = 0$.

This allows the homogenisation of the equation for a single fibre to be developed to an equation for the entire fibre network, using the following procedure. Both sides of equation (21), which is expressed in terms of local coordinates, are multiplied by $f(\varphi)$, and from the left by the inverse transformation matrix $\mathbf{T}^{-1}$ allowing the equation to be expressed in terms of global coordinates,

$$\begin{aligned}\mathbf{T}^{-1}\underline{\mathbf{D}}_f\left(\underline{\boldsymbol{\varepsilon}}^{(3)} + H_2\ddot{\underline{\boldsymbol{\varepsilon}}} + H_1\dot{\underline{\boldsymbol{\varepsilon}}} - \underline{\boldsymbol{\beta}}_f(w^{(3)} + b_2\ddot{w} + b_1\dot{w})\right) f(\varphi) = \\ \mathbf{T}^{-1}\left(\underline{\boldsymbol{\sigma}}_f^{(3)} + S_2\ddot{\underline{\boldsymbol{\sigma}}}_f + S_1\dot{\underline{\boldsymbol{\sigma}}}_f + S_0\underline{\boldsymbol{\sigma}}_f\right) f(\varphi)\end{aligned} \tag{29}$$

The stresses and strains and their derivatives are then transformed into global coordinates according to $\underline{\boldsymbol{\sigma}} = \mathbf{T}\boldsymbol{\sigma}$, $\underline{\boldsymbol{\varepsilon}} = \mathbf{T}\boldsymbol{\varepsilon}$ and $\dot{\underline{\boldsymbol{\sigma}}} = \mathbf{T}\dot{\boldsymbol{\sigma}}$ etc, which leads to

$$\begin{aligned}\mathbf{T}^{-1}\underline{\mathbf{D}}_f\mathbf{T}\left(\boldsymbol{\varepsilon}^{(3)} + H_2\ddot{\boldsymbol{\varepsilon}} + H_1\dot{\boldsymbol{\varepsilon}} - \mathbf{T}^{-1}\underline{\boldsymbol{\beta}}_f(w^{(3)} + b_2\ddot{w} + b_1\dot{w})\right) f(\varphi) = \\ \mathbf{T}^{-1}\mathbf{T}\left(\boldsymbol{\sigma}_f^{(3)} + S_2\ddot{\boldsymbol{\sigma}}_f + S_1\dot{\boldsymbol{\sigma}}_f + S_0\boldsymbol{\sigma}_f\right) f(\varphi)\end{aligned} \tag{30}$$

Finally, an integration of all fibre directions in the plane is performed on both sides of the equation.

$$\begin{aligned}\int_0^\pi \mathbf{T}^{-1}\underline{\mathbf{D}}_f\mathbf{T}\left(\boldsymbol{\varepsilon}^{(3)} + H_2\ddot{\boldsymbol{\varepsilon}} + H_1\dot{\boldsymbol{\varepsilon}} - \mathbf{T}^{-1}\underline{\boldsymbol{\beta}}_f(w^{(3)} + b_2\ddot{w} + b_1\dot{w})\right) f(\varphi)d\varphi = \\ \int_0^\pi \mathbf{I}\left(\boldsymbol{\sigma}_f^{(3)} + S_2\ddot{\boldsymbol{\sigma}}_f + S_1\dot{\boldsymbol{\sigma}}_f + S_0\boldsymbol{\sigma}_f\right) f(\varphi)d\varphi\end{aligned} \tag{31}$$

This integration corresponds to the homogenous strain assumption used in integrating the stress according to equation (27). Equation (31) yields in terms of the constitutive differential equation for the homogenized fibre network material,

$$\mathbf{D}_{fn}\left(\boldsymbol{\varepsilon}^{(3)} + H_2\ddot{\boldsymbol{\varepsilon}} + H_1\dot{\boldsymbol{\varepsilon}} - \boldsymbol{\beta}_{fn}(w^{(3)} + b_2\ddot{w} + b_1\dot{w})\right) = \boldsymbol{\sigma}_{fn}^{(3)} + S_2\ddot{\boldsymbol{\sigma}}_{fn} + S_1\dot{\boldsymbol{\sigma}}_{fn} + S_0\boldsymbol{\sigma}_{fn} \tag{32}$$

which introduces the new properties $\mathbf{D}_{fn}$ and $\boldsymbol{\beta}_{fn}$, defined as

$$\mathbf{D}_{fn} = \int_0^\pi \mathbf{T}^{-1}\underline{\mathbf{D}}_f\mathbf{T}f(\varphi)d\varphi \tag{33}$$

$$\boldsymbol{\beta}_{fn} = \mathbf{D}_{fn}^{-1}\int_0^\pi \mathbf{T}^{-1}f(\varphi)d\varphi\ \ \underline{\mathbf{D}}_f\underline{\boldsymbol{\beta}}_f \tag{34}$$

The calculated elastic stiffness matrix $\mathbf{D}_{fn}$ of the fibre network and the hygroexpansion coefficient vector $\boldsymbol{\beta}_{fn}$ agree with previous purely elastic calculations the of fibre network stiffness [21]. This is an important and surprisingly simple result, one allowing the constitutive properties of the hygroscopic network materials not containing any matrix material to be predicted on the basis of the

properties of the fibre material, homogenous strain being assumed. Hygroscopic network materials which lack a matrix include wood- and cellulose-fibre materials such as fibreboard, oriented strand board and paper.

It is notable that equation (32), which describes the homogenized fibre network, is identical in its structure to equation (21), which describes the single fibre. The only difference is that the elastic stiffness matrix of the single fibre, $\mathbf{D}_f$, is replaced in equation (32) by $\mathbf{D}_{fn}$ and $\boldsymbol{\beta}_f$ is replaced by $\boldsymbol{\beta}_{fn}$. Thus, the spring and dashpot representation used for the single fibre, as shown in Figure 2, is also valid for the homogenized fibre network, $\mathbf{D}_f$ and $\boldsymbol{\beta}_f$ are replaced by $\mathbf{D}_{fn}$ and $\boldsymbol{\beta}_{fn}$. The same set of τ_f, μ_f, α_f and λ_f is associated with the fibre network. This is very useful in numerical implementation of the model, since it means there is no need of a numerical integration of the properties involved in all the fibre directions.

CONSTITUTIVE EQUATION OF THE MATRIX MATERIAL

The constitutive model of the matrix material is assumed to be of the same type as for the fibre material, except for the mechanosorptive creep effect, which is disregarded. The elastic stiffness of the matrix material, $\mathbf{D}_m$, is assumed to be isotropic and to be independent of moisture content. In line with equations (10) - (13) the creep viscosity $\mathbf{C}_{m,cr}$ and the creep stiffness matrix $\mathbf{D}_{m,cr}$ are likewise assumed to not be influenced by the moisture content. Accordingly

$$\mathbf{D}_m = \begin{bmatrix} \frac{1}{E_m} & -\frac{\nu_m}{E_m} & -\frac{\nu_m}{E_m} & 0 & 0 & 0 \\ -\frac{\nu_m}{E_m} & \frac{1}{E_m} & -\frac{\nu_m}{E_m} & 0 & 0 & 0 \\ -\frac{\nu_m}{E_m} & -\frac{\nu_m}{E_m} & \frac{1}{E_m} & 0 & 0 & 0 \\ 0 & 0 & 0 & \frac{1}{2G_m} & 0 & 0 \\ 0 & 0 & 0 & 0 & \frac{1}{2G_m} & 0 \\ 0 & 0 & 0 & 0 & 0 & \frac{1}{2G_m} \end{bmatrix}^{-1} \tag{35}$$

where $G_m = E_m/(2(1+\nu_m))$ and

$$\mathbf{C}_{m,cr} = \frac{1}{\tau_m}\mathbf{D}_m^{-1} \tag{36}$$

$$\mathbf{D}_{m,cr} = \frac{1}{\mu_m}\mathbf{D}_m \tag{37}$$

The hygroexpansion is also assumed to be linear and isotropic, meaning that $\boldsymbol{\beta}_m = \beta_m[\ 1\ \ 1\ \ 1\ \ 0\ \ 0\ \ 0\ ]^T$, where β_m is constant. These assumptions can be shown to give the following constitutive equation for the matrix material:

$$\mathbf{D}_m\left((\dot{\boldsymbol{\varepsilon}} - \boldsymbol{\beta}_m\dot{w}) + \frac{1}{\mu_m\tau_m}(\boldsymbol{\varepsilon} - \boldsymbol{\beta}_m(w - w_0))\right) = \dot{\boldsymbol{\sigma}}_m + \frac{1}{\tau_m}\boldsymbol{\sigma}_m \tag{38}$$

where $w_0 = w(t_0)$ is the initial moisture content of the material. This equation is valid for all orientations of the coordinate system, both local and global, since the matrix material is assumed to be isotropic.

HOMOGENISATION OF THE COMPOSITE MATERIAL

As in the case of the homogenisation of single fibres to a homogenous fibre network material, the homogenisation of the fibre network and the matrix material to a composite material is performed, according to laminate theory, i.e. under the assumption of homogenous strain, by summing the stresses of the constituents and taking account of their relative volume within the composite, schematically shown in Figure 4.

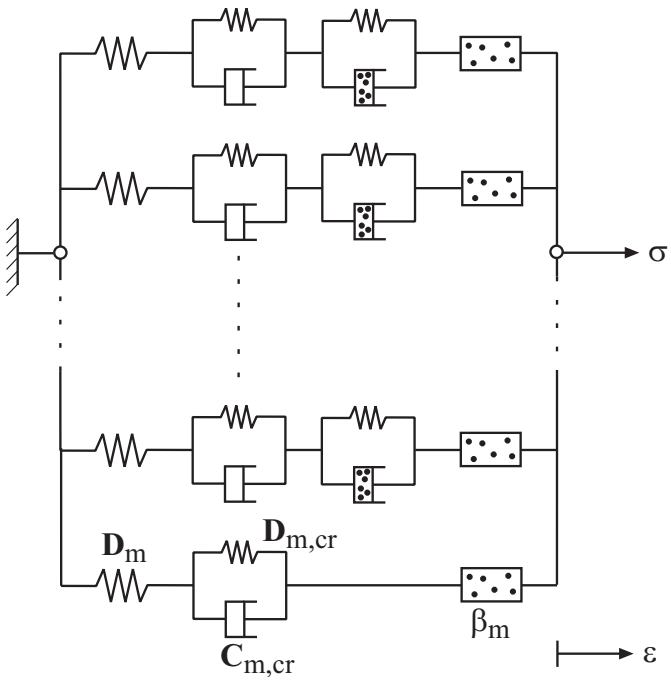

Figure 4: Homogenisation of several fibres and the matrix material with its introduced material parameters.

Since the differential equation for the fibre network (21) comprises zero- to third-order derivatives of the strain, and since the equation for the matrix material (38) comprises zero- and first-order derivatives, the resulting differential equation for the composite material comprises the first to the fourth-order derivatives of the strain. The volume fractions of the fibre phase and the matrix phase are denoted as V_f and V_m, respectively. The equation is calculated from derivatives of the equations above, combined using a scheme contained in equation (39) and analogous to equation (20), the stresses of the fibre network and of the matrix material and its derivatives being the variables contained in the column vector rather than the strains as in equation (20).

$$
\begin{bmatrix}
1 & -V_f & -V_m & 0 & 0 & 0 & 0 & 0 & 0 & 0 & 0 \\
0 & 1 & 0 & S_2 & 0 & \dot{S}_2 + S_1 & 0 & \dot{S}_1 + S_0 & 0 & \dot{S}_0 & 0 \\
0 & 0 & 1 & 0 & \frac{1}{\tau_m} & 0 & 0 & 0 & 0 & 0 & 0 \\
0 & 0 & 0 & 1 & 0 & S_2 & 0 & S_1 & 0 & S_0 & 0 \\
0 & 0 & 0 & 0 & 1 & 0 & \frac{1}{\tau_m} & 0 & 0 & 0 & 0 \\
0 & 0 & 0 & V_f & V_m & 0 & 0 & 0 & 0 & 0 & 0 \\
0 & 0 & 0 & 0 & 0 & 0 & 1 & 0 & \frac{1}{\tau_m} & 0 & 0 \\
0 & 0 & 0 & 0 & 0 & V_f & V_m & 0 & 0 & 0 & 0 \\
0 & 0 & 0 & 0 & 0 & 0 & 0 & 0 & 1 & 0 & \frac{1}{\tau_m} \\
0 & 0 & 0 & 0 & 0 & 0 & 0 & V_f & V_m & 0 & 0 \\
0 & 0 & 0 & 0 & 0 & 0 & 0 & 0 & 0 & V_f & V_m
\end{bmatrix}
\begin{bmatrix}
\boldsymbol{\sigma}^{(4)} \\
\boldsymbol{\sigma}_{fn}^{(4)} \\
\boldsymbol{\sigma}_{m}^{(4)} \\
\boldsymbol{\sigma}_{fn}^{(3)} \\
\boldsymbol{\sigma}_{m}^{(3)} \\
\ddot{\boldsymbol{\sigma}}_{fn} \\
\ddot{\boldsymbol{\sigma}}_{m} \\
\dot{\boldsymbol{\sigma}}_{fn} \\
\dot{\boldsymbol{\sigma}}_{m} \\
\boldsymbol{\sigma}_{fn} \\
\boldsymbol{\sigma}_{m}
\end{bmatrix} =
$$

$$
\begin{bmatrix}
0 \\
\frac{d}{dt}\left(\mathbf{D}_{fn}\left(\boldsymbol{\varepsilon}^{(3)} + H_2\ddot{\boldsymbol{\varepsilon}} + H_1\dot{\boldsymbol{\varepsilon}} - \beta_f(w^{(3)} + b_2\ddot{w} + b_1\dot{w})\right)\right) \\
\mathbf{D}_m\left(\boldsymbol{\varepsilon}^{(4)} + \frac{\mu_m}{\tau_m}\boldsymbol{\varepsilon}^{(3)} - \beta_m(w^{(4)} + \frac{\mu_m}{\tau_m}w^{(3)}\right) \\
\mathbf{D}_{fn}\left(\boldsymbol{\varepsilon}^{(3)} + H_2\ddot{\boldsymbol{\varepsilon}} + H_1\dot{\boldsymbol{\varepsilon}} - \beta_f(w^{(3)} + b_2\ddot{w} + b_1\dot{w})\right) \\
\mathbf{D}_m\left(\boldsymbol{\varepsilon}^{(3)} + \frac{\mu_m}{\tau_m}\ddot{\boldsymbol{\varepsilon}} - \beta_m(w^{(3)} + \frac{\mu_m}{\tau_m}\ddot{w}\right) \\
\boldsymbol{\sigma}^{(3)} \\
\mathbf{D}_m\left(\ddot{\boldsymbol{\varepsilon}} + \frac{\mu_m}{\tau_m}\dot{\boldsymbol{\varepsilon}} - \beta_m(\ddot{w} + \frac{\mu_m}{\tau_m}\dot{w}\right) \\
\ddot{\boldsymbol{\sigma}} \\
\mathbf{D}_m\left(\dot{\boldsymbol{\varepsilon}} + \frac{\mu_m}{\tau_m}\boldsymbol{\varepsilon} - \beta_m(\dot{w} + \frac{\mu_m}{\tau_m}w\right) \\
\dot{\boldsymbol{\sigma}} \\
\boldsymbol{\sigma}
\end{bmatrix} \tag{39}
$$

Solving this system of equations with respect to the first element in the stress vector $\boldsymbol{\sigma}^{(4)}$ results in the differential equation for the composite material

$$
\begin{aligned}
\mathbf{D}_c\left(\boldsymbol{\varepsilon}^{(4)} + \mathbf{K}_3\boldsymbol{\varepsilon}^{(3)} + \mathbf{K}_2\ddot{\boldsymbol{\varepsilon}} + \mathbf{K}_1\ddot{\boldsymbol{\varepsilon}} + \mathbf{K}_0\dot{\boldsymbol{\varepsilon}}\right) - \\
\mathbf{D}_c\left(\boldsymbol{\beta}_c w^{(4)} + \mathbf{b}_3 w^{(3)} + \mathbf{b}_2\ddot{w} + \mathbf{b}_1\dot{w}\right) = \\
\boldsymbol{\sigma}^{(4)} + L_3\boldsymbol{\sigma}^{(3)} + L_2\ddot{\boldsymbol{\sigma}} + L_1\dot{\boldsymbol{\sigma}} + L_0\boldsymbol{\sigma}
\end{aligned} \tag{40}
$$

where

$$
\mathbf{D}_c = V_f\mathbf{D}_{fn} + V_m\mathbf{D}_m \tag{41}
$$

$$
\boldsymbol{\beta}_c = \mathbf{D}_c^{-1}(V_f\mathbf{D}_{fn}\boldsymbol{\beta}_{fn} + V_m\mathbf{D}_m\boldsymbol{\beta}_m) \tag{42}
$$

The coefficients $\mathbf{K}_i$ are matrix-valued linear combinations of $\mathbf{D}_{fn}$ and $\mathbf{D}_m$, the coefficients $\mathbf{b}_i$ are vector-valued linear combinations of $\mathbf{D}_{fn}, \mathbf{D}_m$, $\boldsymbol{\beta}_{fn}$ and $\boldsymbol{\beta}_m$, and L_i are scalar functions of the moisture content, w, and its derivatives.

The influence of the possible porosity in the material can be taken into account. The volume fraction of the porosity is denoted as V_p, such that $V_f + V_m + V_p = 1$. V_p is easily taken into

account of by adding elements of zero stiffness to the model. This does not affect the equations in any other way than through the fact that $V_f + V_m < 1$.

Characteristics of the Differential Equation

Even without making any calculations, it is possible to draw certain conclusions regarding the momentary responses and the long-term behaviour predicted by the differential equation (40). The elastic response, i.e. the momentary strain a short time after loading, is calculated by setting $\boldsymbol{\varepsilon}_{cr} = \boldsymbol{\varepsilon}_{ms} = \boldsymbol{\varepsilon}_h = 0$ for both constituents, i.e. by regarding the creep and mechanosorption dashpots as rigid elements, resulting logically in

$$\boldsymbol{\varepsilon}_e = \boldsymbol{\varepsilon}(t \to 0_+) = \mathbf{D}_c \boldsymbol{\sigma}_0 \tag{43}$$

In approximating the long-term strain in the case of a constant load applied at $t = 0$, the creep and mechanosorption dashpots are set to zero stiffness, resulting in

$$\boldsymbol{\varepsilon}^\infty = (\mathbf{D}_c^\infty)^{-1} \boldsymbol{\sigma}_0 \tag{44}$$

where

$$\mathbf{D}_c^\infty = V_f \mathbf{D}_{fn}^\infty + V_m \mathbf{D}_m^\infty = \frac{V_f \mathbf{D}_{fn}}{1 + \mu_f + \lambda_f / p} + \frac{V_m \mathbf{D}_m}{1 + \mu_m} \tag{45}$$

In the case of constant moisture content λ_f disappears from equation (45), the parameters μ_f, λ_f and μ_m determining the relationship between the momentary strain response of a load and the strain response to the same loading after a long period of time. The parameters τ_f, α_f and τ_m determine how rapidly the material will reach long-term strain, $\boldsymbol{\varepsilon}^\infty$.

ANALYTICAL SOLUTION OF THE SIMPLIFIED EQUATION

As already indicated, the resulting equation for the composite material is a linear fourth-order differential equation with time-dependent matrix-valued coefficients. Such an equation is virtually impossible to solve analytically, numerical methods generally being required to obtain useful results. Only in a simplified case can an analytical solution for controlling the reliability of the numerical results be achieved.

The final differential equation (40) can be simplified by neglecting the stiffness of the three elastic springs parallel-coupled with the two creep dashpots and the moisture rate dashpot, respectively. This lowers the order of the final differential equation in strain by one for each spring that is neglected, neglecting the stiffness of all the springs thus converting the fourth-order differential equation (40) into a first-order differential equation for strain. The constituents are considered in this way to behave as fluids, which in only very exceptional cases can be regarded as a satisfactory physical description of the constituent materials. This is equivalent to setting $\mu_f, \lambda_f, \mu_m >> 1$, which allows equation (40) to be simplified to

$$\ddot{\boldsymbol{\varepsilon}} + \mathbf{F}_1 \dot{\boldsymbol{\varepsilon}} = \mathbf{D}_c^{-1} \left(\ddot{\boldsymbol{\sigma}} + T_1 \dot{\boldsymbol{\sigma}} + T_0 \boldsymbol{\sigma} \right) + \boldsymbol{\beta}_c \ddot{w} + \mathbf{b}_1 \dot{w} \tag{46}$$

where

$$\mathbf{F}_1 = \mathbf{D}_c^{-1}\Bigg[\left(\frac{\dot{p}}{p}+\frac{\tau_m\alpha_f+\tau_m\tau_f p|\dot{w}|-\tau_m^2\tau_f p\dot{|\dot{w}|}-\tau_m^2\tau_f\dot{p}|\dot{w}|-\tau_f\alpha_f}{\tau_m(-\tau_f\alpha_f+\tau_m\alpha_f+\tau_m\tau_f p|\dot{w}|)}\right)V_f\mathbf{D}_{fn} \tag{47}$$

$$+\ \frac{\tau_m\alpha_f^2+2\tau_m\tau_f\alpha_f p|\dot{w}|+\tau_m\tau_f^2p^2|\dot{w}|^2-\tau_m\tau_f^2\alpha_f p\dot{|\dot{w}|}-\tau_m\tau_f^2\alpha_f\dot{p}|\dot{w}|-\tau_f\alpha_f^2-\tau_f^2\alpha_f p|\dot{w}|}{\tau_f\alpha_f(-\tau_f\alpha_f+\tau_m\alpha_f+\tau_m\tau_f p|\dot{w}|)}V_m\mathbf{D}_m\Bigg]$$

$$T_1 = \frac{\tau_m^2\alpha_f^2+2\tau_m^2\tau_f\alpha_f p|\dot{w}|+\tau_m^2\tau_f^2p^2|\dot{w}|^2-\tau_m^2\tau_f^2\alpha_f p\dot{|\dot{w}|}-\tau_m^2\tau_f^2\alpha_f\dot{p}|\dot{w}|-\tau_f^2\alpha_f^2}{\tau_m\tau_f\alpha_f(-\tau_f\alpha_f+\tau_m\alpha_f+\tau_m\tau_f p|\dot{w}|)} \tag{48}$$

$$T_0 = \frac{\tau_m\alpha_f^2+2\tau_m\tau_f\alpha_f p|\dot{w}|+\tau_m\tau_f^2p^2|\dot{w}|^2-\tau_m\tau_f^2\alpha_f p\dot{|\dot{w}|}-\tau_m\tau_f^2\alpha_f\dot{p}|\dot{w}|-\tau_f\alpha_f^2-\tau_f^2\alpha_f p|\dot{w}|}{\tau_m\tau_f\alpha_f(-\tau_f\alpha_f+\tau_m\alpha_f+\tau_m\tau_f p|\dot{w}|)} \tag{49}$$

$$\mathbf{b}_1 = \mathbf{D}_c^{-1}\Bigg[\left(\frac{\dot{q}}{q}+\frac{\dot{p}}{p}+\frac{\tau_m\alpha_f+\tau_m\tau_f p|\dot{w}|-\tau_m^2\tau_f p\dot{|\dot{w}|}-\tau_m^2\tau_f\dot{p}|\dot{w}|-\tau_f\alpha_f}{\tau_m(-\tau_f\alpha_f+\tau_m\alpha_f+\tau_m\tau_f p|\dot{w}|)}\right)V_f\mathbf{D}_{fn}\boldsymbol{\beta}_{fn} \tag{50}$$

$$+\ \frac{\tau_m\alpha_f^2+2\tau_m\tau_f\alpha_f p|\dot{w}|+\tau_m\tau_f^2p^2|\dot{w}|^2-\tau_m\tau_f^2\alpha_f p\dot{|\dot{w}|}-\tau_m\tau_f^2\alpha_f\dot{p}|\dot{w}|-\tau_f\alpha_f^2-\tau_f^2\alpha_f p|\dot{w}|}{\tau_f\alpha_f(-\tau_f\alpha_f+\tau_m\alpha_f+\tau_m\tau_f p|\dot{w}|)}V_m\mathbf{D}_m\boldsymbol{\beta}_m\Bigg]$$

This first-order differential equation for strain is solved by first multiplying both sides with the integrating factor

$$\mathbf{J}(\tilde{t}) = \int_0^{\tilde{t}}\mathbf{F}_1(\hat{t})d\hat{t} \tag{51}$$

and then by integrating both sides from 0 to t two times. This yields

$$\boldsymbol{\varepsilon}(t) = \int_0^t e^{-\mathbf{J}(\tilde{t})}\int_0^{\tilde{t}} e^{\mathbf{J}(\acute{t})}\ \left[\mathbf{D}_c^{-1}\left(\ddot{\boldsymbol{\sigma}}+T_1\dot{\boldsymbol{\sigma}}+T_0\boldsymbol{\sigma}\right)+\boldsymbol{\beta}_c\ddot{w}+\mathbf{b}_1\dot{w}\ \right]\ d\acute{t}\ d\tilde{t} \tag{52}$$

In a still further simplified case of a constant moisture content of the composite material, $\dot{w}=0$, and of a constant load beginning to act at $t=0$, $\boldsymbol{\sigma}(t)=\theta(t)\boldsymbol{\sigma}_0$, where $\theta(t)$ is the Heaviside unit step function, the strain in equation (52) can be written out explicitly:

$$\boldsymbol{\varepsilon}(t) = \left[\left(-\mathbf{I}+\mathbf{F}_1^{-1}(\frac{1}{\tau_f}+\frac{1}{\tau_m})-\mathbf{F}_1^{-2}\frac{1}{\tau_f\tau_m}\right)(1-e^{-\mathbf{F}_1 t})+\mathbf{I}+\mathbf{F}_1^{-1}\frac{t}{\tau_f\tau_m}\right]\theta(t)\ \mathbf{D}_c^{-1}\boldsymbol{\sigma}_0 \tag{53}$$

This equation can be used for verifying correct implementation of the numerical model.

NUMERICAL EXAMPLES

The numerical simulations were performed using a system of first-order differential equations and an implicit Euler scheme. It is assumed that the moisture function $q(w)$ is 1.0 and that the function $p(w)$ is either $p(w)=1.0$ or $p(w)=1-0.015(w-0.04)$. The load is set to $\boldsymbol{\sigma}(t)=\theta(t)\boldsymbol{\sigma}_0=\theta(t)[200\ \ 0\ \ 0\ \ 0\ \ 0\ \ 0]^T$ MPa. The elastic properties of the wood-fibre material are taken from Persson [20] and the moisture dependency from Dinwoodie [7], the time dependent properties being evaluated from tests performed by Hanhijärvi [11]. The properties of melamine formaldehyde are taken from [10, 18]. All parameters defining the time-dependent behaviour ($\tau_f, \mu_f, \alpha_f, \lambda_f, \tau_m$ and μ_m) are evaluated on the basis of test result diagrams, using the least square method. The

volume fractions are assumed to be $V_f = 0.62$ and $V_m = 0.38$. The fibre-orientation is assumed to be planar isotropic, all the fibres thus being aligned randomly in the plane, $f = 1/\pi$. The input values for the properties of the constituents are presented in Tables 1.

Table 1: *Assumed mechanical properties of wood fibres and matrix material.*

Wood fibre Properties						
E_x	$E_y = E_z$	$\nu_{xy} = \nu_{xz}$	ν_{yz}	$G_{xy} = G_{xz}$	G_{yz}	
[MPa]	[MPa]	[-]	[-]	[MPa]	[MPa]	
40 000	5 000	0.2	0.3	4 000	1 920	
β_x	β_y	β_z	τ_f	μ_f	α_f	λ_f
$[1/10^4]$	$[1/10^4]$	$[1/10^4]$	h	[-]	[-]	[-]
1.0	26.0	26.0	2000	0.32	0.24	0.32
Matrix Material Properties						
	E_m	ν_m	β_m	τ_m	μ_m	
	[MPa]	[-]	$[1/10^4]$	$[h]$	[-]	
	9 000	0.3	1.0	36	2.0	

Comparison with the Analytical Solution

Figure 5 compares, under conditions of constant moisture content, $\dot{w} = 0$, the solution to equation (46), both the numerical and the analytical solution to which is presented explicitly in equation (53), with the numerical solution of the complete model in equation (40). The numerical and the analytical solutions of the simplified equation (46) coincide both for ε_x^s and for ε_y^s if the time steps are sufficiently small. The simplified model behaves as a fluid according to

$$\dot{\boldsymbol{\varepsilon}}(t) \cong \frac{1}{\tau_f \tau_m} \mathbf{F}_1^{-1} \mathbf{D}_c^{-1} \boldsymbol{\sigma}_0 \tag{54}$$

its having a constant strain rate as $t >> \tau_f, \tau_m$.

Example of the Calculation of Mechanosorption and of Creep Deformation

Figure 6 shows long-term creep and recovery strains under conditions of constant and of varying moisture content, respectively. Two cases of constant moisture content, $w = 0.04$ and $w = 0.07$, are compared with a third case, having the same set of properties but exposed to a climate such that the moisture content of the material varies between 0.04 and 0.07. The results show the model to be able to mimic the kind of mechanosorptive effect observed in the wood and the wood-based materials, as shown in Figure 1.

Fibre-Orientation and Content

Figure 7, finally, compares the strains obtained for different fibre-orientation distributions. The strain in a composite material having a random fibre-orientation distribution, ε^{CR}, is compared

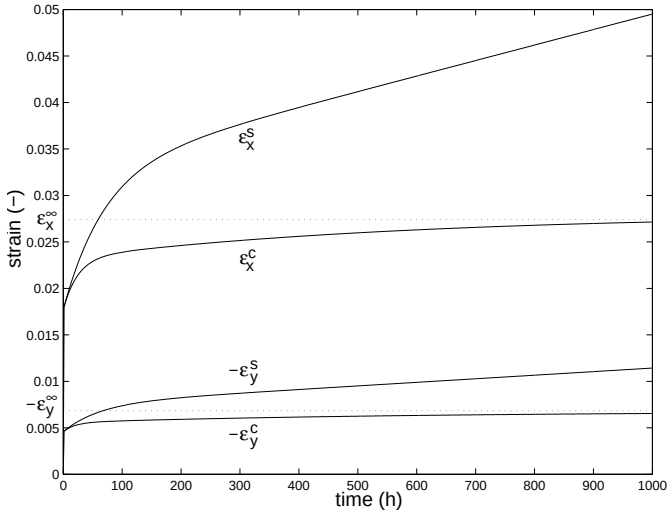

Figure 5: Simplified (ε^s) and complete (ε^c) model at constant moisture and uniaxial load.

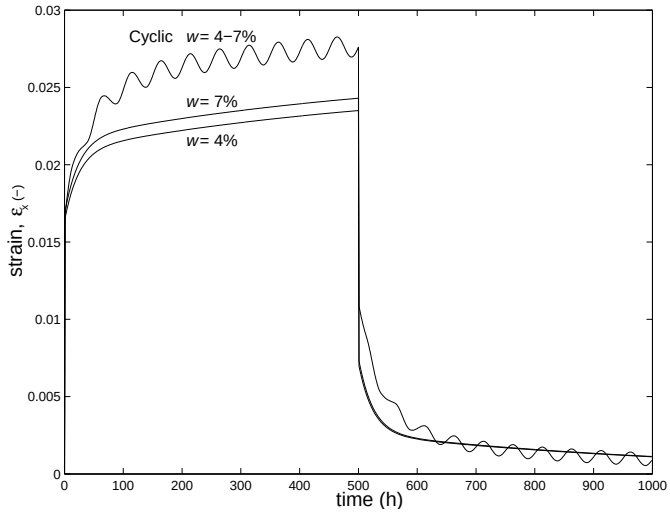

Figure 6: Strain under loading and relaxation under conditions of constant and cyclic varying moisture content.

with that in three different materials containing only fibres, one of them having a random fibre-orientation distribution, ε^{FR}; another being unidirectional, all the fibres being aligned in the loading direction, ε^{F0^o}; and a third likewise being unidirectional but all the fibres being aligned in the direction perpendicular to loading, ε^{F90^o}. The large strains obtained in the latter case reflects the poor stiffness and moisture-effect properties of wood fibres in the cross-fibre direction.

CONCLUDING REMARKS

An analytical three-dimensional model for the moisture dependent behaviour of wood-fibre network composite materials was developed. The model predicts the strain in all directions and at any particular time on the basis of the known properties of the constituents, the proportions, the

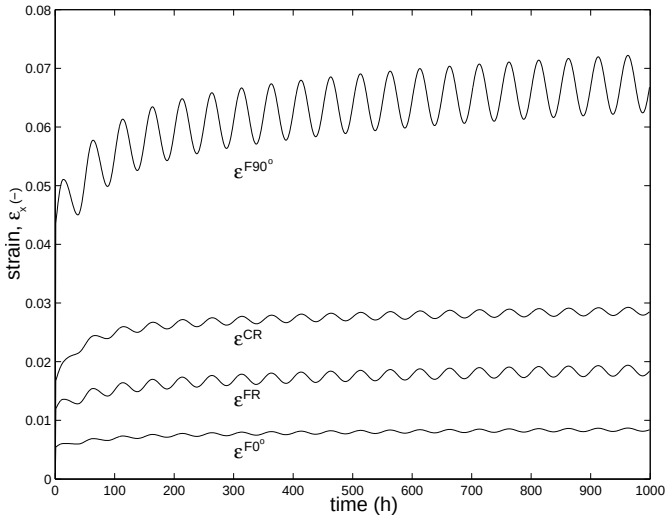

Figure 7: Comparison of unidirectional and randomly aligned fibres.

orientation distribution of the fibres, and the moisture present and the load applied to the material as a function of time. The model is presented in a complete version and a simplified version, where the simplified version is solved analytically. The simplified version of the model can be expected to give reasonably accurate results in the cases of a rapidly varying load and short term constant loading.

The model can be used for optimizing of the make of existing composite materials, for prediction of the properties of not yet existing materials and for analysis of the performance in various types of climatic conditions. The model can moreover be used for sensitivity analyzes that enable identification of critical parameters of the composite and of the course of the loading and the climatic variation.

FUTURE WORK

Before the present model can be used in practical applications two more issues should be investigated: validation and usability. Experimental verification is needed to ensure that the model gives accurate results and to identify limitations of the model. Further, the model should be applied on an industrial composite product to ensure its usability.

The model is based on certain assumptions and simplifications. In order to improve the model some of the assumptions made can be reconsidered:

- The material model can be made more advanced for example by taking into consideration non-linear creep and viscoplasticity. Now all matrices describing creep and mechanosorption are scalar functions multiplied by the stiffness matrix.
- The use of laminate theory, i.e. the assumption of homogenous strain, can be replaced by

an interpolation model between the two cases of homogenous strain and homogenous stress. An example of such interpolation is presented in [21].

- The simplification to regard all time and moisture effects as scalar functions can be generalized.

The above mentioned improvements will however lead to much more extensive calculations. A more advanced material model will also demand a larger number of material parameter values to be known.

ACKNOWLEDGEMENTS

This work was financed by the Swedish Wood Technology Research Colleague, the support of which is gratefully acknowledged. The author would like to thank Prof. Per Johan Gustafsson and Prof. Ola Dahlblom at the Division of Structural Mechanics for their valuable input.

APPENDIX

References

[1] Aboudi, J. (1991). *Mechanics of composite materials*,Elsevier, Amsterdam, The Netherlands, 124-164.

[2] Adl Zarrabi, B. (1998). "Hygro-elastic deformation of high pressure laminates." PhD thesis, Dept. of Building Phys., Chalmers University of Technology, Gothenburg, Sweden.

[3] Alftan, J. (2002). "Micro-mechanical modelling of mechano-sorptive creep in paper." Licentiate dissertation, Department of Solid Mechanics, Royal Institute of Technology, Stockholm, Sweden.

[4] Barbero, E. J. and Luciano, R. (1995). "Micromechanical formulas for the relaxation tensor of linear viscoelastic composites with transversely isotropic fibres." *Int. J. Solid Struct.*, Elsevier, 32(13), 1859-1872.

[5] Bradshaw, R. D. and Brinson, L. C. (1999). "Mechanical response of linear viscoelastic composite laminates incorporating non-isothermal physical aging effects." *Composites Sci. and Techn.*, Elsevier, 59, 1411-1427.

[6] Brauns, J., "Hygromechanical behaviour of wooden composites." *Wood Sci. and Techn.*, Springer, 31(3), 193-204.

[7] Dinwoodie, J. M. (1989). *Wood: nature's cellular, polymeric fibre-composite.* The Institute of Metals, London, 57.

[8] Fellers, C., Panek, J. (2001). "Effect of relative humidity cycling on mechanosorptive creep." *In Moisture and creep effects on paper, board and containers: 5th int. sym.,* Marysville, Victoria, Australia.

[9] Flügge, W. (1975) *Viscoelasticity.* Springer, Berlin.

[10] Hagstrand, P.-O. (1999) "Mechanical analysis of melamine-formaldehyde composites." PhD thesis, Dept. of Polym. Materials, Chalmers University of Technology, Gothenburg, Sweden.

[11] Hanhijärvi, A. (1995). "Modelling of creep deformation mechanisms in wood." PhD thesis, Technical Research Centre of Finland, Espoo.

[12] Holzapfel, G. A. (2001). *Nonlinear solid mechanics.* Wiley, London.

[13] Kaliske M. (2000). "A formulation of elasticity and viscoelasticity for fibre reinforced material at small and finite strains." *Comput. Methods Appl. Mech. Engrg.,* 185, 225-243.

[14] Klasztorny, M., Wilczynski, A. P. (2000). "Constitutive equations of viscoelasticity and estimation of viscoelastic parameters of unidirectional fibrous polymeric composites." J. Comp. Mat., 34(19), 1624-1639.

[15] Luciano, R., Barbero, E. J. (1995). "Analytical expressions for the relaxation moduli of linear viscoelastic composites with periodic microstructure." *Transactions of the ASCE*, 62, 786-793.

[16] *MAPLE - Version 7.0* (2001), "A symbolic computation system of computer algebra system", Waterloo Maple, Inc.

[17] Mårtensson, A. (1992). "Mechanical behaviour of wood exposed to humidity variations." PhD thesis, Dept. of Strucural Engineering, Lund University, Sweden.

[18] Niemz, P. (1993). *Physik des holzes und der holzwerkstoffe.* Leinfelden-Echterdingen: DRW.

[19] Ormarsson, S., *Numerical analysis of moisture-related distortions in sawn timber.* PhD thesis, Dept. of Structural Mechanics, Chalmers University of Technology, Gothenburg, Sweden.

[20] Persson, K. (1997). "Micromechanical modelling of wood and fibre properties." PhD thesis, Div. of Structural Mechanics, Lund University, Sweden.

[21] Stålne, K. (2001). "Modelling of stiffness and hygroexpansion of wood fibre composites." Licentiate dissertation, Div. of Structural Mechanics, Lund University, Sweden.

[22] Stålne, K. and Gustafsson, P.-J. (2002). "Three-dimensional model for analysis of stiffness and hygroexpansion properties of fibre composite materials." *J. Engng. Mech.*, ASCE, 128(6), 654-662.

[23] Stålne, K. and Gustafsson, P.-J. (2008). "Numerical Investigation of the Homogeneous Strain Assumption for Wood Fibre Composite Materials." Rep. No. TVSM-7157, Div. of Structural Mechanics, Lund University, Sweden.

[24] Svensson, S. (1997). "Internal stress in wood caused by climate variations." PhD thesis, Dept. of Strucural Engineering, Lund University, Sweden.

Notation

The following symbols are used in this paper:

$\mathbf{A}$	mechanosorption matrix
$b, \mathbf{b}$	moisture coefficients of diff. eq.
c	cosine of θ
$\mathbf{C}$	creep viscosity matrix
$\mathbf{D}$	stiffness matrix
E	Young's modulus
f	function for fibre-orientation
$\mathbf{F}$	strain coefficient of diff. eq.
G	shear modulus
H	strain coefficient of diff. eq.
$\mathbf{I}$	identity matrix
$\mathbf{J}$	integrating factor
$\mathbf{K}$	strain coefficient of diff. eq.
L	stress coefficient of diff. eq.
m	cosine of φ
n	sine of φ
p	moisture function
q	moisture function
s	sine of θ
S	stress coefficient of diff. eq.
t	time
T	stress coefficient of diff. eq.
$\mathbf{T}$	coord. transformation matrix
V	volume fraction
w	moisture content
α	mechanosorption parameter
$\boldsymbol{\beta}$	hygroexpansion coefficient vector
$\boldsymbol{\varepsilon}$	strain vector
θ	coord. transformation angle
$\theta(t)$	Heaviside unit step function
λ	mechanosorption parameter
μ	creep parameter
ν	poisson's ratio
$\boldsymbol{\sigma}$	stress vector
τ	creep parameter
φ	coord. transformation angle
Ψ	function for fibre-orientation

Superscripts

$\dot{(\ )}, \overline{\dot{(\ )}}$	time derivative of $(\ )$
$(\ )^{(n)}$	n:th derivative of $(\ )$
∞	long term property
c	complete model
C	composite property
F	fibre property
R	random fibre-orientation
s	simplified model

Subscripts

$\underline{(\ )}$	property in local coordinate system
0	initial value
c	composite property
cr	creep
e	elastic (strain)
f	single fibre property
fn	fibre network property
h	hygroexpansion
m	matrix material property
ms	mechanosorptive
p	porosity property

Paper IV

IV

Numerical Investigation of the Homogeneous Strain Assumption for Wood Fibre Composite Materials

Kristian Stålne and Per Johan Gustafsson

Submitted for publication

NUMERICAL INVESTIGATION OF THE HOMOGENEOUS STRAIN ASSUMPTION FOR WOOD FIBRE COMPOSITE MATERIALS

Kristian Stålne,

Prof. Per Johan Gustafsson

Division of Structural Mechanics

Lund University

P.O. Box 118, SE-221 00 Lund

Abstract

The stiffness and hygroexpansion properties of a wood fibre composite material was calculated by means of finite element analysis based homogenisation. The purpose was to investigate if the often used assumption of homogeneous strain is valid when analysing paper based composite materials. The representative volume element, the RVE, consists of in-plane randomly oriented orthotropic fibres, fibre crossings and an isotropic matrix material in the complementary area. The RVE was subjected to cyclic boundary conditions and plane stress. For a fibre volume fraction of 60 percent, which is typical for paper based composite products, the assumption of homogeneous strain was found to overestimate the composite stiffness by approximately 15 percent and underestimate the hygroexpansion by approximately 15 percent as compared to the results of the numerical simulations. These deviations produced by the homogeneous strain assumption can be considered to be within an acceptable range of engineering accuracy for analytical models for simplified analysis of stiffness and hygroexpansion properties of paper based composite materials.

Introduction

High pressure laminate, HPL, is a wood fibre composite composed of craft paper impregnated by phenolic or melamine resin. An important issue concerning wood composites is that of shape stability in relation to moisture content gradients and changes [1]. This entails a need for models that enable analysis and prediction of the hygroexpansion and stiffness properties of wood fibre composites such as HLP.

Various analytical models for analysis of the stiffness properties of fibre composite materials have been developed in recent decades [2]. A common approach is to model the composite as a single

fibre surrounded by matrix material [3,4,5]. These models assumes there to be no interaction between the fibres. Such an assumption is, however, questionable in connection with HPL since the particle phase of this composite material is paper, which is a network of long fibres that are bonded to each other. Another approach that strongly simplifies calculations and may be relevant for HPL composites is to assume homogeneous strain. Such a simplification makes it possible to model also the complex material behaviour of the wood fibres, taking into account creep and mechano-sorptive strains [6]. It has been shown, however, that the homogeneous strain assumption will always overestimate the stiffness of a composite material [7,8]. The aim of this investigation is partly to find out if this overestimation is sufficiently small for the assumption to be acceptable in modelling. In the investigation is moreover the homogeneous strain based prediction of hygroexpansion properties studied.

Developments in the area of numerical simulations by the finite element method have made it possible to model complicated fibre composite material structures, consisting of more than one fibre [9,10,11]. Most of these studies have dealt with estimation of the stiffness properties of plane fabric composites [12,13,14,15,16]. These materials have a weaved fibre phase in which the fibres are crossed over and under each other at right angles. Since the fabric geometry is regular, homogenisation of a single fibre crossing is sufficient to provide a satisfactory estimate of the composite material stiffness. Fibre networks of a more random type have also been studied using numerical simulations [17,18]. There has been no study at a micro mechanical level, however, of the behaviour of network composite materials of irregular geometry. It seems that numerical simulations of hygroexpansion properties of composite materials with an irregular material structure are lacking.

The present investigation is performed by comparing the results from a homogenisation performed under the assumption of homogeneous strain and a numerical homogenisation of the same representative volume element (RVE), a unit cell. The unit cell is a representation of a wood fibre composite with an irregular fibre network, such that of paper. The parameters of the model are the mechanical properties of the constituents, the fibre geometry, the fibre orientation distribution and the fibre volume fraction. The configuration of the fibre network, number and orientation of the fibres, and is created by a Monte Carlo simulation process. This enables a good representation of the micro-structure of the fibre composite material.

The numerical results on stiffness and hygroexpansion are presented for a wide range of fibre volume fractions. The results are compared to those obtained but the homogeneous strain

assumption and also to those obtained by the homogeneous stress assumption. To determine a sufficient size of the RVE, calculations were made for a range of ratios between fibre width and unit cell side length. To determine how fine the finite element mesh needs to be for good numerical accuracy, calculation were made for a range of ratios between size of the finite elements and size of the RVE. The numerical results versus the corresponding results of the homogeneous strain assumption made it possible to make an estimation of the validity of that later assumption when used in modelling of deformations of HPL materials as affected by stress, moisture, moisture changes and time of loading.

The Numerical Model

Figure 1 shows an example of an RVE. In this example there are 5 fibres in the RVE and the RVE is modelled by 30x30 finite elements. The RVE is a square with unit a constant thickness and the finite elements are plane stress square shaped elements of equal size and of the Melosh type with 4 nods. The fibre material is modelled as orthotropic linear elastic and the matrix material as isotropic linear elastic. Also the hygroexpansion properties of the fibres and the matrix are assumed to be orthotropic and isotropic, respectively. The geometry and location of a fibre is defined by pre-defined constant width and randomly selected orientation and location in the RVE. A finite element is assigned the properties of a fibre if more than 50 percent of its volume is within a fibre, and vice versa. In areas of fibre crossings are the finite elements assigned the average stiffness properties of the crossing fibres. Cyclic boundary conditions are employed. This means that the RVE acts as being surrounded by similar RVE:s and assumed to be a small part of an infinitely large volume of composite material. Estimations of material properties of the cellulose fibre and melamine resin are from [19] and [20] and is presented in Table 2 and Table 3, respectively.

The stiffness and hygroexpansion properties of the composite are evaluated by exposing the square unit cell to 4 different loadings: global tensile strain in the *x*-direction, global tensile strain in the *y*-direction, global shear strain in the *x*-*y* plane and increase in moisture content in the fibres and the matrix. The response of the unit cell to these loads is obtained by solving the finite element system of equations. The stiffness tensor of the unit composite cell is the calculated from the mean strains and the boundary traction vectors and the hygroexpansion parameters of the composite cell are obtained from the average strains in the *x*- and *y*-directions when exposing the cell to increased moisture.

The model was implemented in Matlab-code [21], using the free-ware finite element toolbox CALFEM [22] for the definition of the elements and the material properties and for assembling and

solving of the equation system. Evaluation of the composite material properties was then made by means of Matlab.

Table 1: Model parameters

Side length of RVE (mm) = $l_x = l_y$	10 mm
Number of elements/side	20, 30, 50, 75, 100, 150
Fibre width / side length	0.02, 0.04, 0.05, 0.06, 0.08, 0.1, 0.125, 0.15, 0.2, 0.25, 0.3, 0.4
Number of fibres/RVE	Randomly from 1 to 20

Table 2: Fibre material parameters in local coordinates, *x* being the longitudinal direction of the fibre, *y* and *z* being the transverse directions, respectively:

E_x (GPa)	40	ν_{xy} (-)	0.2	G_{xy} (GPa)	4	β_x (-)	$0.01 \cdot 10^{-2}$
E_y (GPa)	5	ν_{xz} (-)	0.2	G_{xz} (GPa)	4	β_y (-)	$0.26 \cdot 10^{-2}$
E_z (GPa)	5	ν_{yz} (-)	0.3	G_{yz} (GPa)	2	β_z (-)	$0.26 \cdot 10^{-2}$

Table 3: Matrix material parameters:

E (GPa)	5.75
ν (-)	0.3
β (-)	$0.01 \cdot 10^{-2}$

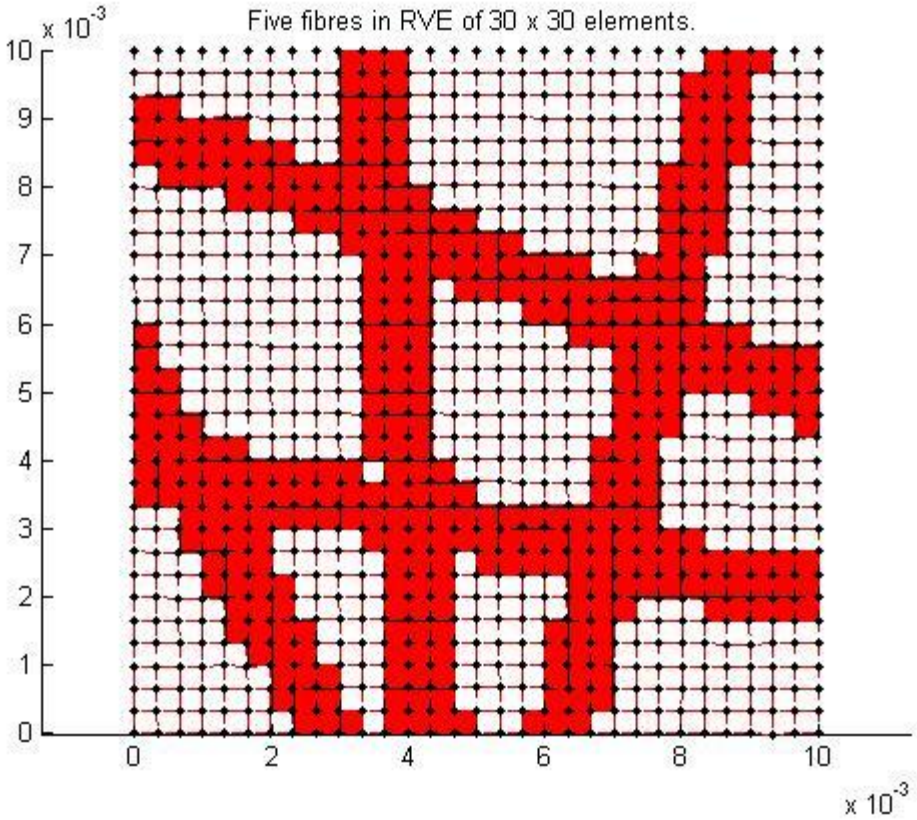

Figure 1: A square unit cell with physical dimensions 10 x 10 mm, with 30x30 elements and 5 fibres with a width relative to unit cell side length of 0.1.

Choice of modelling parameters

A sufficient size of the RVE and a sufficiently fine finite element mesh are needed for representative and accurate numerical results. These modelling parameters were therefore studied before investigating the homogeneous strain assumption.

Figure 2 shows the calculated normalized stiffnesses in the *x*- and *y*-directions as a function of the number of finite elements, *n*, along a side of the RVE. The number of degrees of freedom is $2n^2$ and calculations were made for $n = 20$ to $n = 150$. Simulations with three different fibre configurations showed an accuracy better than 1 percent for $n \geq 50$ for all three different fibre configurations, both in the *x*- and *y*-directions. $n = 50$, corresponding to 2500 elements and 5000 degrees of freedom was estimated to be sufficiently large and was thus used throughout in the subsequent calculations.

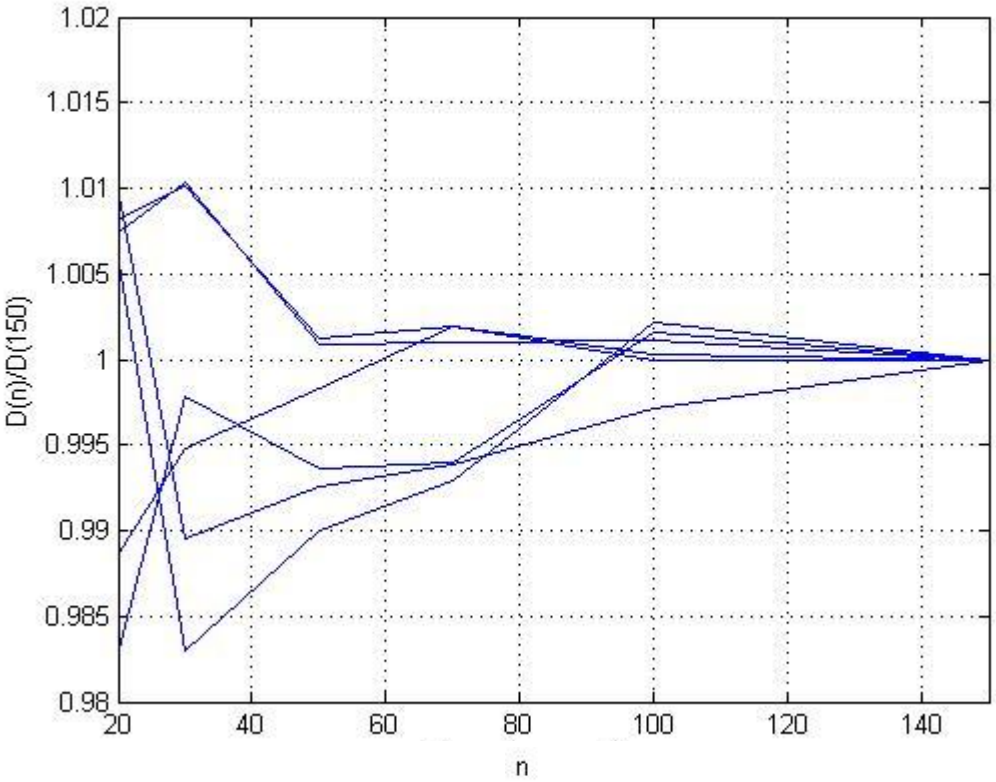

Figure 2. Convergence – the ratio between stiffness at n elements per side and stiffness at 150 elements per side.

The influence of ratio fibre width to cell side length was investigated by performing a large number of simulations for different fibre volume fractions. The simulations were divided into eight groups with a volume fraction within the following intervals: [15-25], [25-35], [35-45], [45-55], [55-65], [65-75], 7[5-85] and [85-95] percent. Different fibre volume fraction was for constant fibre width obtained by change of the number of fibres. This means that any certain interval of fibre volume fraction comprise fibre networks made up of few wide fibres as well as networks made up of many narrow fibres.

Figure 3 shows the stiffnesses found for the fibre volume fraction interval 55-65 percent. The figure also shows a linear regression for stiffness versus fibre width with an estimated inclination k = -3.08 GPa per 100 percent, that is less than the estimated inclination's standard deviation σ = 3.12 GPa per 100 percent.

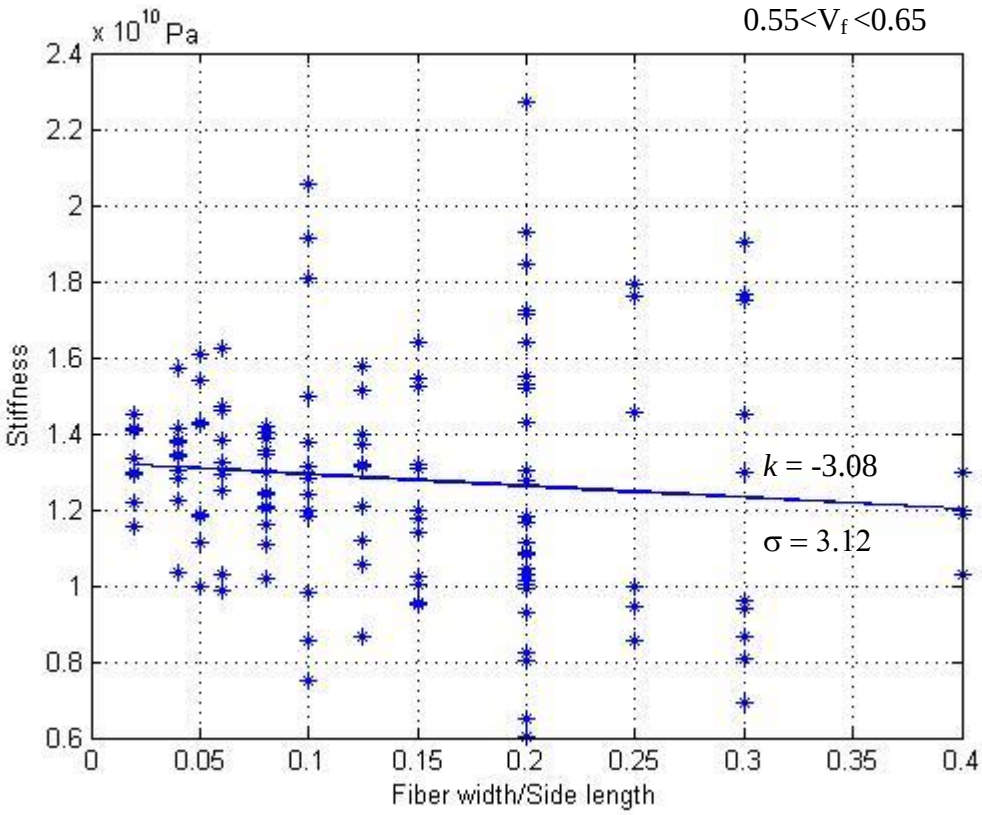

Figure 3. Unit cell stiffness as a function of fibre width relative to side length. Volume fraction of the unit cells are in the interval between 55 and 65 percent.

Figure 4 shows the regression lines for all above mentioned intervals. Higher fibre volume fraction implicates higher stiffness, which means that the regression line from Figure 3 is the fifth line from the bottom and is the line with the largest inclination. The results indicate that there is no significant influence of the ratio fibre width to unit cell length if less than about 0.3. A fibre width of 0.1 times the cell side length was used in the subsequent simulations.

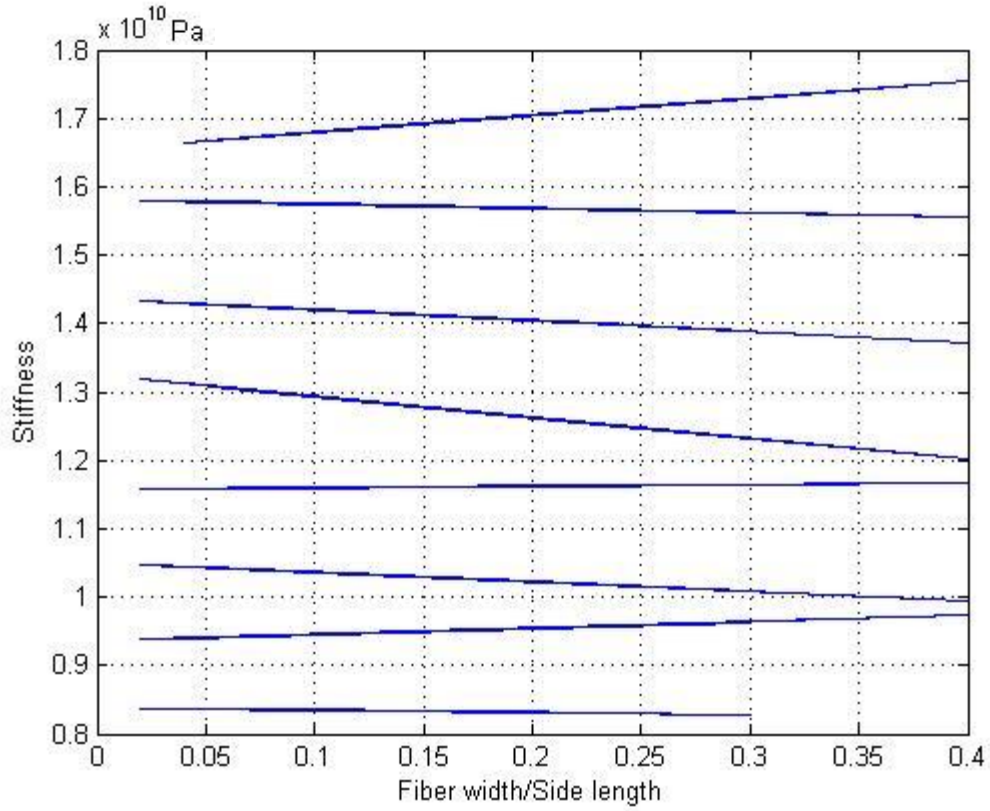

Figure 4. Unit cell stiffness as a function of fibre width relative to side length. All intervals of volume fractions, from bottom and up: 15-25 percent, 25-35 percent up to 85-95 percent.

Results

For investigation of the homogeneous strain and stress assumptions was 100 unit cells generated with a random number of fibres in the range from 1 to 20, oriented and located at random. The stiffness and moisture expansion properties of these cells were determined as described in the above and then, for each individual unit cell, compared to the corresponding results as produced by the homogeneous strain and homogeneous stress assumptions. The homogeneous strain composite material stiffness was calculated as the average material stiffness matrix of the 2500 finite elements and homogeneous stress stiffness was calculated as the inverse of the average compliance matrix for the finite elements. The homogeneous strain and stress composite material moisture expansion properties were calculated in the corresponding manner. The stiffness results are shown in Figure 5 where the 2x3x100=600 stiffnesses are plotted as a function of fibre volume fraction. The upper and lower bounds of the stiffness are for each fibre cell configuration given by homogeneous strain and stress assumptions. In figure 6 is the ratio between the homogeneous strain stiffness and the numerically simulated stiffness shown for the 2x100 stiffness values. This ratio is, as expected, for both directions and for all unit cells greater or equal to 1.0.

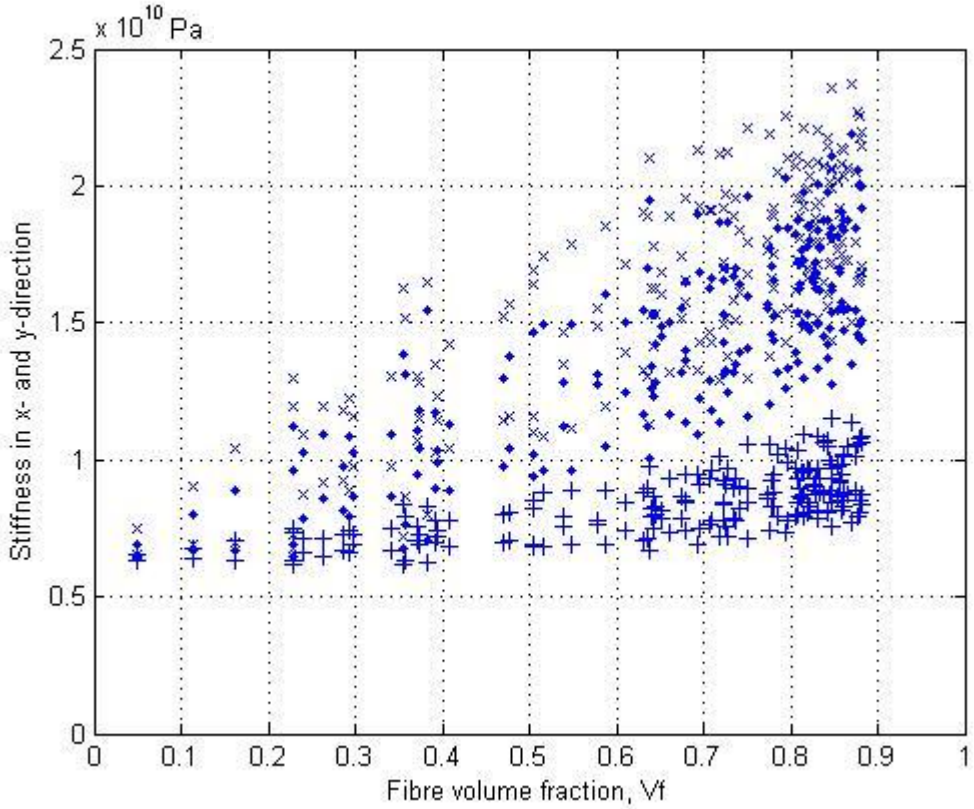

Figure 5. Homogenised stiffness in Pa in *x*- and *y*-directions according to: × – homogeneous strain, • – finite element simulation, + – homogeneous stress assumption.

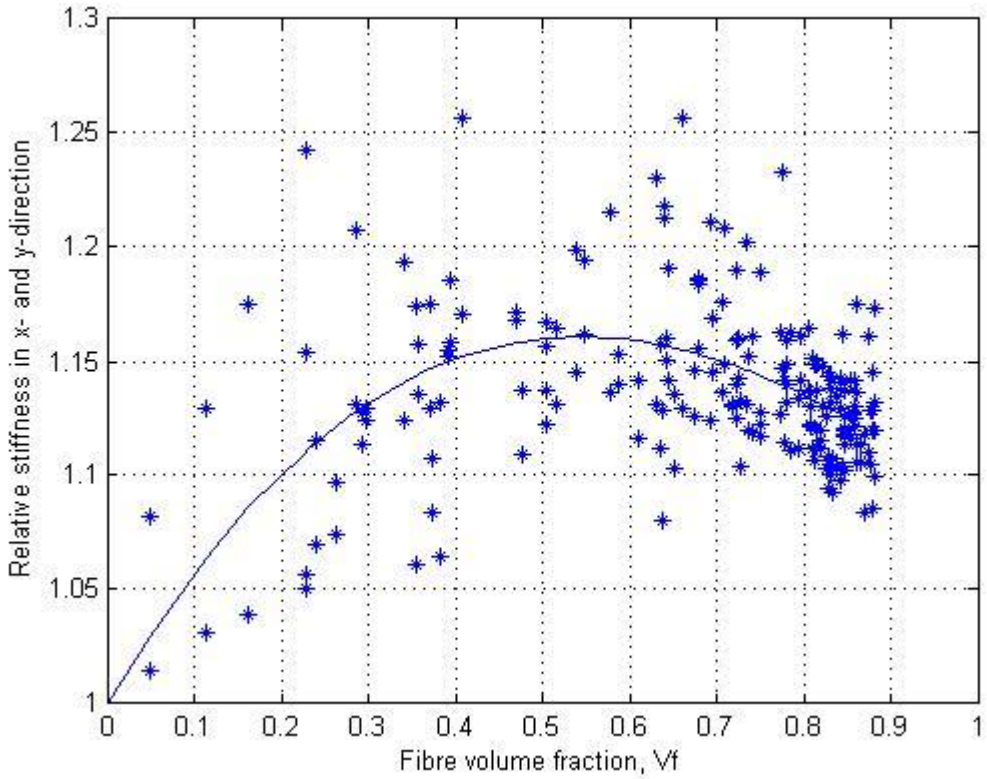

Figure 6. Relative stiffness = stiffness according to homogeneous strain divided by simulated stiffness for each simulated unit cell with a regression line according to least square method.

The free hygroexpansion results are shown i Figure 7. Here the homogeneous strain and stress assumptions are no longer giving bounds for the material properties as is the case of stiffness. This is evident in Figure 8, showing the hygroexpansion of the homogeneous strain assumption divided by the hygroexpansion of the simulations. For fibre volume fractions less than about 0.3 is the hygroexpansion ratio greater than 1, and for V_f greater than about 0.3 less than 1.

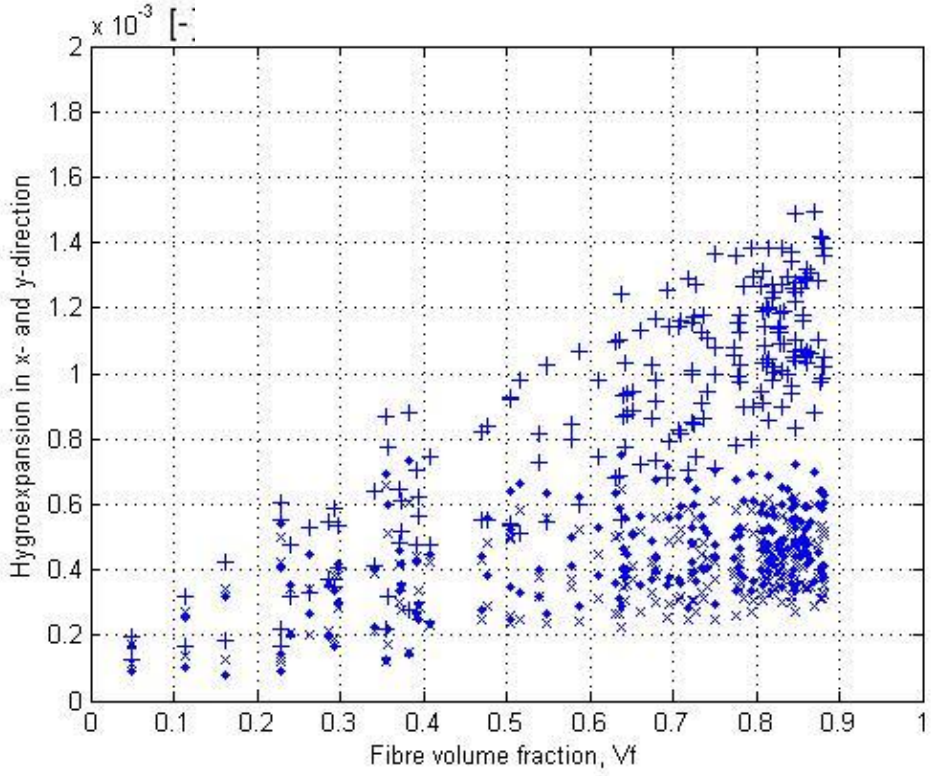

Figure 7. Homogenised hygroexpansion in *x*- and *y*-directions according to: x – homogeneous strain, · – finite element simulation, + – homogeneous stress assumption.

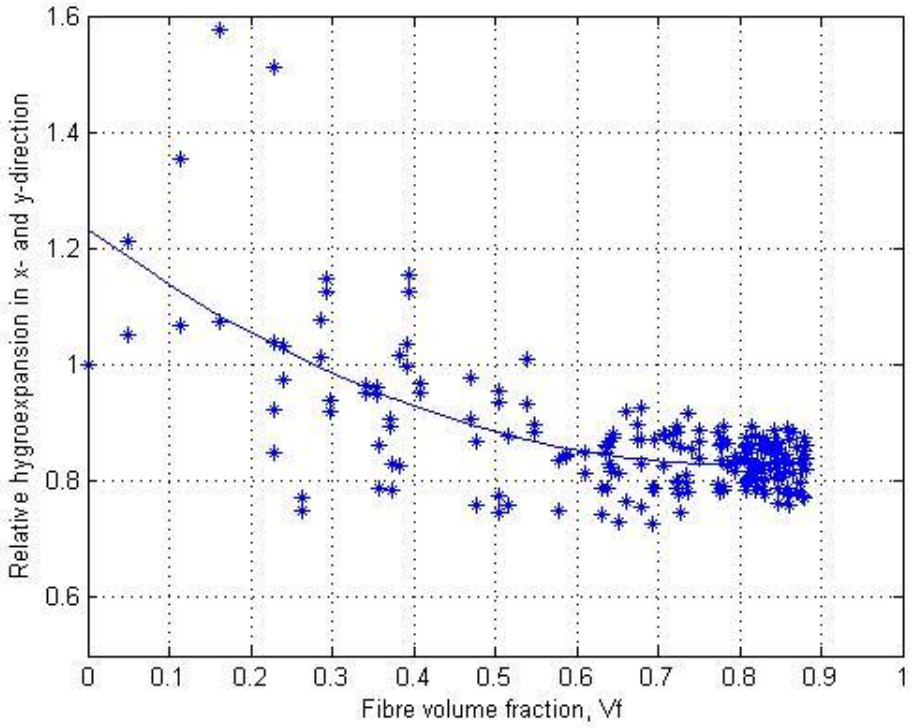

Figure 8. Relative hygroexpansion = hygroexpansion according to homogeneous strain divided by simulated hygroexpansion, with a regression line, calculated according to least square method.

Conclusion

This paper presents a homogenisation of a wood fibre network composite material. The homogenisation was performed using finite element analysis and cyclic boundary conditions and the aim of the analysis was to investigate if the assumption of homogeneous strain is valid for estimating stiffness and hygroexpansion of wood fibre composite materials with an in-plane random fibre orientation distribution.

First modelling parameters in terms required size and required finite element mesh of the RVE were determined. An RVE with a side length 10 times the fibre width and represented by a uniform finite element mesh with 50x50 elements were found to be sufficient. In the subsequent analysis were 100 RVE:s with various fibre volume fraction and with random orientation and location of the fibres analysed with respect to stiffness and hygroexpansion.

The results from the homogenisations show that the homogeneous strain assumption overestimates the simulated stiffness by approximately 15 percent and underestimates the simulated hygroexpansion by approximately 15 percent at the most interesting fibre volume fraction, which is around 60 percent. The deviation of the results of the homogeneous strain assumption from the results of the simulations is not greater than it can be justified to use the assumptions in analytical modelling of HPL materials. There is also a possibility to introduce a correction factor to an analytical model to take the deviation into account.

Acknowledgements

This work was financed by the Swedish Wood Technology Research Colleague, which is gratefully acknowledged. The authors would also like to thank the Structural Mechanics division for support and helpful discussions.

References

[1] Stålne K. Modelling of Stiffness and Hygroexpansion of Wood Fibre Composites. Licentiate Thesis. 2001. Div of Structural Mechanics, Lund University.
[2] Hashin Z. Analysis of Composite Materials – A survey. J Appl Mech 1983;50:481-505.
[3] Eshelby JD. The Determination of the Field of an Elliptical Inclusion and Related Problems. Proceedings of the Royal Society. London. 1957;A(241):376-396.
[4] Mori T, Tanaka K. Average Stress in Matrix and Average Elastic Energy of Materials with Misfitting Inclusions. Acta Metallurgica 1973;21:571-574.
[5] Stålne K, Gustafsson PJ. A 3D Model for Analysis of Stiffness and Hygroexpansion Properties of Fibre Composite Materials. J Eng Mat 2002;128(6):654-662.
[6] Stålne K. 3D Homogenisation of Hygroscopic Anisotropic Fibre Network Composite. Report TVSM-7156, Div. of Structural Mechanics, Lund University, Sweden.
[7] Aboudi J. Mechanics of Composite Materials. Elsevier: Amsterdam, The Nederlands, 1991.
[8] Hill R. Elastic Behaviour of a Crystalline Aggregate. Proceedings of the Physical Society, 1951;Section A:349-354.
[9] Christman T, Needleman A, Suresh S. On Microstructural Evolution and Micromechanical Modelling of Deformation of a Whisker-reinforced Metal-Matrix Composite. Mat Sci Eng 1989;A107:49-61.
[10] Baldwin JD, Altan MC, Rajamani K. Structural Analysis of an Injection Molded Short-Fiber-Reinforced Disc. J of Mat Proc and Manu Sci. 1997;6:123-145.
[11] Ghassemieh E, Nassehi V. Stiffness Analysis of Polymeric Composites Using the Finite Element Method. Adv in Pol Tech. 2001;20:42-57.
[12] Dasgupta A, Agarwal RK, Bhandarkar SM. Three-Dimensional Modeling of Woven-Fabric Composites for Effective Thermo-Mechanical and Thermal Properties. Comp Sci Tech 1996;56:209-223.
[13] Thom H. Finite Element Modelling of Plain Weave Composites. J Comp Mat 1999;33:1491-1510.
[14] Falzon PJ, Herszberg I. Effects of Compaction on the Stiffness of Plain Weave Fabric RTM Composites. J Comp Mat 1996;30:1210-1247.
[15] Whithcomb JD, Chapman CD, Tang X. Derivation of Boundary Conditions for Micromechanics Analysis of Plain and Satin Weave Composites. J Comp Mat 2000;34:724-747.
[16] Ishmar H, Schroter F, Streicher F. Modeling and Numerical Simulation of the Mechanical Behaviour of Woven SiC/SiC regarding a Three Dimensional Unit Cell. Computational Mat Sci 2000;19:320-328.
[17] Nilsen N, Niskanen K. A 3D Simulation Model for Paper Structure. Progress in Paper Physics – A Seminar Proceedings. 1996.
[18] Stahl DC, Cramer SM. A Three-Dimensional Network Model for a Low Density Fibrous Composite. J Eng Mat Tech 1998;120:126-130.
[19] Person K. Micromechanical Modelling of Wood and Fibre Properties. Doctoral Thesis 2001. Div of Structural Mechanics, Lund University.
[20] Hagstrand PO. Mechanical Analysis of Melamine-Formaldehyde Composites. Doctoral Thesis 1999. Chalmers University of Technology.
[21] Matlab 7.4. R2007a. The Math Works Inc., Natick, Ma, USA.
[22] CALFEM – A Finite Element Toolbox to MATLAB. Version 3.3. TVSM-9001.

Paper V

V

Measurement of Hygro-Mechanical Properties of a High-Pressure Laminate Composite Material

Kristian Stålne and Per Johan Gustafsson

Submitted for publication

Measurement of Hygro-Mechanical Properties of a High-Pressure Laminate Composite Material

Kristian Stålne, Per Johan Gustafsson
Division of Structural Mechanics, Lund University
P.O. Box 118, SE–221 00 Lund, Sweden

ABSTRACT: The hygro-mechanical behaviour of a high pressure laminate material, consisting of paper impregnated with melamine-formaldehyde resin with two different fibre volume fractions, has been characterised. The materials have been tested with regards to strength, stiffness, creep under short and long term loading, hygroexpansion, moisture uptake and mechanosorption at various constant and varying moisture contents. All in-plane strain components were recorded in most of the tests. An empirical model was developed to characterise the strain development at various load and moisture conditions. The materials show a significant accelerated creep at varying moisture, i.e. mechanosorption.

KEY WORDS: Wood fibre composites, high pressure laminate, elastic properties, creep, stiffness, moisture, mechanosorption, hygroexpansion.

Introduction

High-pressure laminate, HPL, is a wood fibre composite material whose usage has increased during the recent decades. HPL is used in building industry, in such applications as flooring and panelling, and as interior surface material in sanitary applications. It is made of craft paper impregnated with phenolic or melamine formaldehyde, the latter being used as the surface layer, making it hard and scratch resistant. Besides being environmentally friendly and cheap, there is an advantage in using cellulose fibres due to the good adhesion to the melamine resin improving mechanical properties such as stiffness and strength.

A key issue concerning wood based materials and composites is that of shape stability at long term loading and varying climate. A change in moisture content in the material, or an uneven moisture distribution can lead to large deformations. The deformation due to moisture change can by possible mechanosorption effect be increased by simultaneously acting load. In order to promote an increased use of HPL in more demanding environments a number of models have been developed to predict

the laminates behaviour under such conditions [1-3]. In order to enable verification of such models there is a need for experimental characterisation of the hygro-mechanical strain development properties of HPL materials at varying load and moisture conditions. The short term ramp loading properties of HPL materials at constant moisture have been investigated in a number of studies [4-6]. Any investigation of mechanical behaviour under long time loading and varying climate has not been found available in literature.

Models for analysis of creep and mechanosorption have for wood and wood-based materials such as fibre board and paper been presented in [7-10]. Mechanosorption have been studied and reported also for non organic hygroscopic materials, such as concrete [11].

The aim of the present study is to determine the actual hygro-mechanical behaviour of HPL by means of experimental tests. HPL materials with two fibre volume fractions are tested and most test comprise tensile loading in one direction with recording of the strain in the load direction and the transverse direction. By such determination it is possible to identify features of the strain development performance of HPL and to get a quantitative basis for calibration and verification of theoretical models. Based on the test results an empirical model is developed in this paper. The model comprises a number of Kelvin elements and is used to evaluate the presence of mechanosorption. 10 material parameters are needed and determined in order to characterise the material in uniaxial tension. The model can be used directly for the two qualities of HPL tested and is suited for validation of more general micro-mechanics based composite models, e.g. [12].

Materials and Method

Material

The high pressure laminates tested are made up of several layers of craft paper (S&H 023) impregnated with melamine formaldehyde. They were cured at a temperature of 190 centigrade and a pressure of 2.6 MPa. The composite is orthotropic due to a symmetric and continuous fibre orientation distribution curve with approximately 1.8 times higher fibre frequency in the papers machine direction, denoted the *y*-direction, than in the papers cross direction, denoted the *x*-direction. The laminate was cut into test pieces of size $200 \times 30 \times 1$ mm, Figure 1. The testing program comprised two composite materials, denoted O53 and O58, with different fibre volume fractions, V_f = 53 % and V_f = 58 %. Dry density, mass content ratios and volume fractions of fibres and pores are indicated in Table 1. The volume fractions were estimated from the measured density and mass ratio, assuming the densities of the fibre and matrix constituents to be ρ_f = 1500 kg/m^3 [13, 14] and ρ_m = 1480 kg/m^3 [5], respectively.

Table 1. *Density and content fractions of the two materials tested.*

Material	Mass content ratios, $\kappa = m_m/m_f$	Measured density, ρ [kg/m^3]	Porosity, V_p	Fibre volume fraction, V_f
O53	0.74	1380	0.075	0.53
O58	0.61	1400	0.063	0.58

Figure 1. *Two specimens, one with aluminium plates glued to the ends.*

Conditioning and preparation of specimens

The specimens were after manufacture and cutting stored for more than 6 months in a climate chamber with 50 % relative humidity, RH. The specimens were then separated into three groups and further conditioned for more than 2 months in 30, 50 or 70 % RH, respectively. Weighings were made to ensure moisture equilibrium before the start of testing. All conditioning and testing were made at a constant temperature, 23 °C. All tests involving mechanical load related to centric tensile loading in the *y*-direction. The load was applied by means of two pairs of aluminium plates that were glued and screwed to the ends of the specimen, Figure 1.

Testing program

The testing program is indicated in Table 2. Six kinds of tests, A – F, were carried out for the two materials O53 and O58. Most testing series comprised 4 nominally equal tests each. The tests of creep at various loads were made only for material O53 and only one or two nominally equal tests were made at each of the seven load levels. Completing tests relating to the hygroexpansion of a third material, O56, with a fibre volume fraction of 56%, were also made, although not indicated in Table 2. In the below is further information, about the test equipment and the 6 kinds of tests.

Table 2. *Testing program. Abbreviations: NOS = number of specimens, O53 = material with V_f = 53%, O58 = material with V_f = 58%, HTM = hydraulic testing machine, DOL = duration of load test rig, DSP = digital speckle photography.*

Test	A: Strength, stiffness	B: Stiffness, short time creep	C: Long time creep	D: Creep of various load	E: Hygro-expansion and sorption isotherms	F: Mechano-sorption
Loading	Ramp loading until failure, ~3 min	Ramp loading 38 s+20 min at 31 MPa	Constant load, ~5 weeks at 33 MPa	Constant loads: 10, 16, 21, 26, 33, 33, 37 and 42 MPa	Unloaded	Constant load, ~5weeks, 33 MPa
Loading device	HTM	HTM	DOL	DOL	Small test rig	DOL
Strain measurement	Extenso-meter	Extenso-meter	DSP	DSP	DSP	DSP
Climate (% RH)	50	30, 70	30, 50, 70	50	Varying: 20-30-50-70-88-80-70-50-30-0	Varying: 30-70-30-70-30-70...
NOS O53	-	4, 4	4, 4, 4	1+1+1+1+ 2+1+1= 8	4	4
NOS O58	4	4, 4	4, 4, 4	-	4	4

Test equipment

The ramp loading tests, A, and the short time creep tests, B, were carried out by a conventional servo hydraulic material testing machine. The specimens were clamped to holders in each end and loaded with an axial tensile force, Figure 2. The strain in the *y*-direction was determined by two extensometers, one at each side of the specimens, and the load was recorded by a conventional load cell. The measuring length of the extensometers was 50 mm.

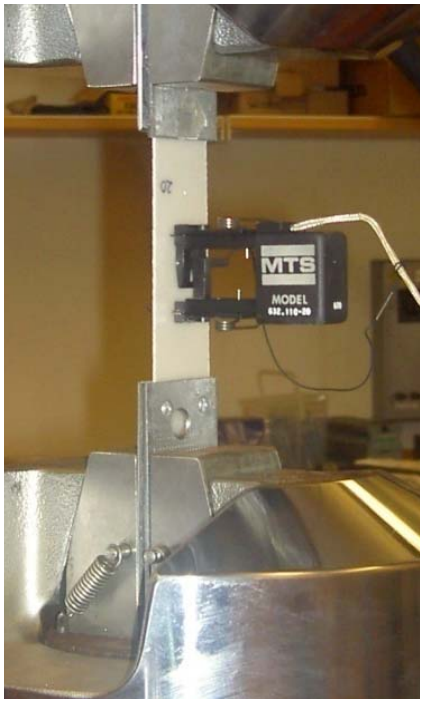

Figure 2. *Testing machine with clamped specimen and one extensometer.*

The specimens for the long time loading tests, C, D and F, were loaded in a duration of load test rig, each specimen exposed to loading from the weight of a number of steel plates hanging in the specimen, Figure 3. The rig allowed simultaneous testing of eight specimens. The rig was further more designed for strain determination as described below by means of a digital camera.

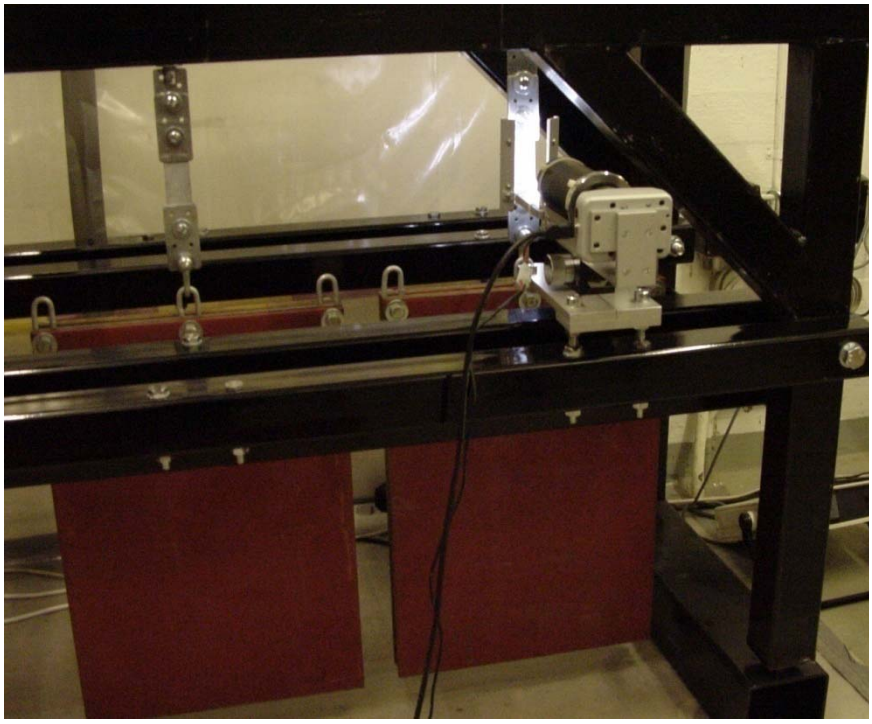

Figure 3*. Test rig with specimen loaded with steel plates and camera placed in holders.*

The tests of free hygroexpansion, E, were carried out by means of a small special purpose test rig that held the specimen plane and fixed when taking pictures for strain evaluation. The tests involving changing relative humidity were made in a room where the RH could be changed between different levels from 10 to 88 % at a rate of about 1 % per minute.

The strain measurements in the long time creep tests and the hygroexpansion tests, C-F, were made by means of a technique called digital speckle photography, DSP, which is based on a theory developed by Sjödahl [15]. DSP uses image correlation in order to evaluate the deformation field of the surface of a specimen from the difference between two digital images. From the deformation field all in-plane strain components, i.e. ε_x, ε_y and γ_{xy}, can be evaluated. The surfaces were before testing sprayed with small drops of black paint in order to obtain a random black and white pattern, which is needed for the image correlation. The DSP measurement equipment was specially built for the present tests and the deformation field evaluation was made by a correlation algorithm developed by Sjödahl [15].

Results

Stiffness, strength and Poisson's ratio

The materials tensile strength σ_f in the *y*-direction and the stiffness E_y were evaluated by means of the ramp loading tests A and B. The rate of loading was 25 N/s until failure. The tests were carried out to get information about the stress vs. strain performance and the stiffness and the strength of the O58 material when loaded in the *y*-direction. Strength tests were made only for material O58 and only at RH = 50 %. The results are presented in Table 3 and illustrated in Figure 4. Stiffnesses were evaluated as the initial inclination of the stress-strain curve. Poisson's ratio ν_{yx} was evaluated from the loading phase of the long time creep test, C. The definition of ν_{yx} is here ratio $-\varepsilon_x/\varepsilon_y$ for uniaxial load in the *y*-direction.

Table 3. *Strength and stiffness properties at various RH.*

	RH = 50%	RH = 30%		RH = 50%		RH = 70 %	
Material	σ_f (std) (MPa)	E_y (std) (GPa)	ν_{yx} (std) (-)	E_y (std) (GPa)	ν_{yx} (std) (-)	E_y (std) (GPa)	ν_{yx} (std) (-)
O53	-	11.6 (0.3)	0.32 (0.05)	-	0.36 (0.08)	11.2 (0.2)	0.36 (0.05)
O58	117 (2)	13.8 (0.2)	0.31 (0.09)	13.8 (0.1)	0.35 (0.07)	13.7 (0.6)	0.35 (0.04)

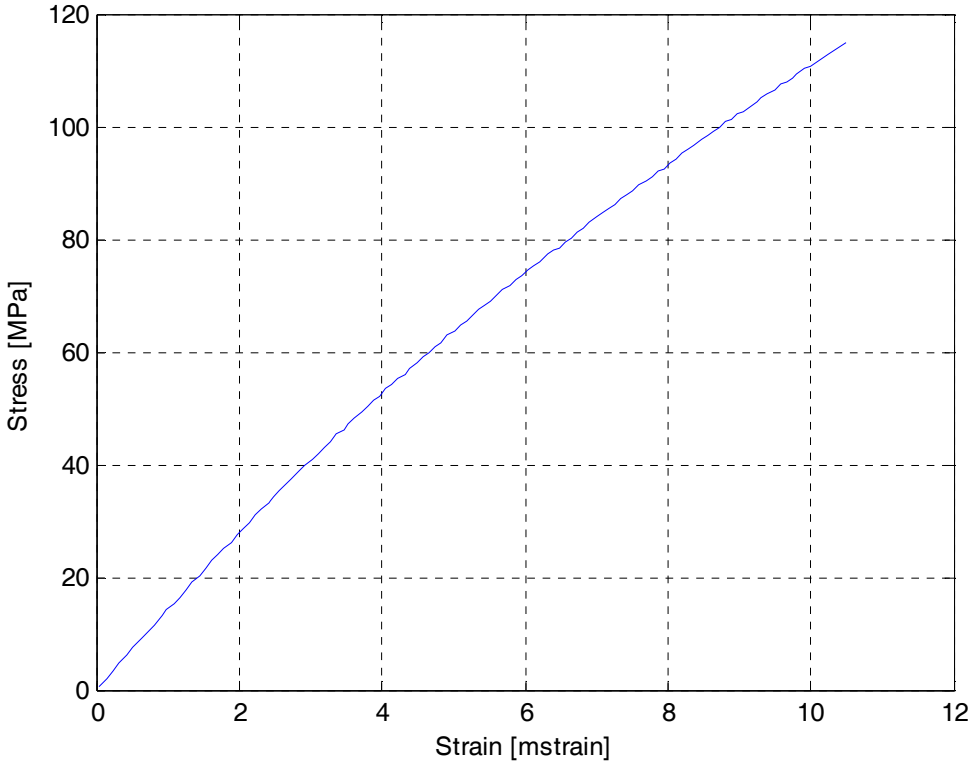

Figure 4. *Strength test on material O58 at 50 % RH.*

Short time creep

In test B both materials O53 and O58 were loaded up to about 30 % of the materials strength at relative humidities of 30 and 70 %.The specimens were first exposed to loading with 25 N/s for about 38 s, and then a constant load of 940 N, corresponding to a tensile stress of 31 MPa, for 20 minutes. The ramp loading part of the test was carried out to get further information about the stiffness of the materials and the second constant load part of the test was for evaluating the creep strain development during a short time of loading. The equipment for long time creep testing is not well suited for strain determination at short time loading. The recorded total strains versus time at different RH are presented in Table 4.

Table 4. *Short time loading strains in the y-direction in mstrain.*

Material		ε (std)		
		t = 38 s	t = 0.1 h	t = 0.3 h
O53	RH = 30%	2.68 (0.06)	2.80 (0.08)	2.86 (0.08)
	RH = 70%	2.84 (0.03)	3.06 (0.01)	3.17 (0.01)
O58	RH = 30%	2.26 (0.04)	2.40 (0.05)	2.46 (0.05)
	RH = 70%	2.34 (0.02)	2.50 (0.03)	2.58 (0.04)

Long time creep

The specimens were slowly exposed to loading by gradual release of a lever jack that carried the weight of the steel plates. The time from zero load to the full load, 980 N, was about 1-2 minutes. This load was kept constant during the entire creep test, about 5 weeks. The strains ε_x and ε_y, were recorded by the DSP system both during the loading procedure and several times during the creep test period. The strains recorded during the loading procedure are, however, not considered to be very accurate due to practical difficulties. The tests were made under constant climate for three different RH: 30, 50 and 70 %. The result from the long time creep tests, C, are presented in Table 5 and 6, which for different loading time show mean and standard deviations of the total strains in the *y*-, and the *x*-direction. The strain at full loading at $t = 0$ was set equal to the corresponding strain in the *y*-direction at the short time creep tests at $t =$ 38 s. The strain in the *y*-direction was for the times $t = 0.1$ h and $t = 0.3$ h measured both during the short time test, B, and of the long time test, C. Comparison between Table 4 and 5 shows good agreement between the strain recorded at these two overlapping instants of time. The results are illustrated also in Figure 5, showing mean total strain for each group of tests. The creep in the *y*-direction increases with an increase in moisture content, whereas creep in the *x*-direction decreases with an increase in moisture content. At 50 and 70 % RH is the creep in the *x*-direction virtually zero.

Table 5. *Long time total strain in the y-direction with standard deviations.*

Material		$\varepsilon_y \cdot 10^3$ (std $\cdot 10^3$)					
		$t = 0.1$ h	$t = 0.3$ h	$t = 1$ h	$t = 10$ h	$t = 100$ h	$t = 700$ h
O53	30%	2.80 (0.04)	2.86 (0.02)	2.92 (0.04)	2.94 (0.06)	3.00 (0.08)	3.30 (0.09)
	50%	2.93 (0.10)	2.96 (0.13)	3.07 (0.12)	3.16 (0.12)	3.58 (0.24)	4.04 (0.27)
	70%	3.06 (0.05)	3.16 (0.05)	3.29 (0.06)	3.62 (0.08)	4.56 (0.15)	5.40 (0.20)
O58	30%	2.40 (0.04)	2.43 (0.02)	2.47 (0.01)	2.53 (0.03)	2.70 (0.03)	2.99 (0.07)
	50%	2.45 (0.08)	2.46 (0.10)	2.45 (0.08)	2.61 (0.12)	2.88 (0.08)	3.10 (0.18)
	70%	2.50 (0.06)	2.59 (0.08)	2.69 (0.11)	2.83 (0.10)	3.40 (0.18)	4.07 (0.12)

Table 6. *Long time total strain in the x-direction with standard deviations.*

Material		$-\varepsilon_x \cdot 10^3$ (std $\cdot 10^3$)					
		$t = 0.1$ h	$t = 0.3$ h	$t = 1$ h	$t = 10$ h	$t = 100$ h	$t = 700$ h
O53	30%	0.95 (0.28)	1.00 (0.04)	1.05 (0.05)	1.30 (0.05)	1.83 (0.12)	2.29 (0.23)
	50%	0.99 (0.02)	1.06 (0.05)	1.11 (0.06)	1.26 (0.15)	1.21 (0.35)	1.40 (0.30)
	70%	1.06 (0.04)	1.10 (0.04)	1.15 (0.04)	1.27 (0.05)	1.07 (0.02)	1.09 (0.03)
O58	30%	0.77 (0.03)	0.78 (0.01)	0.82 (0.02)	1.11 (0.04)	1.78 (0.05)	2.24 (0.16)
	50%	0.77 (0.02)	0.81 (0.04)	0.82 (0.09)	0.82 (0.15)	0.68 (0.25)	0.78 (0.21)
	70%	0.82 (0.03)	0.87 (0.06)	0.88 (0.07)	1.00 (0.06)	0.95 (0.15)	0.88 (0.11)

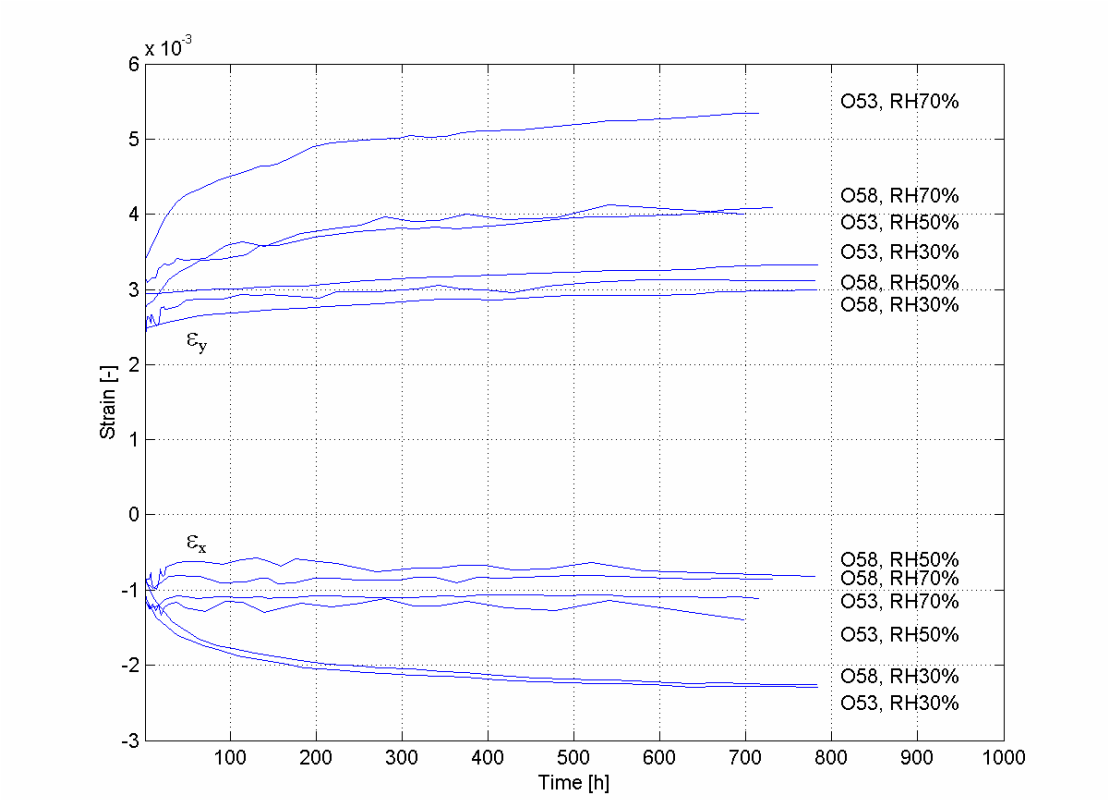

Figure 5. *Long time creep curves in y- and x-direction.*

Creep at various loads

Eight nominally equal specimens were exposed to different magnitudes of load. The loading was decided by the number of weight plates. The eight specimens were exposed to 2, 3, 4, 5, 6, 6, 7 and 8 plates, respectively, each plate having a weight of about 163 N. The tests were made to find out if and when the creep is linear, i.e. if the creep strain is proportional to the load level. The results from the measurement D of creep strain in material O53 at different loads and RH = 50 % are presented in Table 7. The table shows the creep strain, $\varepsilon_c = \varepsilon - \varepsilon_e$, divided by the stress σ. Recorded ratio ε_c/σ is scattered for t = 1 h and t = 10 h, but there is no significant influence of σ, neither at t = 1 h, 10 h, 100 h, nor at 1000 h. Thus the creep strain can be regarded to be proportional to the stress, i.e. the creep can be regarded as linear, at least for $\sigma \leq 44$ MPa.

Table 7: *Ratio creep strain ε_c to stress σ at various load levels for material O53.*

Loading stress σ (MPa)	t = 1 h $\varepsilon_c/\sigma \cdot 10^6$ (MPa^{-1})	t = 10 h $\varepsilon_c/\sigma \cdot 10^6$ (MPa^{-1})	t = 100 h $\varepsilon_c/\sigma \cdot 10^6$ (MPa^{-1})	t = 1000 h $\varepsilon_c/\sigma \cdot 10^6$ (MPa^{-1})
11	4.7	11.2	26.8	38.4
16	1.5	8.7	21.3	31.4
22	5.4	15.0	26.4	43.5
27	2.0	9.0	21.7	34.4
33	5.4	14.9	26.7	41.0
33	3.1	13.7	24.3	39.6
38	3.6	12.3	25.4	40.7
44	2.8	10.7	22.2	38.6

Moisture equilibrium curves and sorption isotherms

The hygroexpansion properties were evaluated by measuring the strain field at different moisture content. The specimens were stored for a long time in 50 % RH and then conditioned until equilibrium in 20-30-50-70-90-80-70-50-30-0 % RH. The last desorption was made by drying the specimens completely in an oven. The time to reach equilibrium in each climate was approximately 8 days. The sorption isotherms were obtained by weighing of the specimens. The specimen's free hygroexpansion were during the entire procedure evaluated using the DSP system. This expansion and shrinkage was evaluated for the *x*- and *y*-directions. The moisture content, *w*, was determined according to $w = (m - m_o)/m_o$, where m_o is the dry weight of the material. The RH was kept constant at each level until the moisture content was stabilised. The materials diffusivity was estimated from the equilibrium curves, assuming 1 dimensional Fickian flow, to be approximately $D_w = 9$ m^2/s for both materials. The moisture equilibrium curves of the materials O53 and O58 are shown in Figure 6. The values shown are the means for the four specimens tested of each material. The lowest and the highest RH levels 20 % and 90 %, respectively, could not be maintained by the climate room until the specimens reached equilibrium.

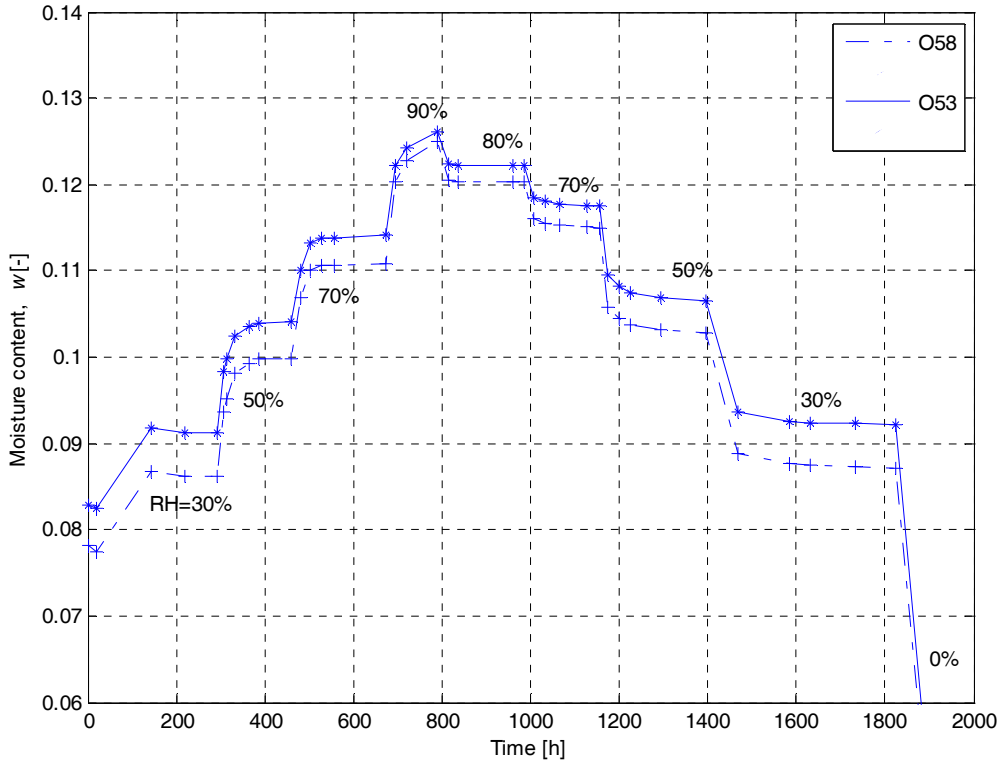

Figure 6. *Moisture equilibrium curves for O53 and O58.*

Sorption curves were evaluated from the moisture equilibrium curves. The result is indicated in Table 8, showing the moisture content *w* at equilibrium of different RH. Mean value and standard deviation of the four specimens of each material are indicated. Both materials show a small hysteris effect. The results for 20 and 90 % RH may not be accurate since equilibrium was not reached.

Table 8. *Sorption isotherms: mean value and (standard deviation) of the equilibrium moisture content w at different RH.*

Material	20 %	30 %	50 %	70 %	90 %	80 %	70 %	50 %	30 %
O53	0.082 (0.0003)	0.091 (0.0002)	0.104 (0.0003)	0.114 (0.0002)	0.126 (0.0002)	0.122 (0.0002)	0.118 (0.0002)	0.107 (0.0002)	0.092 (0.0002)
O58	0.078 (0. 0004)	0.086 (0. 0004)	0.100 (0. 0005)	0.111 (0. 0005)	0.125 (0. 0007)	0.121 (0. 0007)	0.115 (0. 0006)	0.103 (0. 0005)	0.087 (0.0004)

Hygroexpansion

The free hygroexpansion strain was measured at the same time and for the same specimens as the moisture equilibrium curves and the sorption isotherms. The hygroexpansion coefficients of the materials were then evaluated from the hygroexpansion strains and the moisture content for the following intervals of RH: 30 to 50 %, 50 to 70 %, 70 to 50 % and 50 to 30 %. The two in-plane hygroexpansion coefficients are defined as $\beta_y = \Delta\varepsilon_y / \Delta w$ and $\beta_x = \Delta\varepsilon_x / \Delta w$.

Table 9 shows for the two materials means and standard deviations of $\Delta\varepsilon_y$, $\Delta\varepsilon_x$, Δw, β_y and β_x for the four humidity intervals. Average values of β_y and β_x are also shown.

Table 9. *Hygroexpansion coefficients in y- and x-direction.*

	RH	30% → 50%	50% → 70%	70% → 50%	50% → 30%	Average
O53	$\Delta\varepsilon_y \cdot 10^3$ (std) / $\Delta w \cdot 10^3$ (std) = β_y (std)	2.00 (0.2) / 12.8 (0.4) = 0.157 (0.02)	1.52 (0.2) / 10.1 (0.3) = 0.151 (0.02)	–1.62 (0.2) / –11.0 (0.3) = 0.148 (0.02)	–2.52 (0.1) / –14.4 (0.3) = 0.175 (0.01)	0.158
	$\Delta\varepsilon_x \cdot 10^3$ (std) / $\Delta w \cdot 10^3$ (std) = β_x (std)	2.81 (0.1) / 12.8 (0.4) = 0.220 (0.01)	2.27 (0.2) / 10.1 (0.3) = 0.225 (0.02)	–2.32 (0.03) / –11.0 (0.3) = 0.212 (0.006)	–3.49 (0.09) / –14.4 (0.3) = 0.242 (0.008)	0.225
O58	$\Delta\varepsilon_y \cdot 10^3$ (std) / $\Delta w \cdot 10^3$ (std) = β_y (std)	1.51 (0.04) / 13.7 (0.7) = 0.111	1.17 (0.07) / 11.0 (0.7) = 0.106	–1.34 (0.09) / –12.1 (0.8) = 0.110	–1.88 (0.14) / –15.8 (0.6) = 0.119	0.112
	$\Delta\varepsilon_x \cdot 10^3$ (std) / $\Delta w \cdot 10^3$ (std) = β_x (std)	3.03 (0.18) / 13.7 (0.7) = 0.222 (0.006)	2.38 (0.13) / 11.0 (0.7) = 0.215 (0.02)	–2.54 (0.13) / –12.1 (0.8) = 0.210 (0.02)	–3.85 (0.06) / –15.8 (0.6) = 0.244 (0.01)	0.223

The hygroexpansion coefficient β_x is larger than β_y, as could be expected from the fibre orientation distribution. If comparing the two materials, there is no significant difference in β_x. Coefficient β_y is, on the other hand, significantly lower for O53 than for O58. This unexpected result indicating less hygroexpansion in the y-direction for the material with more fibres was verified by doing the entire hygroexpansion test twice. Here only the result of the first set of tests is presented. The second set of tests gave almost exactly the same result.

Mechanosorption

In addition to the long time creep tests at constant climate, a set of eight specimens were exposed to the same loading at cyclically changing RH. The humidity was kept at 70 % for 1 week, then at 30 % for 1 week, than at 70 % for 1 week, and so on. The specimens were before the application of the load stored for over one month in 70 % RH. The test was made to evaluate possible accelerated creeping due to varying moisture content, i.e. possible mechanosorptive behaviour of the material.

The total strains ε_y and ε_x were measured for the two materials O53 and O58. These recorded total strains are shown as a function of time in Figure 7. The curves are mean curves for each group of specimens. It is evident that the two materials differ with respect to ε_y.

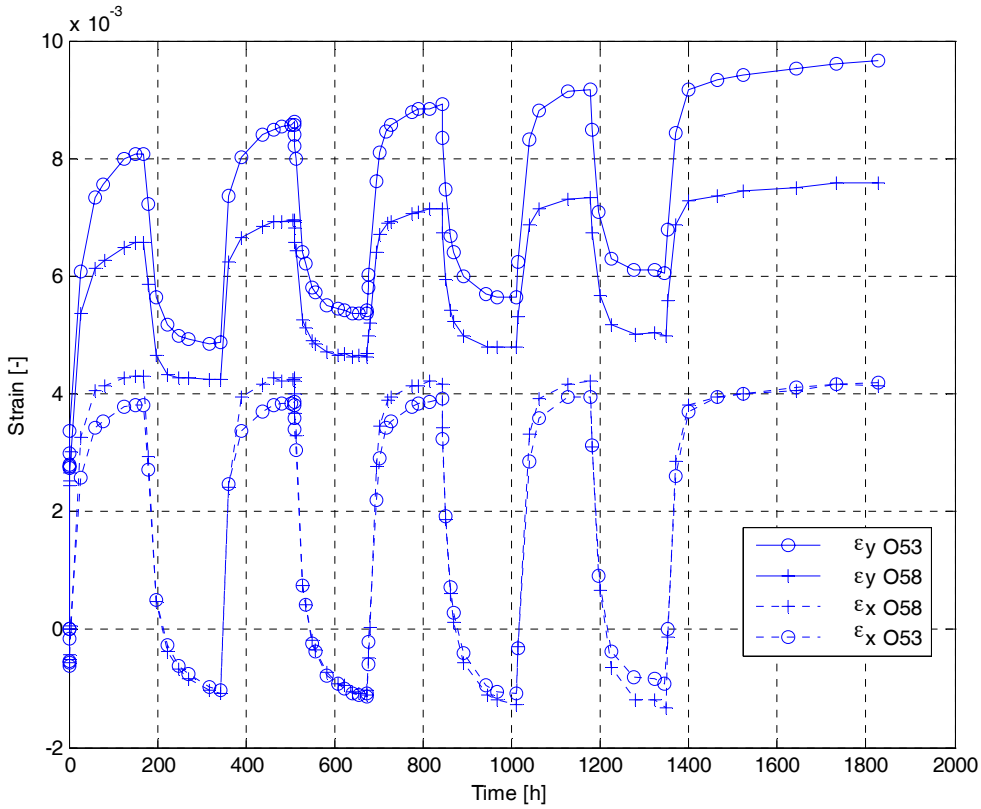

***Figure 7**. Strain at constant load and with RH cycled between 30% and 70%, starting at 30%.*

Analysis

In order to evaluate the presence of mechanosorption an empirical one dimensional material model for the two composite materials is developed by means of the data from the measurements of stiffness, creep, mechanosorption and hygroexpansion. The model proposed in [12] and illustrated in Figure 8, calculates the total strain as the sum of the elastic, creep, mechanosorption and hygroexpansion strain.

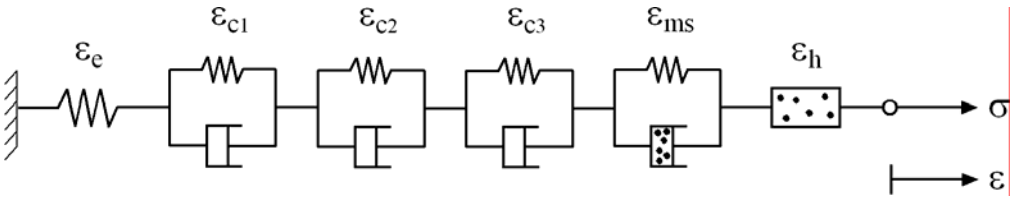

***Figure 8**. Total strain calculated as the sum of elastic, creep, mechanosorption and hygroexpansion strain.*

If the change in moisture content |dw| can be regarded as constant over a number of cycles the total strain $\varepsilon(t)$ at time t is for the stress history $\sigma(t)$ given by the model as:

$$\varepsilon(t) = \frac{\sigma_0(t)}{E} + \int_0^t \frac{\sigma(t')}{E}\left(\sum_{i=1}^{N}\frac{\mu_i}{\tau_i}\cdot e^{\frac{t'-t}{\mu_i\tau_i}} + \frac{|\dot{w}|}{\alpha}\cdot e^{-\frac{t'-t}{\alpha\lambda}|\dot{w}|}\right) + \beta\cdot\dot{w}\,dt \qquad (1)$$

where $N = 3$ and where μ_i, τ_i, α, λ and β are different material parameters. Linear creep is accordingly assumed as suggested, by the results in Table 8. For constant stress, $\sigma(t) = \sigma_0$, is Equation 1:

$$\varepsilon(t) = \frac{\sigma_0}{E}\left(1 + \int_0^t\left(\sum_{i=1}^{N}\frac{\mu_i}{\tau_i}\cdot e^{\frac{t'-t}{\mu_i\tau_i}} + \frac{\lambda|\dot{w}|}{\alpha}\cdot e^{\frac{t'-t}{\alpha\lambda}|\dot{w}|}\right)dt\right) + \beta\cdot(w - w_0) \qquad (2)$$

The creep strain is in the present application modelled by three Kelvin elements, each with a spring and a parallel dashpot. Three elements, $N = 3$, were found to be sufficient for accurate modelling of the creep test data. This means that a total of 10 material parameters are needed for definition of the uniaxial strain performance of a material. The modulus of elasticity, $E = E_y$, is given in Table 4. E_y does not seem to be significantly affected by the relative humidity and was in the present application assumed to be moisture independent with E_y = 11.4 GPa for material O53 and E_y = 13.8 GPa for material O58.

The 3+3 parameters μ_i and τ_i that define the creep properties were determined by least square fit to the creep results for ε_y indicated in Figure 5. The numerical values are given in Table 10. The creep performance seems, unlike the elastic stiffness E_y to be affected by the relative humidity, at least in terms parameters μ_3 and τ_3, representing the rate of creep at long time loading. In the present analysis of creep at varying moisture were the creep parameters assumed to vary linear with w, the linear variation being according to the parameter values determined at RH = 30 % and 70 %.

The mechanosorption parameters λ and α were determined by fit to the test results in Figure 6 and were assumed to be moisture independent. The hygroexpansion coefficient $\beta = \beta_y$ was in accordance with Table 9 made equal to 0.158 for material O53 and 0.112 for material O58.

Table 10. *Creep and mechanosorption material parameters.*

Material		μ_1	τ_1	μ_2	τ_2	μ_3	τ_3	λ	τ
O53	30%	0.036	0.017	0.066	0.44	0.42	1940	2500	150
	70%	0.062	0.020	0.106	0.50	0.62	104		
O58	30%	0.040	0.012	0.070	0.23	0.21	245	2000	150
	70%	0.038	0.014	0.081	0.23	0.52	131		

The moisture absorption and desorption shown in Figure 4 from a moisture content w_1 to a moisture content w_2 are for the present test specimens described by an exponential function according to Equation 3.

$$w_2 = w_1 + (w_2 - w_1) \cdot \left(1 - e^{-\frac{t}{\tau_w}} \right) \tag{3}$$

where the time constant is estimated to τ_w = 20 h from the moisture equilibrium curves in Figure 6.

Figure 9 and 10 show the total strains measured in the mechanosorption tests and according to the model, without mechanosorption. The constant stress, σ, is 33 MPa. It is evident that the two HPL materials show a significant mechanosorptive effect. The development of the total strain at varying moisture can not be explained by creep and hygroexpansion.

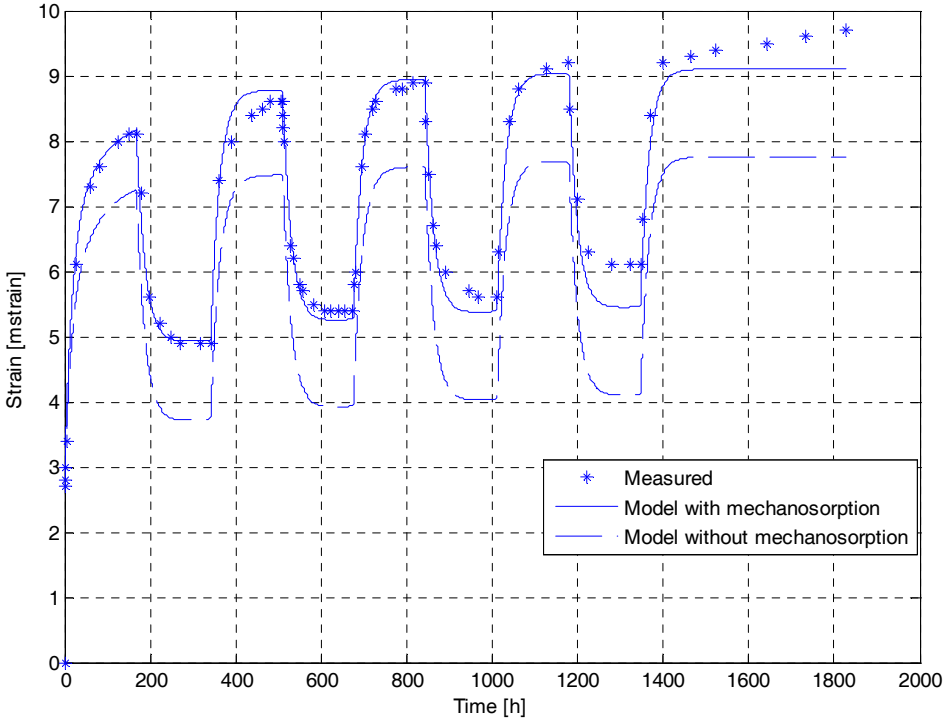

Figure 9. *Total strain ε_y for material O53 at varying moisture.*

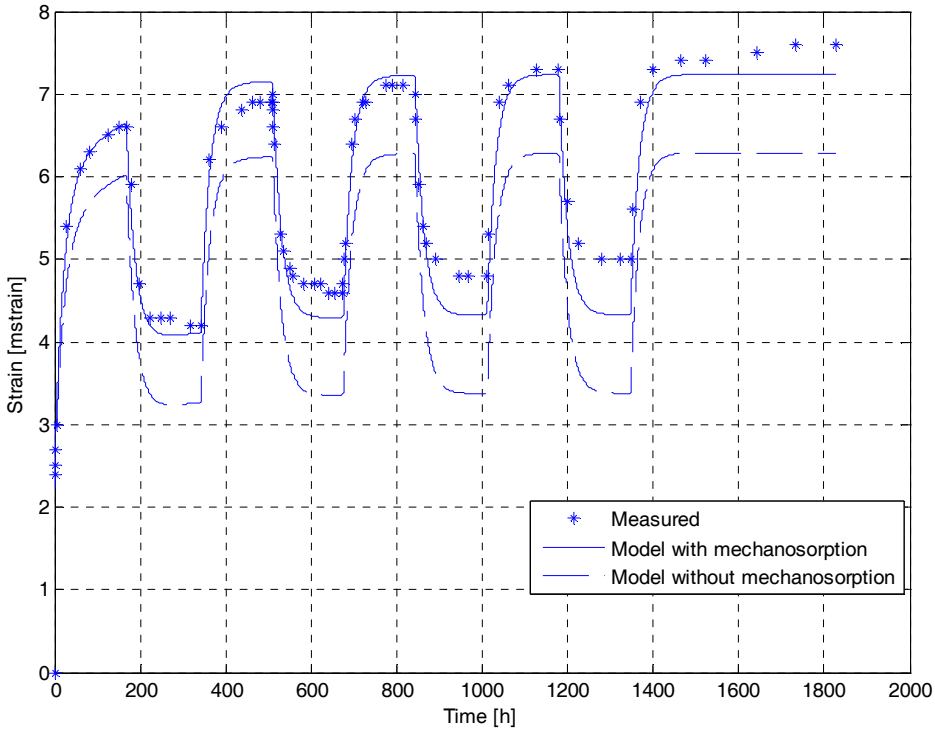

Figure 10. *Total strain ε_y for material O58 at varying moisture.*

Concluding discussion

The hygro-mechanical properties of two high pressure laminate materials with different fibre volume fraction have been tested. Moisture equilibrium curves, sorption isotherms, as well as elastic, creep, hygroexpansion and mechanosorption strains were recorded.

The elastic stiffness was not found to be effected by the moisture level. As expected, an increase in fibre volume fraction gave a higher material stiffness and a decrease in creep strain. The hygroexpansion coefficients in the *x*-direction, i.e. the cross machine direction of the paper, are equal for the two materials, but differ significantly in the *y*-direction, where β_y is higher for material O53. This is worth noting since O53 contains a lower amount of fibres than material O58. The hygroexpansion coefficients were found to be about constant in the interval of moisture content corresponding to RH = 30 % to 70 %, and also about the same at adsorption and desorption.

Short time and long time creep tests were combined to evaluate the creep of the two materials. The creep strains are highly dependent on the moisture content. At high moisture content the creep strain is much larger in the loading direction than at lower moisture content. In the transverse direction it is the opposite, i.e. the transverse creep strain is larger at lower moisture content. This could imply that the materials at

conditioning had not yet fully expanded or contracted, although the moisture content was in balance.

It was also found that the creep is linear, i.e. the creep strain is proportional to the stress, up to at least to a stress corresponding to about 40 % of the short term ramp loading strength. The strain under a constant load and varying relative humidity was also tested in order to evaluate the presence of mechanosorption.

An empirical model of the strain as the sum of the elastic, creep, mechanosorption and hygroexpansion strain was created. Creep and mechanosorption strains were modelled as a number of serial coupled Kelvin elements. Indata to the model were evaluated by fitting the model to the curves from the measurements of stiffness, creep, mechanosorption and hygroexpansion, respectively. The evaluation show significantly increased creep strain under varying moisture content. It is thus evident that the performance of HPL is significantly affected by mechanosorption.

Acknowledgments

This work was financed by the Swedish Wood Technology Research Colleague, which is gratefully acknowledged.

References

1. **Brauns, J.** Hygromechanical Behaviour of Wooden Composites. 1997, Vol. 31(3).
2. **Stålne, K., Gustafsson, P.-J.** Three-Dimensional Model for Analysis of Stiffness and Hygroexpansion properties of Fibre Composite Materials. *Journal of Engineering Mechanics, ASCE.* 2002, Vol. 128 (6).
3. **Neagu, R.C., Gamstedt, E. K., Berthold, F.** Stiffness contribution of various wood Fibers to composite materials. *Journal of Composite Materials.* 2006, Vol. 40(8).
4. **Voigt, B.** *New Melamine-Formaldehyde Composites.* Licentiate Dissertation, Department of Polymeric Materials, Chalmers University of Technology, Sweden, 2001.
5. **Hagstrand, P.-O.** *Mechanical Analysis of Melamine-Formaldehyde Composites.* Doctoral Thesis, Department of Polymeric Materials, Chalmers University of Technology, Sweden, 1999.
6. **Adl Zarrabi, B.** *Hygro-Elastic Deformation of High Pressure Laminates.* Doctoral Thesis, Division of Building Material, Chalmers University of Techology, Sweden, 1998.
7. **Mårtensson, A.** *Mechanical Behaviour of Wood Exposed to Humidity Variations.* Doctoral Thesis, Department of Structural Engineering, Lund Institute of Technology, Sweden, 1992.
8. **Hahnijärvi, A.** *Modelling of Creep Deformation Mechanisms in Wood.* Doctoral Thesis, Technical Research Centre of Finland, Espoo, 1995.

9. **Alftan, J.** *Micro-Mechanically Based Modeling of Mechano-sorptive Creep in Paper.* Doctoral Thesis, Department of Solid Mechanics, Royal Institute of Technology, Sweden, 2004.
10. **Strömbro, J.** *Micro-Mechanical Mechanisms for Deformation in Polymers-Material Structures.* Doctoral Thesis, Department of Solid Mechanics, Royal Institute of Technology, Sweden, 2008.
11. **Pickett, G.** The Effect of Change in Moisture-Content of the Creep of Concrete under a Sustained Load. *Journal of the American Concrete Institute.* 1942, Vol. 13(4), ss. 333-355.
12. **Stålne, K.** *3D Homogenisation of Hygroscopic Anisotropic Fibre Network Composites.* Division of Structural Mechanics, Lund Institute of Technology, Sweden, 2008.
13. **Dinwoodie, J. M.** *Wood – Nature's Cellular, Polymeric Fibre-composite.* The Institute of Metals, London, UK., 1989.
14. **Persson, K.** *Mícromechanical Modelling of Wood and Fibre Properties.* Doctoral Thesis, Division of Structural Mechanics, Lund Institute of Technology, Sweden, 2000.
15. **Sjödahl, M.** *Electronic Speckle Photogrphy applied to In-plane Deformation and Strain Field Measurements.* Doctoral Thesis, Division of Experimental Mechanics, Luleå University of Technology, Sweden, 1995.
16. **Marklund, E.** *Modelling the Mechanical Performance of Natural Fiber Composites.* Doctoral Thesis, Division of Polymer Engineering, Luleå University of Technology, Sweden, 2007.
17. **Dahlblom, O.** *Constitutive Modelling and Finite Element Analysis of Concrete Structures with Regard to Environmental Influence.* Report TVSM-1004, Division of Structural Mechanics, Lund Institute of Technology, Sweden, 1987.
18. **The Math Works Inc.** *Matlab - The Language of Technical Computation.* Natick, Ma, USA, 2007.

Appendix A

A

Analysis of Fibre Composite Models for Stiffness and Hygroexpansion

Kristian Stålne

Abstract

The report deals with analytical models for the elastic properties and hygroexpansion of fibre composite materials. Cases of homogeneous strain and homogeneous stress both for 2D and 3D states of stress are studied. Interpolation between the two cases is also taken up, its being shown that the interpolation is unambiguous and fulfills the coordinate invariance principle.

1 Introduction

The use of fibre composite materials for obtaining a combination of stiffness, strength and low weight has increased in recent years, resulting in a need for better models to predict the properties and behaviour of a composite material from the properties of the constituents. Of the many different homogenisation and network mechanics models in this area today [1, 2, 3], that provided by the Halpin-Tsai equations [4] which has been in considerable use ever since the 1960s, largely for short fibre composites, appears to be the most dominant one.

The models to be considered illustrate different ways in which the stiffness matrix and the hygroexpansion of a composite material can be calculated. The indata for calculating the stiffness consists of the stiffness matrices of the materials, their component volume fractions and the orientation distribution of the fibres. The hygroexpansion of the composite is estimated on the basis of the free hygroexpansions of the constituents. The results consists of bounds for the stiffness and the hygroexpansion and an interpolation between the two extremes using a generalisation based on the method of weighted power means.

The report takes up coordinate transformations for stresses, strains and stiffness matrices, as well as summation of stiffness matrices and integration of them over the fibres in theri entirety, followed by the consideration of hygroexpansion as well. An interpolation model for the case of plane stress is also taken up. The model is shown, through use of matrix theory and an alternative definition of the stress and strain vectors, to be coordinate-invariant. The model is, finally, generalised to three dimensions.

2 Transformation of stresses and strains

For a coordinate system rotated by the angle φ stresses in the plane can be transformedas follows [5]:

$$\begin{aligned} \sigma_x &= \sigma_X \cos^2\varphi + \sigma_Y \sin^2\varphi + 2\tau_{XY}\sin\varphi\cos\varphi \\ \sigma_y &= \sigma_X \sin^2\varphi + \sigma_Y \cos^2\varphi - 2\tau_{XY}\sin\varphi\cos\varphi \\ \tau_x &= -\sigma_X \sin\varphi\cos\varphi + \sigma_Y \sin\varphi\cos\varphi + \tau_{XY}(\cos^2\varphi - \sin^2\varphi) \end{aligned} \tag{1}$$

where x-y are the local coordinates and X-Y the global coordinates.

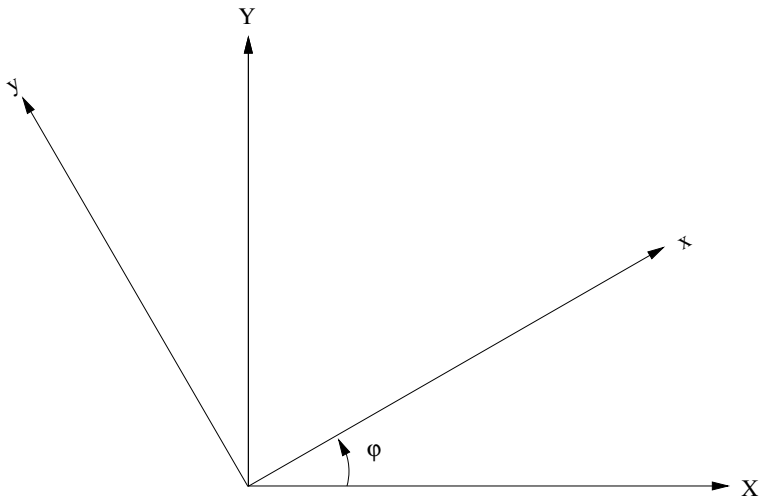

Figure 1: *Rotation of the coordinate system by the angle φ from the global coordinate system (X-Y) to the coordinate system of the fibres. x-y.*

In matrix notation, this can be written as

$$\begin{bmatrix} \sigma_x \\ \sigma_y \\ \tau_{xy} \end{bmatrix} = \begin{bmatrix} m^2 & n^2 & 2mn \\ n^2 & m^2 & -2mn \\ -mn & mn & m^2 - n^2 \end{bmatrix} \begin{bmatrix} \sigma_X \\ \sigma_Y \\ \tau_{XY} \end{bmatrix} \tag{2}$$

where $m = \cos\varphi$ and $n = \sin\varphi$. This in turn can be written as

$$\overline{\boldsymbol{\sigma}} = \mathbf{T}\boldsymbol{\sigma} \tag{3}$$

Henceforth, overlining ($\overline{\boldsymbol{\sigma}}$, $\overline{\boldsymbol{\epsilon}}$) will be used to indicate local stress, local strain, etc.

The same transformation rules apply to the strain as well:

$$\begin{bmatrix} \epsilon_x \\ \epsilon_y \\ \epsilon_{xy} \end{bmatrix} = \begin{bmatrix} m^2 & n^2 & 2mn \\ n^2 & m^2 & -2mn \\ -mn & mn & m^2 - n^2 \end{bmatrix} \begin{bmatrix} \epsilon_X \\ \epsilon_Y \\ \epsilon_{XY} \end{bmatrix} \tag{4}$$

Observe that $\epsilon_{xy} = \frac{1}{2}\gamma_{xy}$ and that $\epsilon_{XY} = \frac{1}{2}\gamma_{XY}$. If the shear strain is denoted as γ_{XY} the transformation matrix changes to

$$\begin{bmatrix} \epsilon_x \\ \epsilon_y \\ \gamma_{xy} \end{bmatrix} = \begin{bmatrix} m^2 & n^2 & mn \\ n^2 & m^2 & -mn \\ -2mn & 2mn & m^2 - n^2 \end{bmatrix} \begin{bmatrix} \epsilon_X \\ \epsilon_Y \\ \gamma_{XY} \end{bmatrix} \tag{5}$$

or in brief notation

$$\overline{\boldsymbol{\epsilon}} = \mathbf{T}^{-T}\boldsymbol{\epsilon} \tag{6}$$

where $\mathbf{T}^{-T}$ is the inverse of the transpose of $\mathbf{T}$. The difference between the transformation of stress and of strain can be eliminated by use of ϵ_{xy} instead of γ_{xy} and be compensated for in the stiffness matrix by doubling the element $\overline{Q_{44}}$. Henceforce $\boldsymbol{\epsilon} = \begin{bmatrix} \epsilon_X & \epsilon_Y & \gamma_{XY} \end{bmatrix}^T$. Observe that

$$\mathbf{T}^T \neq \mathbf{T}^{-1} \tag{7}$$

3 The stiffness matrix under homogeneous conditions

3.1 The fibre network in a homogeneous state of strain

The fibres are considered as being orthotropic discs of differing orientation. It is assumed that under conditions of homogeneous strain all fibres are under the same strain at all points. This is equivalent to laminate theory. The stiffness matrix, $\mathbf{D}$, can be calculated by transforming the fibre stiffness matrix obtained for each orientation and summing over the latter. The constitutive equation $\overline{\boldsymbol{\sigma}} = \overline{\mathbf{D}}\overline{\boldsymbol{\epsilon}}$ for the fibres in the local coordinate system, in its extensive form, is

$$\overline{\boldsymbol{\sigma}} = \frac{1}{1 - \nu_{xy}\nu_{yx}} \begin{bmatrix} E_x & \nu_{yx}E_x & 0 \\ \nu_{xy}E_y & E_y & 0 \\ 0 & 0 & (1 - \nu_{xy}\nu_{yx})G_{xy} \end{bmatrix} \overline{\boldsymbol{\epsilon}} \tag{8}$$

Combined with the transformation equation for stresses and strains, this gives

$$\boldsymbol{\sigma} = \mathbf{T}^{-1}\overline{\boldsymbol{\sigma}} = \mathbf{T}^{-1}\overline{\mathbf{D}}\overline{\boldsymbol{\epsilon}} = \mathbf{T}^{-1}\overline{\mathbf{D}}\mathbf{T}^{-T}\boldsymbol{\epsilon} \tag{9}$$

In terms of the global coordinates, the stiffness matrix can then be written as

$$\mathbf{D} = \mathbf{T}^{-1}\overline{\mathbf{D}}\mathbf{T}^{-T} \tag{10}$$

The resulting stiffness matrix for the fibre network as a whole can be calculated by summing (integrating) over all of the fibres.

$$\mathbf{D}_f = \int_0^{\pi} \mathbf{T}^{-1}\overline{\mathbf{D}}\mathbf{T}^{-T} \cdot f(\varphi) d\varphi \tag{11}$$

where $f(\varphi)$ is the fibre orientation distribution function, which has the form $f(\varphi) = A + B\cos^2\varphi$ and is examined more closely in section 6.2. For an isotropic orientation distribution, $f(\varphi) = \frac{1}{\pi}$ whereas for an orthotropic orientation distribution of 1:p, where p is how many times higher the fibre density is in the x-direction than in the y-direction, $f(\varphi)$ becomes

$$f(\varphi) = \frac{2}{\pi} \cdot \frac{1 + (p-1)cos^2\varphi}{p+1} \tag{12}$$

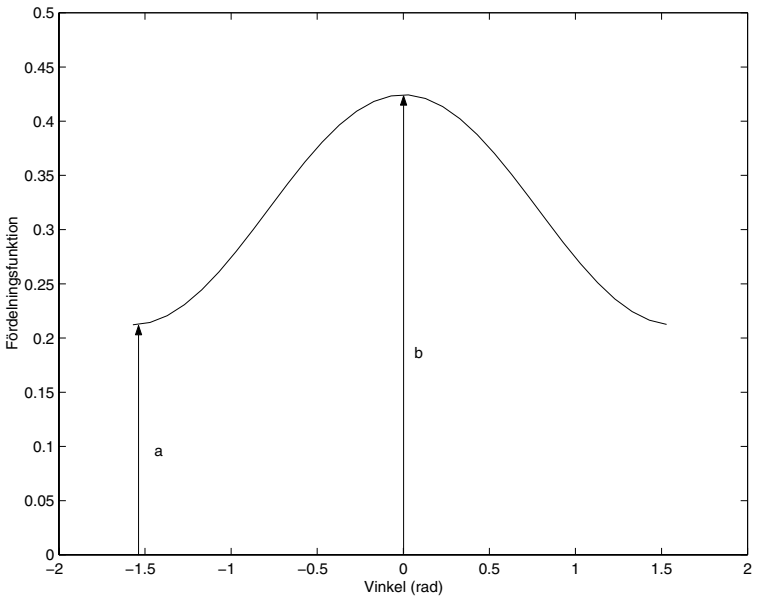

Figure 2: *The fibre orientation distribution function* $f(\varphi)$. $p = \frac{b}{a}$

3.2 Fibre network at homogeneous state of stress

In this case the stress at all points is assumed to be equal and stiffness of the fibre network is achived by summing of all strains. In the case of homogeneous strain all stiffness matrices was summed, here all compliance matrices are summed, $\mathbf{S} = \mathbf{D}^{-1}$. According to the above

$$\mathbf{D} = \mathbf{T}^{-1}\overline{\mathbf{D}}\mathbf{T}^{-T}$$

gives

$$\mathbf{S} = \mathbf{D}^{-1} = (\mathbf{T}^{-1}\overline{\mathbf{D}}\mathbf{T}^{-T})^{-1} = \mathbf{T}^{T}\overline{\mathbf{D}}^{-1}\mathbf{T} = \mathbf{T}^{T}\overline{\mathbf{S}}\mathbf{T} \tag{13}$$

Summarising all compliance matrices gives

$$\mathbf{S}_f = \int_0^{\pi} \mathbf{T}^{T}\overline{\mathbf{S}}\mathbf{T} \cdot f(\varphi)d\varphi \tag{14}$$

or

$$\mathbf{D}_f = \left[\int_0^{\pi} \mathbf{T}^{T}\overline{\mathbf{D}}^{-1}\mathbf{T} \cdot f(\varphi)d\varphi\right]^{-1} = \left[\int_0^{\pi} (\mathbf{T}^{-1}\overline{\mathbf{D}}\mathbf{T}^{-T})^{-1} \cdot f(\varphi)d\varphi\right]^{-1} \tag{15}$$

3.3 Stiffness matrices of composite materials with two phases

If another material is added to the fibre network, the components stiffness matrices can be summarised, weighted with the volume fractions respectively, in analogy with the integration

$$\mathbf{D}_c = V_m\mathbf{D}_m + V_f\mathbf{D}_f \tag{16}$$

according to the model of parallel coupling. That can also be done using the serial coupling model

$$\mathbf{D}_c = \left(V_m\mathbf{D}_m^{-1} + V_f\mathbf{D}_f^{-1}\right)^{-1} \tag{17}$$

4 Hygroexpansion

The free hygroexpansion of a fibre is denoted $\overline{\boldsymbol{\epsilon}}^0$ in the local coordinate system of the fibre and is defined

$$\overline{\boldsymbol{\epsilon}}^0 = \begin{bmatrix} \epsilon_L \\ \epsilon_T \\ 0 \end{bmatrix} = p(\xi) \begin{bmatrix} \epsilon_L(max) \\ \epsilon_T(max) \\ 0 \end{bmatrix} \tag{18}$$

where $p(\xi)$ is the relative strain as a function of the relative humidity, ξ, $\epsilon_L(max)$ and $\epsilon_T(max)$ are the hygroexpansion at saturated humidity [7].

4.1 Serial coupling

The simplest way of calculating the hygroexpansion of a composite material is the serial coupling model. The total strain is the sum of the strains of all components multiplied with the respective volume fractions

$$\boldsymbol{\epsilon}_c^0 = V_1\boldsymbol{\epsilon}_1^0 + V_2\boldsymbol{\epsilon}_2^0 \tag{19}$$

where $\boldsymbol{\epsilon}_1^0$ and $\boldsymbol{\epsilon}_2^0$ are the components free hygroexpansion strains. For k number of components the total strain is

$$\boldsymbol{\epsilon} = \sum_{i=1}^{k} V_i\boldsymbol{\epsilon}_i^0 \tag{20}$$

The corresponding integral for all fibre directions the total strain $\boldsymbol{\epsilon}_f^0$ of the fibre network becomes

$$\boldsymbol{\epsilon}_f^0 = \int_0^\pi \boldsymbol{\epsilon}^0 \cdot f(\varphi)d\varphi = \int_0^\pi \mathbf{T}^T\overline{\boldsymbol{\epsilon}}^0 \cdot f(\varphi)d\varphi \tag{21}$$

4.2 Parallel coupling

Parallel coupling means a homogeneous state of strain, which at a constrained hygroexpansion leads to the stress

$$\boldsymbol{\sigma} = V_1\boldsymbol{\sigma}_1 + V_2\boldsymbol{\sigma}_2 \tag{22}$$

where $\boldsymbol{\sigma}_1 = \mathbf{D}_1\boldsymbol{\epsilon}_1^0$ and $\boldsymbol{\sigma}_2 = \mathbf{D}_2\boldsymbol{\epsilon}_2^0$. This stress gives the free hygroexpansion strain

$$\boldsymbol{\epsilon}_c^0 = \mathbf{D}_c^{-1}\boldsymbol{\sigma} = V_1\mathbf{D}_c^{-1}\mathbf{D}_1\boldsymbol{\epsilon}_1^0 + V_2\mathbf{D}_c^{-1}\mathbf{D}_2\boldsymbol{\epsilon}_2^0 \tag{23}$$

where $\boldsymbol{\epsilon}_1^0$ and $\boldsymbol{\epsilon}_2^0$ are the constituents free hygroexpansion strains. A general expression for k number of material is

$$\boldsymbol{\epsilon}^0 = \sum_{i=1}^{k} V_i\mathbf{D}_c^{-1}\mathbf{D}_i\boldsymbol{\epsilon}_i^0 \tag{24}$$

and the integration for all fibres in a network is

$$\boldsymbol{\epsilon}_f^0 = \mathbf{D}_c^{-1}\int_0^\pi \boldsymbol{\sigma} \cdot f(\varphi)d\varphi = \int_0^\pi \mathbf{D}_c^{-1}\mathbf{T}^{-1}\overline{\mathbf{D}\boldsymbol{\epsilon}}^0 \cdot f(\varphi)d\varphi \tag{25}$$

or

$$\boldsymbol{\epsilon}_f^0 = \int_0^\pi \mathbf{D}_c^{-1}\mathbf{D}\mathbf{T}^T\overline{\boldsymbol{\epsilon}}^0 \cdot f(\varphi)d\varphi \tag{26}$$

5 An interpolation model

The idea of this model is to make a mathematical interpolation between the cases of parallel and serial coupling. One way to achieve this is by inserting a potence, "α" over all matrices. The parameter α works as a fitting parameter and can be fitted to measurements but also estimated regarding to the geometry of the composite.

$$\mathbf{D}_c^\alpha = V_m \mathbf{D}_m^\alpha + V_f \mathbf{D}_f^\alpha \tag{27}$$

here $\alpha = 1$ corresponds to the parallel coupling case and $\alpha = -1$ corresponds to the serial coupling case. The idea comes from the compendium in building materials [7] where it is described in one dimension, i.e. for scalar properties:

$$E_c^\alpha = V_m E_m^\alpha + V_f E_f^\alpha \tag{28}$$

which for $n \to 0$ appproaches

$$E_c = E_m^{V_m} E_f^{V_f} \tag{29}$$

which is the geometrical mean of E_m och E_f.

According to Wall [8] even the Halpion-Tsai equations can be seen as an interpolation between arithmetic mean, $\alpha = 1$, and harmonic mean, $\alpha = -1$. He also mensions the weighted potence mean, equation (28), for scalar properties.

5.1 Calculation of $\mathbf{D}^\alpha$

The potence, α, inserted is an operation carried out on the entire matrix, and not elementwise. Like other matrix functions this operation is done by diagonalising the matrix and performing the operation on the diagonal elements

$$\mathbf{D}^\alpha = (\mathbf{Q}\mathbf{\Lambda}\mathbf{Q}^{-1})^\alpha = \mathbf{Q}(\mathbf{\Lambda})^\alpha \mathbf{Q}^{-1} = \mathbf{Q} \begin{bmatrix} \lambda_1^\alpha & 0 & 0 \\ 0 & \lambda_2^\alpha & 0 \\ 0 & 0 & \lambda_3^\alpha \end{bmatrix} \mathbf{Q}^{-1} \tag{30}$$

The requirement for this to be possible is that $\mathbf{D}$ is diagonalisable and positively difinite, which easily can be shown if $\mathbf{D}$ is linear elastic.

5.2 Problem

Now the corresponding procedure for hygroexpansion is analysed. For a composite with two constituents the equations (19) and (23) are combined to

$$\boldsymbol{\epsilon}^0 = V_1 (\mathbf{D}_c^{-1}\mathbf{D}_1)^{\frac{\alpha+1}{2}} \boldsymbol{\epsilon}_1^0 + V_2 (\mathbf{D}_c^{-1}\mathbf{D}_2)^{\frac{\alpha+1}{2}} \boldsymbol{\epsilon}_2^0 \tag{31}$$

Still $\alpha = 1$ corresponds to parallel coupling and $\alpha = -1$ to serial coupling. One small problem is that the strain $\boldsymbol{\epsilon}_c^0$ not equals the free strains of the constituents when they are set to be equal $\boldsymbol{\epsilon}_1^0 = \boldsymbol{\epsilon}_2^0$ for all α. $\boldsymbol{\epsilon}_c^0$ is only equal to $\boldsymbol{\epsilon}_1^0$ and $\boldsymbol{\epsilon}_2^0$ when $\alpha = 1$ or $\alpha = -1$.

It is desirable to perform the calculation of the stiffness matrix and the hygroexpansion strain for a fibre network for all α even for the integration of the fibre orienation directions.

$$\mathbf{D}_f = \left[\int_0^\pi (\mathbf{T}^{-1} \overline{\mathbf{D}} \mathbf{T}^{-T})^\alpha \cdot f(\varphi) d\varphi \right]^{1/\alpha} \tag{32}$$

and for hygroexpansion

$$\boldsymbol{\epsilon}_f^0 = \int_0^\pi (\mathbf{D}_c^{-1} \mathbf{D})^{\frac{\alpha+1}{2}} \mathbf{T}^T \overline{\boldsymbol{\epsilon}}^0 \cdot f(\varphi) d\varphi \tag{33}$$

The big problem is that this calculation of $\mathbf{D}_f$ is depending on the coordinate system used. When equation (27) is solved it is natural to chose the coordinate system in the fibres direction of orthotropy (MD), but now the fibres will be weighted differently depending on the alignment. Regardless of this fact it is unacceptable for a fysical law to be dependent on the chosen coordinate system. One example is

$$\mathbf{D}_c^\alpha = V_m \mathbf{D}_m^\alpha + V_f \mathbf{D}_f^\alpha$$

which for another arbitrary chosen coordinate system can be written as

$$(\mathbf{T}^{-1} \overline{\mathbf{D}}_c \mathbf{T}^{-T})^\alpha = V_m (\mathbf{T}^{-1} \overline{\mathbf{D}}_m \mathbf{T}^{-T})^\alpha + V_f (\mathbf{T}^{-1} \overline{\mathbf{D}}_f \mathbf{T}^{-T})^\alpha$$

In order to make this coordinate invariant there have to be a way of getting rid of all $\mathbf{T}$. For example

$$(\mathbf{T}^{-1})^\alpha \overline{\mathbf{D}}_c^\alpha (\mathbf{T}^{-T})^\alpha = V_m (\mathbf{T}^{-1})^\alpha \overline{\mathbf{D}}_f^\alpha (\mathbf{T}^{-T})^\alpha + V_f (\mathbf{T}^{-1})^\alpha \overline{\mathbf{D}}_m^\alpha (\mathbf{T}^{-T})^\alpha \tag{34}$$

Unfortunatly this simplification, or any other, is not possible since

$$\mathbf{A}^\alpha \mathbf{B}^\alpha \neq (\mathbf{AB})^\alpha \tag{35}$$

thus the coordinate invariance not can be shown.

5.3 Redefinition of stress and strain vectors

The solution of the problem of coordinate invariance is defining the stress and strain vectors as

$$\boldsymbol{\sigma} = \begin{bmatrix} \sigma_x \\ \sigma_y \\ \sqrt{2}\,\sigma_{xy} \end{bmatrix}, \; \boldsymbol{\epsilon} = \begin{bmatrix} \epsilon_x \\ \epsilon_y \\ \sqrt{2}\,\epsilon_{xy} \end{bmatrix} \tag{36}$$

This is not new, it is mentioned in "The Mechanics of Constitutive Modelling [10] briefly together with a few references. With this definition the stress and strain vectors are transformed using the same transformation matrix,

$$\overline{\boldsymbol{\sigma}} = \mathbf{T}\boldsymbol{\sigma}, \; \overline{\boldsymbol{\epsilon}} = \mathbf{T}\boldsymbol{\epsilon}, \tag{37}$$

The, now orthogonal, transformation matrix is defined as

$$\mathbf{T} = \begin{bmatrix} m^2 & n^2 & \sqrt{2}mn \\ n^2 & m^2 & -\sqrt{2}mn \\ -\sqrt{2}mn & \sqrt{2}mn & m^2 - n^2 \end{bmatrix} \tag{38}$$

5.4 Some matrix theory

The reason of defining the shear strain and shear stress components with the factor $\sqrt{2}$ instead of as in equation(2), (4) and (5) is that the stiffness matrix, $\mathbf{D}$, now is independent of in which coordinate system it is calculated. The new choice of strain and stiffness definitions gives the two necessary properties:

1) The stiffness matrix is symmetric and positively definite. This can be shown by using thermodynamics which states that the strain energy, W, allways is positive when the strains are not equal to zero. This can be written

$$W = \frac{1}{2}\boldsymbol{\epsilon}^T\mathbf{D}\boldsymbol{\epsilon} < 0 \tag{39}$$

which is equivalent to $\mathbf{D}$ being positively definite. In that case the spectre of the matrix is positive, i.e. all eigenvalues of $\mathbf{D}$ are positive if the matrix is symmetric. This means that there are no unpleasant involvements of complex numbers which arises when a negative base is raised to non-integer potence.

2) The transformation of the strains are carried out in the same way as for the stresses. This is decisive when the coordinate invariance is shown. The constitutive relation is now:

$$\overline{\boldsymbol{\sigma}} = \overline{\mathbf{D}}\overline{\boldsymbol{\epsilon}} = \frac{1}{1-\nu_{xy}\nu_{yx}} \begin{bmatrix} E_x & \nu_x E_y & 0 \\ \nu_x E_y & E_y & 0 \\ 0 & 0 & (1-\nu_{xy}\nu_{yx})\cdot 2G_{xy} \end{bmatrix} \overline{\boldsymbol{\epsilon}} \tag{40}$$

The stiffness matrix is transformed as

$$\boldsymbol{\sigma} = \mathbf{T}^{-1}\overline{\boldsymbol{\sigma}} = \mathbf{T}^{-1}\overline{\mathbf{D}}\overline{\boldsymbol{\epsilon}} = \mathbf{T}^{-1}\overline{\mathbf{D}}\mathbf{T}\boldsymbol{\epsilon}$$

$$\Rightarrow$$

$$\mathbf{D} = \mathbf{T}^{-1}\overline{\mathbf{D}}\mathbf{T} \tag{41}$$

When the engineering strains (5) are used only condition 1) is fulfilled and when the tensor components (4) are used only condition 2) is fulfilled. With the new definition both conditions are fulfilled.

When the coordinate invariance of the stiffness matrix is to be shown, the following equation is used [11]

$$f(\mathbf{B}^{-1}\mathbf{A}\mathbf{B}) = \mathbf{B}^{-1}f(\mathbf{A})\mathbf{B} \tag{42}$$

where f is a arbitrary function defined on As specter, which is the set of As eigenvalues. $\mathbf{B}$ is an arbitrary inversible matrix. Observe the similarity with equation (30). The equation (42) can be proved by potence serie expanding the function $f(\mathbf{B}^{-1}\mathbf{A}\mathbf{B})$. The equation

$$\mathbf{D}_c^\alpha = V_m\mathbf{D}_m^\alpha + V_f\mathbf{D}_f^\alpha \tag{43}$$

can now in an arbitrarily oriented coordinate system be written

$$(\mathbf{T}^{-1}\overline{\mathbf{D}}_c\mathbf{T})^\alpha = V_m(\mathbf{T}^{-1}\overline{\mathbf{D}}_m\mathbf{T})^\alpha + V_f(\mathbf{T}^{-1}\overline{\mathbf{D}}_f\mathbf{T})^\alpha$$

With equation (42) this gives

$$\mathbf{T}^{-1}\overline{\mathbf{D}}_c^\alpha\mathbf{T} = V_m\mathbf{T}^{-1}\overline{\mathbf{D}}_c^\alpha\mathbf{T} + V_f\mathbf{T}^{-1}\overline{\mathbf{D}}_f^\alpha\mathbf{T}$$

Multiplication with $\mathbf{T}$ from left and with $\mathbf{T}^{-1}$ from right gives

$$\overline{\mathbf{D}}_c^\alpha = V_m\overline{\mathbf{D}}_c^\alpha + V_f\overline{\mathbf{D}}_f^\alpha \tag{44}$$

and the coordinate invariance is proved.

6 Generalisation to three dimensions

In the three dimensional case the fibre orientation is described as a projection on a unit semisphere with the radius 1. The spherical coordinates on the semisphere represent the two angles, φ and θ, where θ is the angle between the positive z-axis ($0 \leq \theta \leq \pi$) and the fibre and φ is the angle between the fibres projection at the X-Y plane and the X-axis in the positive direction ($0 \leq \varphi \leq \pi$). The angles are shown in figure 3.

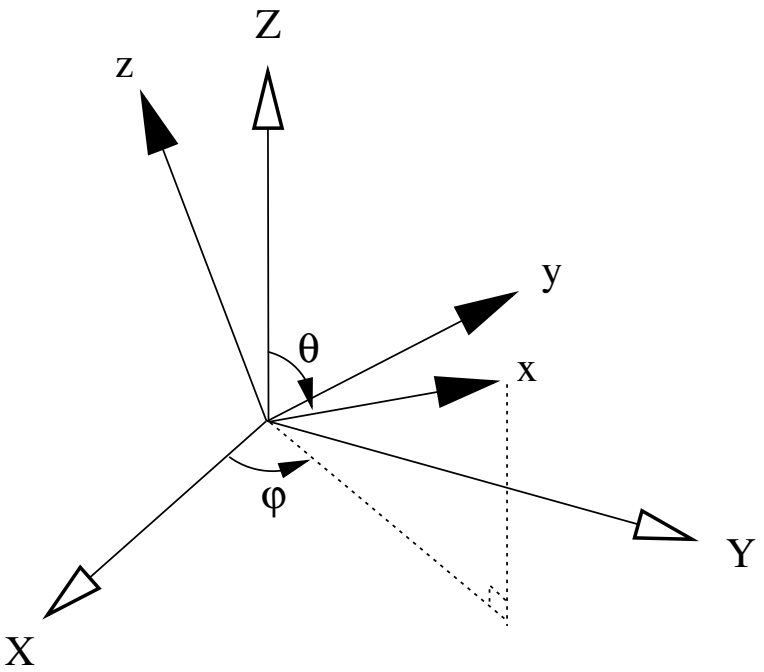

Figure 3: *Coordinate transformation in three dimensions.*

The coordinate system of the fibre has been chosen such that the x-axis coincides with the fibres longitudinal direction. The fibres are assumed to have transversaly isotropic stiffness properties in the $y-z$ plane. This means that the y-axis principally can be chosen arbitrily, orthogonal to the x-axis, but simplest is to place it in the X-Y plane, i.e.

$$\overline{\boldsymbol{e}}_y = \frac{\boldsymbol{e}_Z \times \overline{\boldsymbol{e}}_x}{|\boldsymbol{e}_Z \times \overline{\boldsymbol{e}}_x|} \tag{45}$$

6.1 Coordinate transformation

The change of base from the the local coordinate system of the fibre, (x, y, z), to the global, (X, Y, Z), is defined such that the transformation of the stress

becomes

$$\overline{\boldsymbol{\sigma}} = \mathbf{T}\boldsymbol{\sigma} \tag{46}$$

where the stress in the fibres coordinates, $\overline{\boldsymbol{\sigma}}$, and in the global coordinates, $\boldsymbol{\sigma}$, are defined

$$\overline{\boldsymbol{\sigma}} = \begin{bmatrix} \sigma_x \\ \sigma_y \\ \sigma_z \\ \sqrt{2}\tau_{xy} \\ \sqrt{2}\tau_{xz} \\ \sqrt{2}\tau_{yz} \end{bmatrix}, \boldsymbol{\sigma} = \begin{bmatrix} \sigma_X \\ \sigma_Y \\ \sigma_Z \\ \sqrt{2}\tau_{XY} \\ \sqrt{2}\tau_{XZ} \\ \sqrt{2}\tau_{YZ} \end{bmatrix} \tag{47}$$

The transformation matrix, $\mathbf{T}$, is derived first by deciding the transformation of the stress and strain tensor

$$\sigma_{ij} = a_{iq}a_{jm}\overline{\sigma}_{qm} \tag{48}$$

where a_{ij} according to basic linear algebra are derived

$$[a_{ij}] = \begin{bmatrix} sm & sn & c \\ sn & m & -cn \\ c & 0 & s \end{bmatrix} \tag{49}$$

Then the components of σ_{ij} are identified at which the transformation matrix, after a correction with a factor $\sqrt{2}$, can be written

$$\mathbf{T} = \begin{bmatrix} s^2m^2 & s^2n^2 & c^2 & \sqrt{2}s^2mn & \sqrt{2}csm & \sqrt{2}csn \\ n^2 & m^2 & 0 & -\sqrt{2}mn & 0 & 0 \\ c^2m^2 & c^2n^2 & s^2 & \sqrt{2}c^2mn & -\sqrt{2}csm & -\sqrt{2}csn \\ -\sqrt{2}smn & \sqrt{2}smn & 0 & s(m^2-n^2) & -cn & cm \\ -\sqrt{2}csm^2 & -\sqrt{2}csn^2 & \sqrt{2}cs & -2csmn & -m(c^2-s^2) & -n(c^2-s^2) \\ \sqrt{2}cmn & -\sqrt{2}cmn & 0 & -c(m^2-n^2) & -sn & sm \end{bmatrix} \tag{50}$$

where the cosine and the sine of the angles are

$$\begin{aligned} m &= \cos\varphi \\ n &= \sin\varphi \\ c &= \cos\theta \\ s &= \sin\theta \end{aligned} \tag{51}$$

The strains are transformed identically

$$\overline{\boldsymbol{\epsilon}} = \mathbf{T}\boldsymbol{\epsilon} \tag{52}$$

with

$$\overline{\boldsymbol{\epsilon}} = \begin{bmatrix} \epsilon_x \\ \epsilon_y \\ \epsilon_z \\ \sqrt{2}\epsilon_{xy} \\ \sqrt{2}\epsilon_{xz} \\ \sqrt{2}\epsilon_{yz} \end{bmatrix}, \boldsymbol{\epsilon} = \begin{bmatrix} \epsilon_X \\ \epsilon_Y \\ \epsilon_Z \\ \sqrt{2}\epsilon_{XY} \\ \sqrt{2}\epsilon_{XZ} \\ \sqrt{2}\epsilon_{YZ} \end{bmatrix} \tag{53}$$

The transformation of the stiffness matrix is now like before

$$\mathbf{D} = \mathbf{T}^{-1}\overline{\mathbf{D}}\mathbf{T} \tag{54}$$

6.2 Orientation distribution function

The three dimensional distribution function, $\Psi(\varphi, \theta)$, indicates how high the fibre density is in a certain direction. The number of fibres at the surface element dS on the unit semisphere is $V = \Psi(\varphi, \theta)dS$ and the share within a certain interval of angle, $\varphi_1 \leq \varphi \leq \varphi_2$ and $\theta_1 \leq \theta \leq \theta_2$, is

$$V = \int_{\varphi_1}^{\varphi_2}\int_{\theta_1}^{\theta_2} \Psi(\varphi, \theta)dS = \int_{\varphi_1}^{\varphi_2}\int_{\theta_1}^{\theta_2} \Psi(\varphi, \theta)\sin\theta d\varphi d\theta \tag{55}$$

since $dS = r^2 \sin\theta d\varphi d\theta = \sin\theta d\varphi d\theta$. $r^2 \sin\theta$ is a scale factor ($h_\varphi = r\sin\theta$ and $h_\theta = r$). The distribution function is assumed to be separable in the φ- and the θ direction such that

$$\Psi(\varphi, \theta) = f(\varphi) \cdot g(\theta) \tag{56}$$

where $f(\varphi)$ is the same as in the two dimensional case (12). Both function are normalised according to

$$V = \int_0^{\pi}\int_0^{\pi} \Psi(\varphi, \theta)\sin\theta d\varphi d\theta = \int_0^{\pi} f(\varphi)d\varphi \cdot \int_0^{\pi} g(\theta)\sin\theta d\theta = 1 \cdot 1 \tag{57}$$

At an isotropic distribution f and g are constants. It can easily be shown that $f = \frac{1}{\pi}$ and $g = \frac{1}{2}$. The distribution functions are assumed to be of the form

$$\begin{aligned} f(\varphi) &= A + B\cos^2\varphi \\ g(\theta) &= D + E\sin^2\theta \end{aligned} \tag{58}$$

With this form it is very easy to evaluate the integral of the transformed stiffness matrices.

6.3 Integration of all fibres

Now the stiffnesses are summarised for all fibres according to the assumption of homogeneous strain

$$\mathbf{D}_f = \int_0^{\pi} \int_0^{\pi} \mathbf{T}^{-1} \overline{\mathbf{D}} \mathbf{T} \cdot \Psi(\varphi, \theta) \sin\theta \, d\varphi d\theta \tag{59}$$

It is also here possible to perform the interpolation using the parameter α

$$\mathbf{D}_f = \left[\int_0^{\pi} \int_0^{\pi} \mathbf{T}^{-1} \overline{\mathbf{D}}^{\alpha} \mathbf{T} \cdot \Psi(\varphi, \theta) \sin\theta \, d\varphi d\theta \right]^{1/\alpha} \tag{60}$$

7 Concluding remarks

This report describes how the stresses and strains are transformed in the plane as well as in the space. This have made it possible to summarise the fibres and the matrix material stiffness matrices to different kinds of means for the entire composite under the state och homogeneous strain and homogeneous state of stress. This corresponds to the upper and the lower extreme values for the stiffness of the composite. Analogous moisture induced strain, hygroexpansion, have been summarised, which also can be used e.g. at strains caused by an increase in temperature.

The novelty here is the interpolation between the cases of parallel coupling and serial coupling according to the method of weighted potence mean is expanded from usage on scalar properties to usage on material stiffness properties at two- and three dimensional states of stress. The parameter, α, controlling the interpolation can be adapted to fit measurement data or eventually be estimated according to the geometry of the composite. By a suitable definition of stress and strain vectors the interpolation method has been shown to be coordinate invariant and computed stiffnesses are thus unambigous.

One drawback using the model in its present form is that it does not take the geometry of the fibres into consideration. One example is if it would be applied on a glassfibre-epoxy composite where the fibres as well as the matrix material are isotropic and where all fibres are aligned in one direction. The longitudinal and transversal stiffensses differ often, typically with a factor 3-4, which can not be predicted by this model. One interpretation is that the material have different α in the different directions. In order to take the fibre geometries in consideration there might be a possibility of performing som sort of homogenisation of a single fibre in a small environment of matrix material.

7.1 Future work

A similair interpolation between serial and parallel coupling for hygroexpansion were studied. One problem here was that the function did not behave in a, physically speaking, reliable way in all situations. One example is when both components hygroexpansion properties where set to be equal. Then the composites hygroexpansion should be equal to the of the comsitituents. The hygroexpansion was equal to the constituents for the cases of $\alpha = 1$ and $\alpha = -1$, but not in between. One alternative, although not as elegant mathematically speaking, is to make a linear interpolation between parallel coupling and serial coupling

$$\boldsymbol{\epsilon}_c^0 = \frac{1+\alpha}{2}\boldsymbol{\epsilon}_p^0 + \frac{1-\alpha}{2}\boldsymbol{\epsilon}_s^0 \tag{61}$$

where $\boldsymbol{\epsilon}_p^0$ is the composites free hygroexpansion computed under parallel coupling and $\boldsymbol{\epsilon}_s^0$ under serial coupling. Other possibilities can also come into consideration.

One detail worth investigation is what happens at when $\alpha \to 0$ which corresponds to the geometrical mean. It is uncertain if it is as easy as in the scalar case, equation (29), and if it is unambigous. It may not be of greater practical importance since it is possible to choose a value of α sufficiently close to 0. But it is still desirable to show that the theory is defined in the entire interval $-1 \leq \alpha \leq 1$.

References

[1] Aboudi, J. Mechanics of Composite Materials, Elsevier, NY (1991)

[2] Hashin, Z. The Elastic Moduli of Fiber-Reinforced Materials, Journal of Applied Mechanics (1964)

[3] Heyden, S. A Network Model Applied to Cellulose Fibre Materials, Progress in Paper Physics (1996)

[4] Halpin, JC. Kardos, JC. The Halpin-Tsai equations: A review. Polym. Eng. Sci. (1976)

[5] Benham, PP. Mechanics of Engineering Materials, Addison, Harlow (1996)

[6] Heyden, S. How to derive an analytical network mechanics theory, Division of Structural Mechanics, Lund University (1998)

[7] Hillerborg, A. Kompendium i Byggnadsmateriallära FK, Lund (1986)

[8] Wall, P. A Comparison of Homogenisation, Hashin-Shtrikman Bounds and the Halpin-Tsai Equations, Institutionen för Matematik, Luleå Tekniska Universitet (1994)

[9] Nevander, LE. Fukthandbok. Svensk byggtjänst, Schmids (1981)

[10] Ottosen, NS. Ristinmaa, M, The Mechanics of Constitutive Modelling, Division of Solid Mechanics, Lund University (1996)

[11] Spanne, S. Föreläsningar i matristeori, Department of Mathematics, Lund University (1994)

Appendix B

B

Measurement of Strain using Digital Speckle Photography

Kristian Stålne

Measurement of Strain using Digital Speckle Photography

Kristian Stålne
Division of Structural Mechanics, Lund University
P.O. Box 118, SE–221 00 Lund, Sweden

ABSTRACT: This appedix presents the theory and application of optical strain measurement by means of a system based on the principal of digital speckle photography, DSP. The DSP system comprises a digital camera that is connected to a laptop computer. The measurement is carried out by taking a number of pictures of the specimen's surface. An image correlation algorithm calculates the displacement field of the measurement area. From this all in-plane components of the strain field are evaluated by differentiating the deformation field. Results from a measurement performed by the DSP system are compared to results from simultaneously made measurements by means of an extensometer on a sample exposed to a tensile loading. The comparison shows a good correspondence between the methods. Finally, examples of performed measurements using the DSP system are presented.

KEY WORDS: Digital Speckle Photography, DSP, Strain field, Optical Strain Gauge, Non-destructive testing.

Introduction

Materials testing with contact free strain measurements is an important field and it has several advantages compared to conventional testing, using e.g. extensometers and foil strain gauges. An optical strain gauge that employs image correlation technique can measure all in-plane components of the strain on a surface of a specimen. It can measure the strain of fragile surfaces where conventional gauges cannot access, e.g. paper. It measures the deformation field, and thus the in-plane components of the strain field, of a larger area instead of single points. The measurement is robust so that it can compensate for a rigid body movement made by, e.g. moving the camera between the photographs being taken. It can also be built without any large investments, the presented system required investments of less than € 5 000 in 2002. Today the price of components, computers and cameras, is significantly lower and a corresponding system would cost below € 2 000.

Overview of the Camera System

The image capturing part of the DSP system comprises a camera with additional hardware, shown in Figure 1.

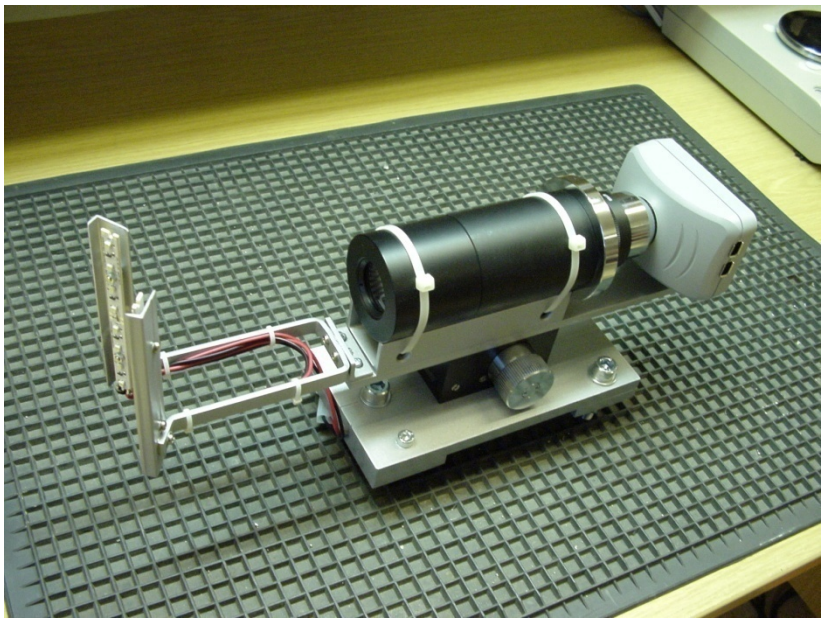

Figure 1. *Digital camera with mounting and light ramp.*

On the camera is mounted a 19 cm long black telecentric objective lens system with a fixed magnification of 0.38. This gives a fixed measurement area of 16 × 20 mm^2, which can only be changed by changing the lens. Telecentric means that the magnification stays constant even if the surface moves in the out-of-plane, i.e. z-direction or the direction of the optical axis. This gives a small magnification error and a large depth of field. In front of the objecive there are two light ramps with diode lamps for lighting of the specimen. The distance between the specimen and the camera is approximately 35 cm.

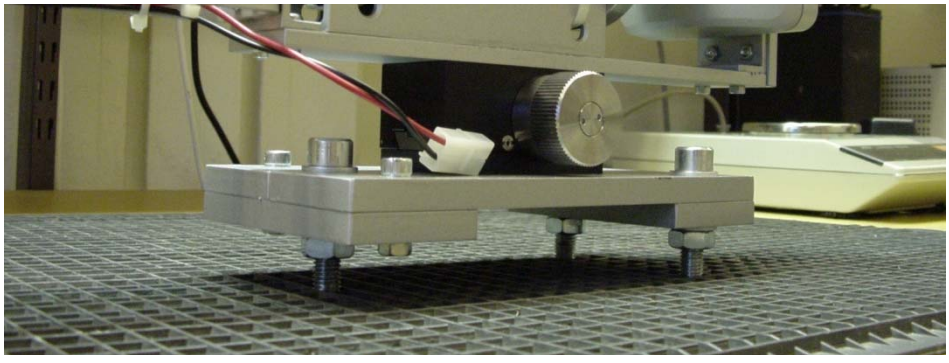

Figure 2. *Supporting points of the camera mounting.*

The camera is mounted on a translator which can be adjusted horisontally in order to find the focal point. The translator is fastened to a foundation that rests on three supporting points, that are used to place the camera at an exact location, shown in Figure 2.

The camera, PixeLink, is a digital camera with 1280×1024 pixels, where 1 pixel is 15 μm wide. It is connected to a laptop with a firewire. With the provided camera software it can capture 1 image per 10 s in automatic mode. The computer is a Dell Inspiron 8600 with a 2.4 GHz processor with PixeLink software for camera control and MatLab 6.1 [1], which is used for image processing and calculation of the strain field.

Theory and Measurement Procedure

The theory behind the DSP system is developed by Prof. Mikael Sjödahl at the Division of Experimental Mechanics at Luleå University of Technology. The DPS measurement technique is based on an image correlation algorithm developed by Sjödahl [2]. The function of the system is illustrated by the following measurment example:

First, the surface the specimen is sprayed by drops of black paint, speckles. This creates a speckle pattern of the surface, shown in Figure 3 a) and b).

Figure 3. a) *Preparation of surface by spraying droplets of black paint.*
b) *Random speckle pattern created by spraying.*

The desirable size of the speckles is approximately 10 pixels. An alternative method to spraying black paint is using laser speckles, which are produced by illuminate the surface by means of a laser.

Next, the surface is clamped in a loading device according to Figure 4 a), and an image is taken by the camera at $t = t_0$. After exposing the specimen to a loading in Figure 4 b), another image is taken by the camera at $t = t_1$ according to Figure 4 c).

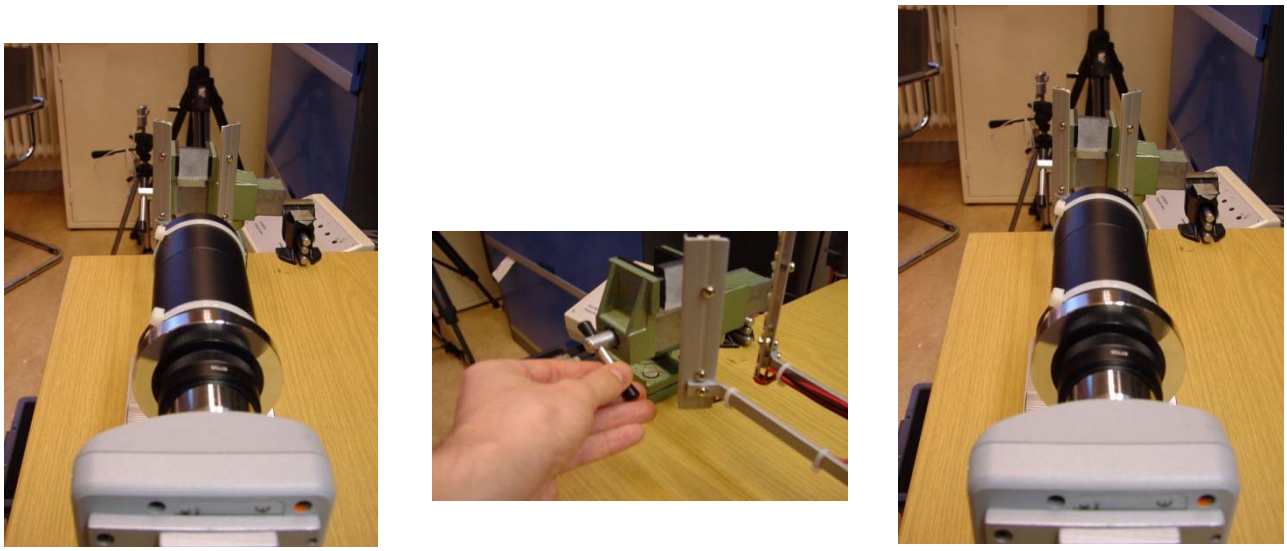

Figure 4 a) *Image 1 taken at* $t = t_0$, ***b)*** *specimen is exposed to a loading,* ***c)*** *image is taken at* $t = t_1$.

The images are now imported to a Matlab-routine that divides the images into sub-images according to Figure 5, giving a deformation field of 320 measurement points.

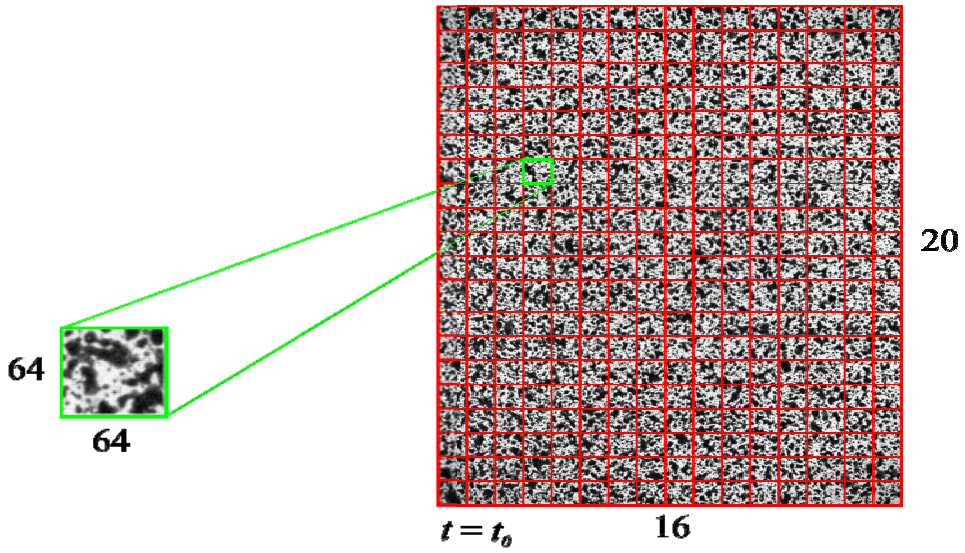

Figure 5. *Image divided into* 16×20 *sub-images of* 64×64 *pixels each.*

The sub-images from the image taken at $t = t_0$ are correlated to the corresponding sub-images from the image taken at $t = t_1$ according to Figure 6. This correlation is performed by the DSP correlation algorithm [2]. The correlation of the respective sub-images result in a deformation vector (u, v) for each measurement point of the measurement area which is described by the coordinates (x, y), where u and v are the deformations in the x- and the y-direction, respectively. The correlation function $C(x,y)$ is defined as

$$C(x,y) = f(s,t) \circ g(s,t) = \int_{-\infty}^{\infty}\int_{-\infty}^{\infty} f(s,t) \cdot g(s+x,t+y)\,ds\,dt$$

The deformation vector (u,v) is evaluated as the position of the maximum of the correlation function, $C(x,y)$. Using the correlation algorithm the deformation is calculated with an accuracy of 1 % of a pixel under ideal conditions [2, 3].

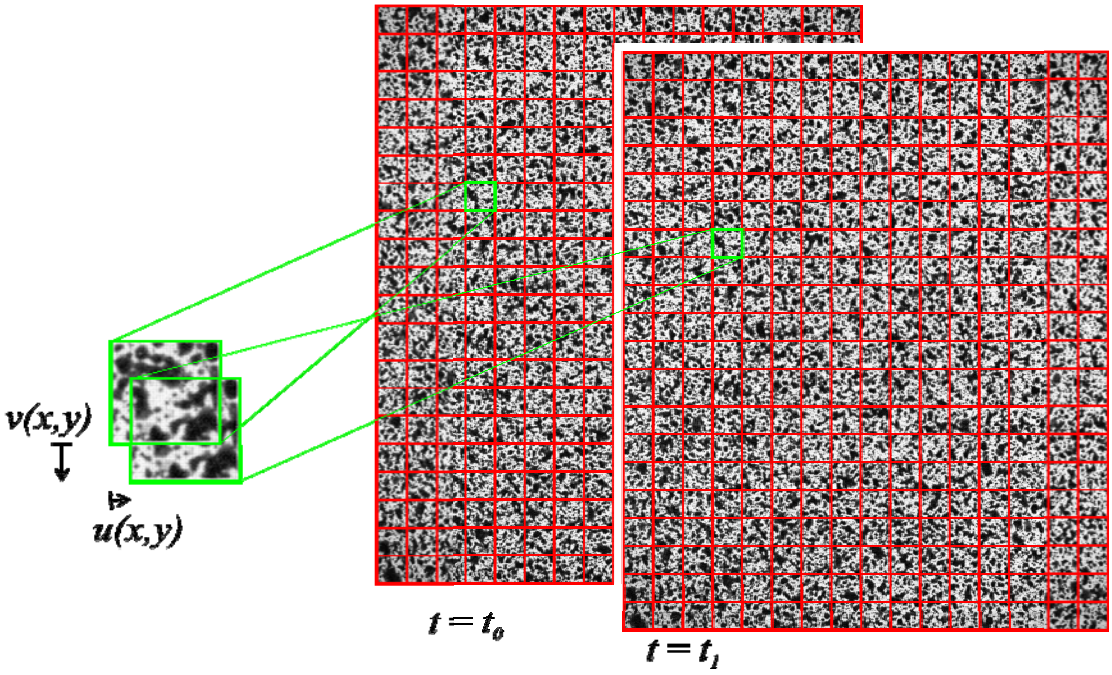

Figure 6. *Correlation between corresponding sub-images of the two images.*

The u- and the v- components of the deformation are separated from each other and plotted as functions of the coordinate according to Figure 7 a) and b).

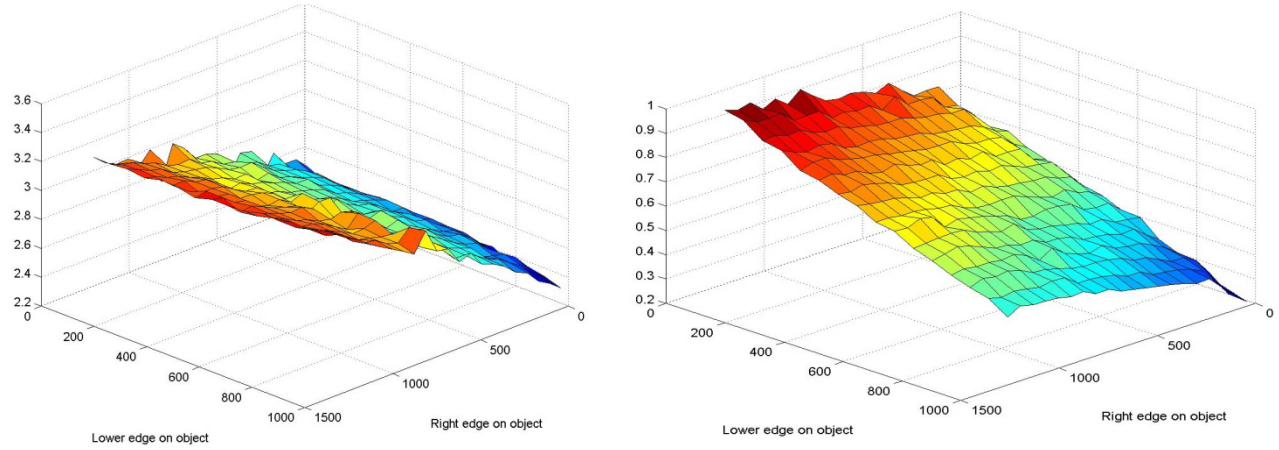

Figure 7. a) *u-component of deformation, u(x,y),* ***b)*** *v-component of deformation, v(x,y).*

The deformation fields are fitted to inclined planes, assuming a constant strain field. Thus the fitted deformation fields u_p and v_p can be expressed as

$$u_p = u_0 + a_x + b_y$$

and

$$v_p = v_0 + c_x + d_y,$$

from which the strains can be evaluated as the space derivatives of the deformation fields according to

$$\Delta\varepsilon_x = a,$$
$$\Delta\varepsilon_y = d \text{ and}$$
$$\Delta\varepsilon_{xy} = \frac{b+c}{2}$$

The calculated standard deviations of the strains that are evaluated from the inclined planes are typically the order of magnitude of 10^{-5}.

There is also a possibility of measuring the strain increment between several time intervals, e.g. at ramp loading tests or long time creep tests. In this case there are two possibilities of measuring the strain: single reference image or incremental reference image. Single reference means that an image in the beginning of the sequence is chosen as a reference that all other images are correlated to. Incremental reference means that every image is correlated to the previous image. Both principles are illustrated in Figure 8.

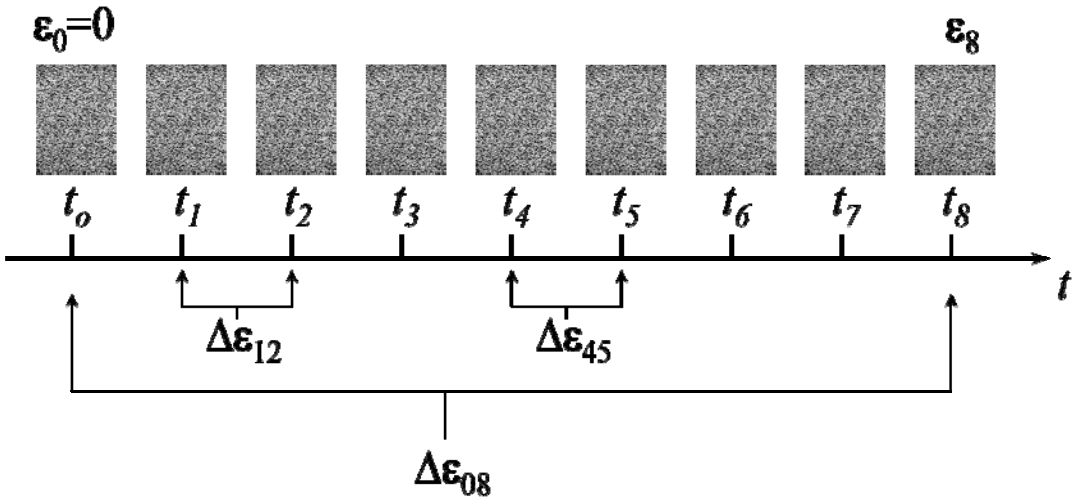

Figure 8. *Single reference compared to incremental reference.*

In the case of single reference the strain at $t = t_8$ is calculated according to

$$\varepsilon_8 = \varepsilon_0 + \Delta\varepsilon_{08},$$

and in the case of incremental reference, the same strain is calculated according to

$$\varepsilon_8 = \varepsilon_0 + \Delta\varepsilon_{01} + \Delta\varepsilon_{12} + \Delta\varepsilon_{23} + \Delta\varepsilon_{34} + \Delta\varepsilon_{45} + \Delta\varepsilon_{56} + \Delta\varepsilon_{67} + \Delta\varepsilon_{78}$$

The disadvantage with single reference is that it uses the same reference image that it can induce such large rigid body-movement that the correlation algorithm cannot trace the deformation. The disadvantage with the incremental reference is that any systematic error that may occur at a correlation gets magnified for each calculation, whereas the single reference only needs one calculation for all strains. The principle is illustrated in Figure 8. The advantage with incremental reference is that it is stable with regards to rigid body movements, as long as images are captured with sufficiently close. The two approaches are compared by means the results from two measurements, shown in Figure 9 and 10.

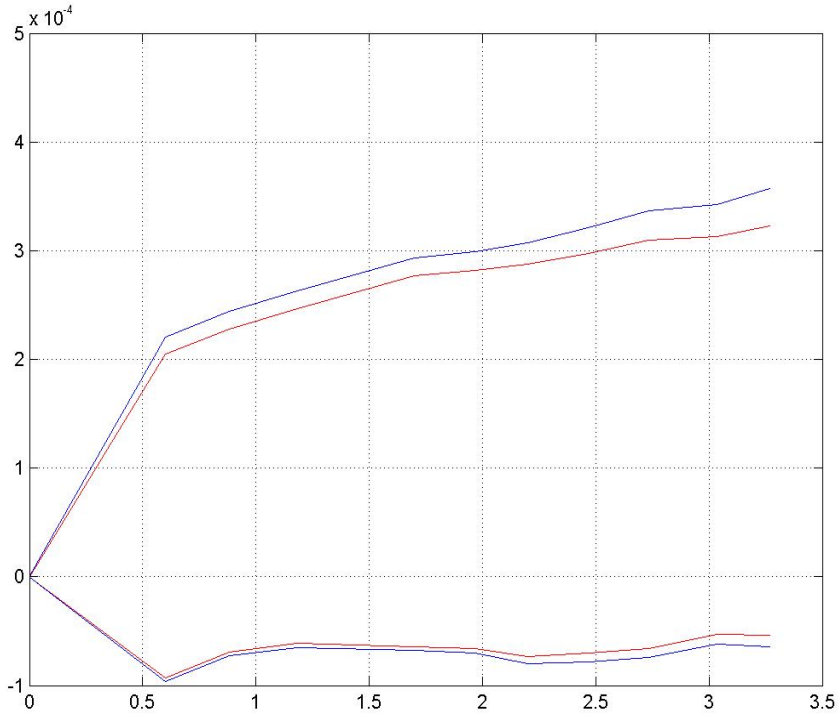

Figure 9. *Strain (-) in the loading and transverse direction as a function of time (min). Specimen is a high pressure laminate exposed to a tensile loading. Red line = incremental reference, blue line = single reference.*

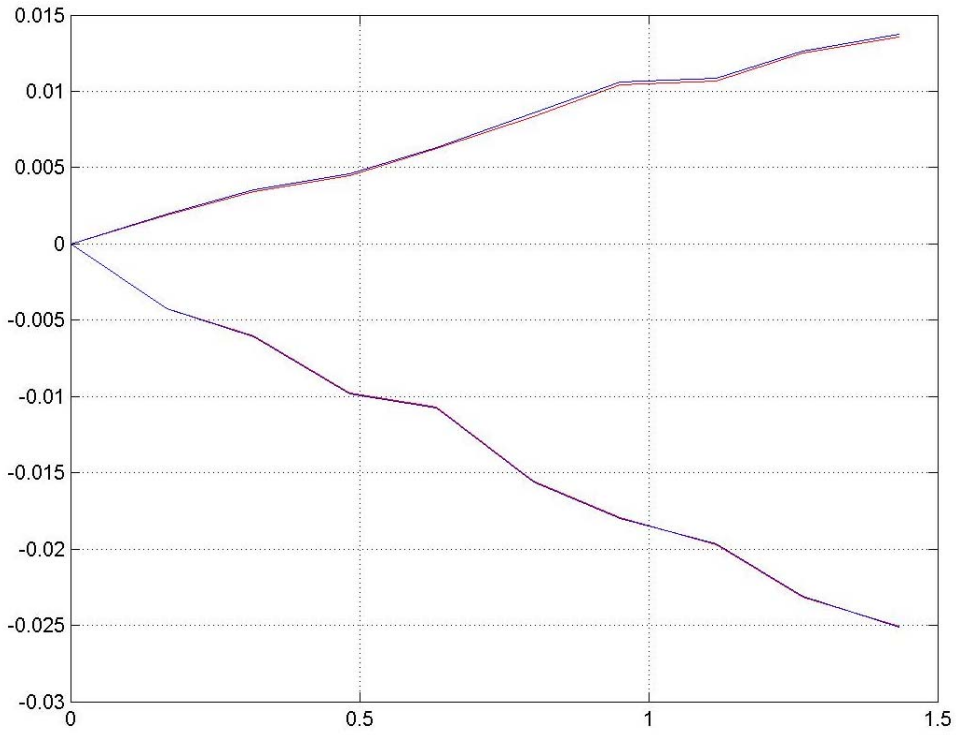

Figure 10. *Strain (-) in the loading and transverse direction as a function of time (min). Specimen is a rubber cube exposed to compression in the x-direction. Red line = incremental reference, blue line = single reference.*

The comparisons show no significant difference, and henceforth incremental reference is used due to its stability to rigid body movements.

Verifying Measurements

Verifications were made by means of two measurements on specimen made up of high pressure laminate. The specimen was clamped to a materials testing machine and exposed to an increasing tensile load with a loading rate of 50 N/s. During the loading the strain was recorded by means of the DSP system using incremental and single reference, and by means of an extensometer mounted at the back side of the specimen. The results from the first measurements are presented in Figure 11.

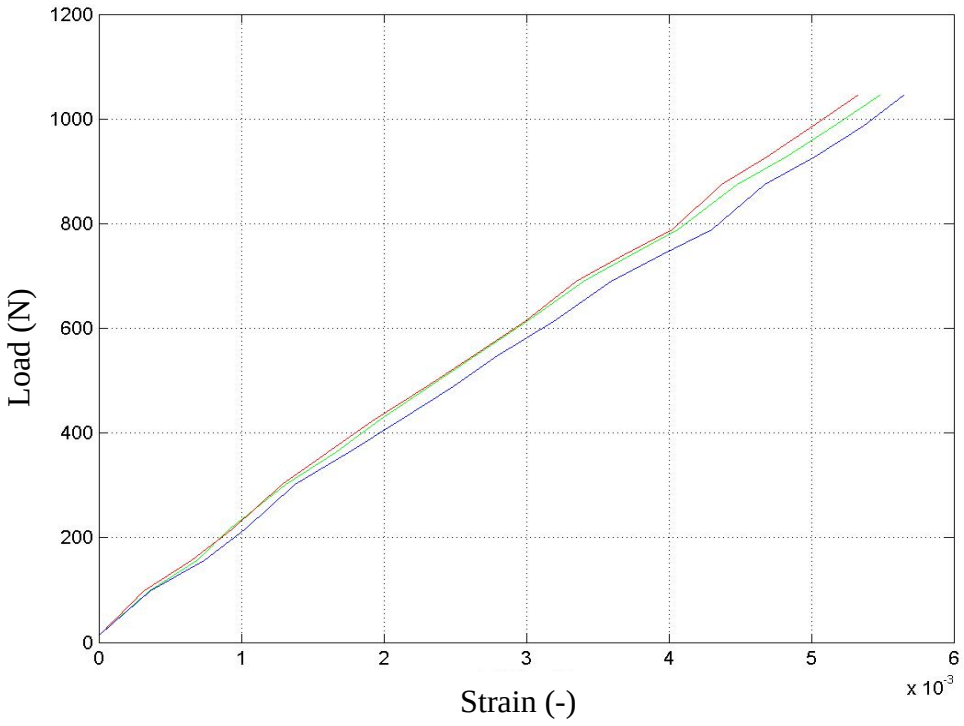

Figure 11. *First test: strain (-) measured by extensiometer (green), DSP – incremental (red) and – single (blue), as a function of load (N).*

In the second test, shown in Figure 12, DSP single reference (blue line) fails to correlate due to large rigid body movement. Results from calculations using incremental reference shows good correspondence to results from extensometer.

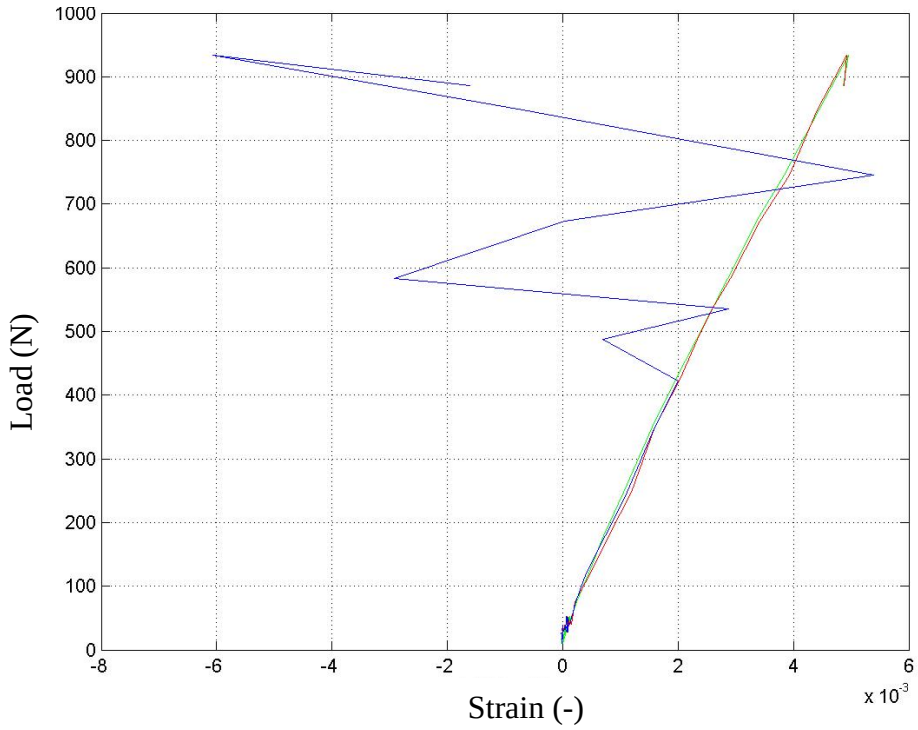

Figure 12. *Second test: strain (-) measured by extensometer (green), DSP – incremental (red) and – single (blue), as a function of load (N).*

Figure 13 shows the same diagram with a magnification of the strain in the beginning of the course of loading, before the ramp loading begins. The variations of the strain due to a fluctuation in loading are captured by all strain measurement techniques.

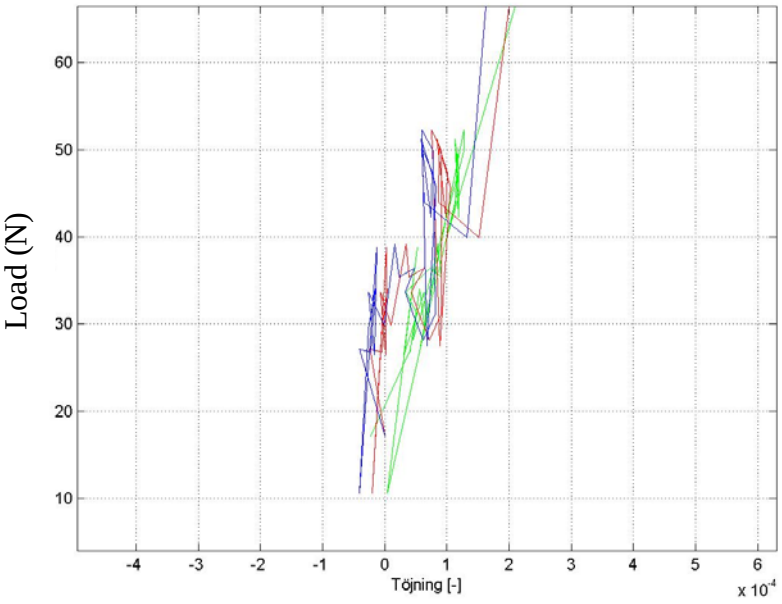

Figure 13. *Second test: strain (-) as a function of load (N).*

Applications

The DSP system has successfully been employed for measurements of the strain in the following applications:

Long time creep tests on several specimens simultaneously: 8 specimens were exposed to constant loading at different climates for several weeks. The DSP system recorded the strain for each of the specimen, one at a time by moving the camera from one position to the next. The load rig had fixed mounts so that the camera could be placed in the same position at each measurement time. All in-plane components of the strain field were evaluated at each time.

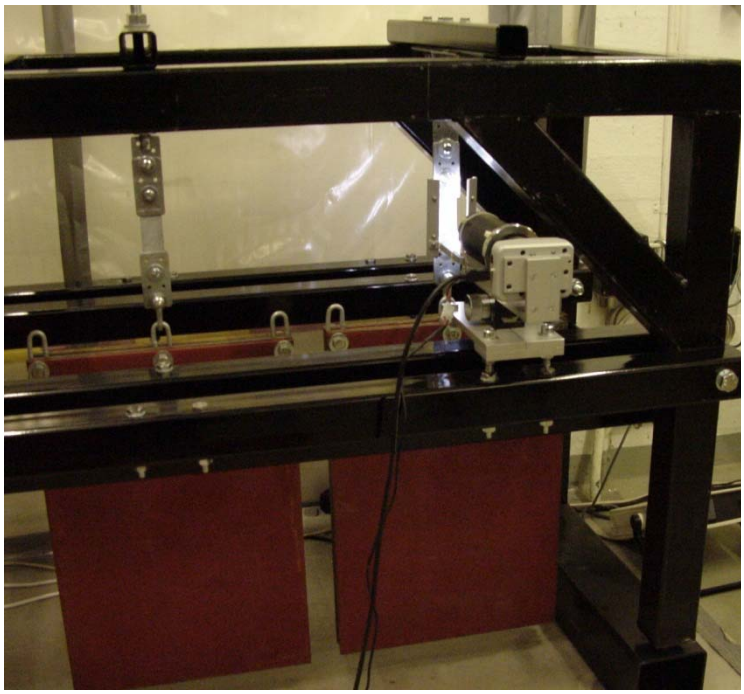

Figure 14. *Long time creep tests of several specimens of high pressure laminate simultaneously.*

Tensile and compression tests of paper: In the next application printing paper was tested exposed to a tensile loading of single paper specimens and compressive loading of piles of paper. The strain field was recorded as the paper was loaded until failure, which is illustrated in Figure 15 a) – d). Evaluated in-plane strains of the single paper specimen are presented in Figure 16. From the measurements performed on the paper specimens, all components of the stiffness tensor could be evaluated. Figure 17 illustrates a compression test of an inclined paper pile in order to evaluate the two out-of-plane shear elastic modulus of the paper pile.

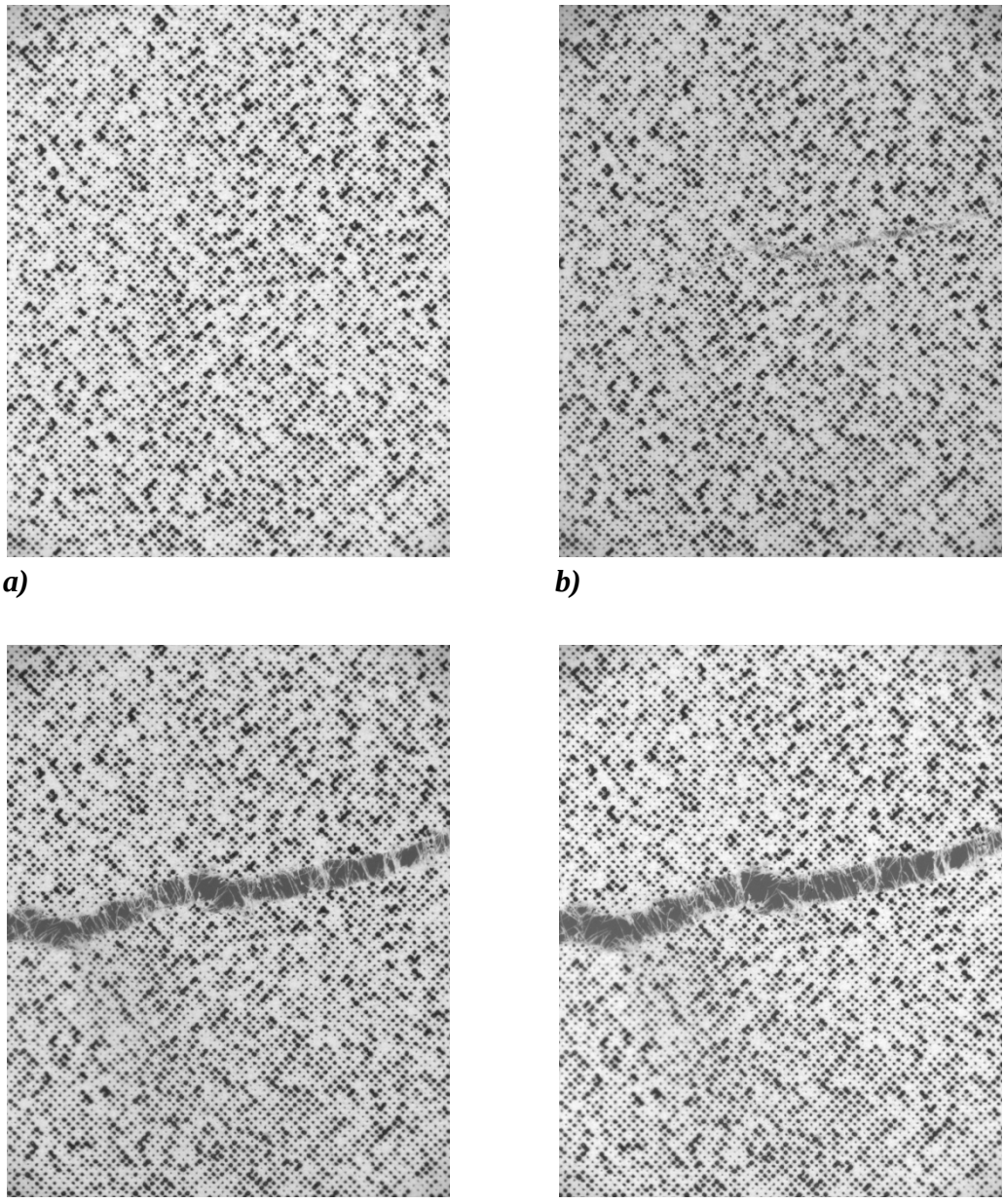

a) ***b)***

c) ***d)***

Figure 15. a) – d) *Paper specimen exposed to tensile force until failure. Size of measurement area is 20 ×16 mm.*

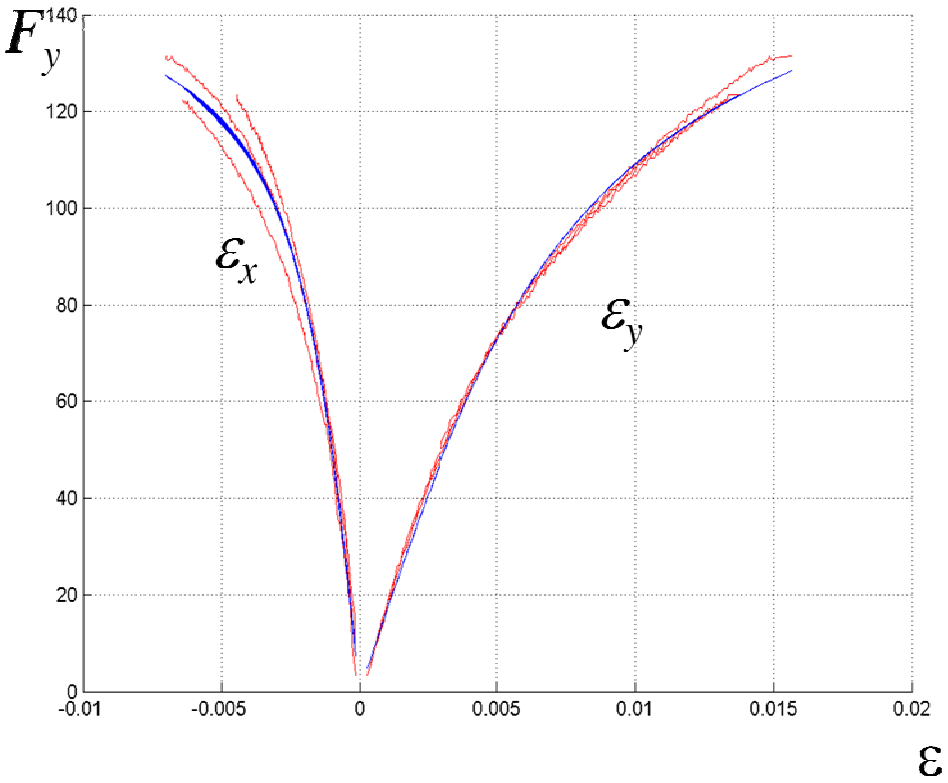

Figure 16. *Measured strains in the loading direction, ε_y, and the transverse direction, ε_x, in red with arctan curves in blue fitted according to least squares.*

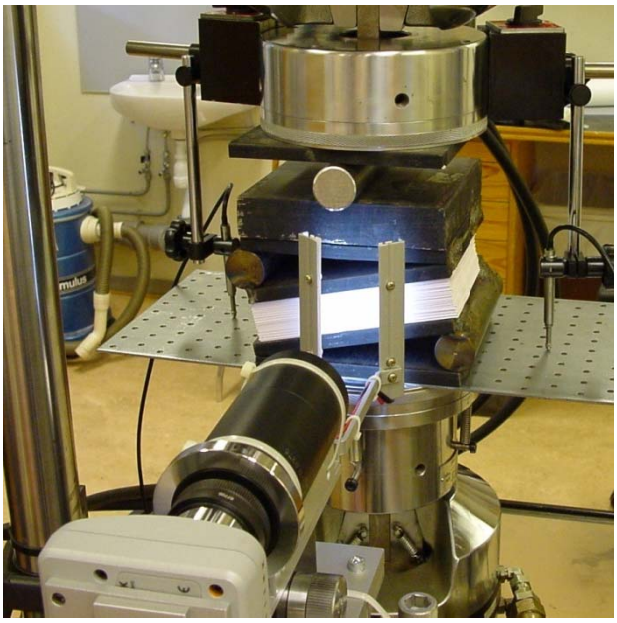

Figure 17. *Compression tests of paper piles. The paper pile is exposed to a compressive force with an inclination. The DSP system records all in-plane strain components of the surface of the pile.*

Conclusions

The optical DSP strain measurement system has been presented. The system measures all in-plane components of the strain of a specimen with high accuracy without affecting the surface other than by spraying droplets of paint. By using incremental reference the strain can be evaluated even with large rigid body movements of the specimen. The verifying tests show a good correspondence between the strain results from the DSP system and from strains measured by an extensometer. The DSP system has been employed successfully in a number of applications. In none of the applications were conventional strain gauges an alternative.

Acknowledgements

The building of the strain measurement system presented was financed by the Structural Mechanics Division at Lund University. The camera hardware as well as the load rig was built by Mr Thord Lundgren at the Structural Mechanics Division and the programming and evaluation was carried out by the author. The correlation algorithm was kindly provided by Prof. Mikael Sjödahl at the Division of Experimental Mechanics, Luleå University of Technology, which is gratefully acknowledged.

References

[1] The Math Works Inc. *Matlab - The Language of Technical Computation.* Natick, Ma, USA, 2007.

[2] Sjödahl, M. *Electronic Speckle Photography applied to In-plane Deformation and Strain Field Measurements.* Doctoral Thesis, Division of Experimental Mechanics, Luleå University of Technology, Sweden, 1995.

[3] **Stålne, K**. *Uppbyggnad av en Optisk Töjningsgivare*. Masters dissertation, Division of Experimental Mechanics, Luleå University of Technology, Division of Materials Engineering, Lund University, Sweden, 1998.